QUANTIFICATION OF THERMOELECTRIC ENERGY SCAVENGING OPPORTUNITY IN NOTEBOOK COMPUTERS

A THESIS SUBMITTED TO
THE BOARD OF CAMPUS GRADUATE PROGRAMS OF
MIDDLE EAST TECHNICAL UNIVERSITY,
NORTHERN CYPRUS CAMPUS

BY

REHA DENKER

IN PARTIAL FULLFILLMENT OF THE REQUIREMENTS
FOR
THE DEGREE OF MASTER OF SCIENCE
IN
SUSTAINABLE ENVIRONMENT AND ENERGY SYSTEMS

AUGUST 2012

Approval of the thesis:

QUANTIFICATION OF THERMOELECTRIC ENERGY SCAVENGING OPPORTUNITY IN NOTEBOOK COMPUTERS

submitted by **REHA DENKER** in partial fulfillment of the requirements for the degree of **Master of Science in Sustainable Environment and Energy Systems (SEES) program, Middle East Technical University, Northern Cyprus Campus (METU-NCC)** by,

Prof. Dr. Erol Taymaz
Chair of the **Board of Graduate Programs** _____

Asst. Prof. Dr. Ali Muhtaroğlu
Program Coordinator, **SEES Program** _____

Asst. Prof. Dr. Ali Muhtaroğlu
Supervisor, **Electrical Engineering Dept.** _____

Examining Committee Members:

Asst. Prof. Dr. Eray Uzgören
Mechanical Engineering Dept., METU-NCC _____

Asst. Prof. Dr. Ali Muhtaroğlu
Electrical Engineering Dept., METU-NCC _____

Assoc. Prof. Dr. Haluk Külah
Electrical Engineering Dept., METU _____

Inst. Dr. Murat Sönmez
Mechanical Engineering Dept., METU-NCC _____

Asst. Prof. Dr. Volkan Esat
Mechanical Engineering Dept., METU-NCC _____

Date: August 16th, 2012

I hereby declare that all information in this document has been obtained and presented in accordance with academic rules and ethical conduct. I also declare that, as required by these rules and conduct, I have fully cited and referenced all material and results that are not original to this work.

Name, Last name :

Signature :

ABSTRACT

QUANTIFICATION OF THERMOELECTRIC ENERGY SCAVENGING OPPORTUNITY IN NOTEBOOK COMPUTERS

Denker, Reha

M.S., Sustainable Environment and Energy Program
Supervisor: Asst. Prof. Dr. Ali Muhtaroğlu
Co-Supervisor: Assoc. Prof. Dr. Haluk Külah

August 2012, 104 pages

Thermoelectric (TE) module integration into a notebook computer is experimentally investigated in this thesis for its energy harvesting opportunities. A detailed Finite Element (FE) model was constructed first for thermal simulations. The model outputs were then correlated with the thermal validation results of the selected system. In parallel, a commercial TE micro-module was experimentally characterized to quantify maximum power generation opportunity from the combined system and component data set. Next, suitable "warm spots" were identified within the mobile computer to extract TE power with minimum or no notable impact to system performance, as measured by thermal changes in the system, in order to avoid unacceptable performance degradation. The prediction was validated by integrating a TE micro-module to the mobile system under test. Measured TE power generation power density in the carefully selected region of the heat pipe was around 1.26 mW/cm^3 with high CPU load. The generated power scales down with lower CPU activity and scales up in proportion to the utilized opportunistic space within the system. The technical feasibility of TE energy harvesting in mobile computers was hence experimentally shown for the first time in this thesis.

Keywords: Thermoelectric Energy Harvesting, Thermoelectric Power Generation, Mobile Computers, Sustainable Energy

ÖZ

DİZÜSTÜ BİLGİSAYARLARDA TERMOELEKTRİK ENERJİ ÜRETİM OLANAĞININ SAYISAL OLARAK İNCELENMESİ

Denker, Reha

Yüksek Lisans, Sürdürülebilir Çevre ve Enerji Sistemleri Programı

Tez Yöneticisi: Yrd. Doç. Dr. Ali Muhtaroğlu

Ortak Tez Yöneticisi: Doç. Dr. Haluk Külah

Ağustos 2012, 104 sayfa

Bu çalışmada, dizüstü bir bilgisayara eklenen termoelektrik kapsül vasıtasıyla enerji üretimi fırsatları deneysel olarak incelenmiştir. Isıl simulasyonlar için detaylı bir sonlu analiz modeli hazırlanmıştır. Bu modelden elde edilen sonuçlar daha sonra test sisteminden toplanan bulgularla bağdaştırılmıştır. Aynı zamanda ticari bir termoelektrik mikro kapsülü deneysel olarak karakterize edilmiş ve bu kapsül ile sistemin hangi koşullarda azami güç üretimi için elverişli olacağı sayısal olarak analiz edilmiştir. Akabinde, dizüstü bilgisayar içerisinde thermoelektrik kapsül için uygun olabilecek "sıcak noktalar" belirlenmiştir. Bu noktaların belirlenmesi esnasında ısıl ölçümler sürekli göz önünde tutulmuş ve sistemin aşırı ısınmasına veya performans kaybına sebep olmayacak noktaların seçilmesi özellikle dikkate alınmıştır. Önceki aşamalarda yapılan tahminlerin doğrulanması için çalışır durumdaki test sistemine termoelektrik kapsüller eklenmiştir. Mikroişlemci yüksek iş yüküyle çalışırken, ısı boruları civarındaki termoelektrik güç üretim yoğunluğu 1.26 mW/cm^3 olarak ölçülmüştür. Üretilen güç miktarı, mikroişlemci faaliyeti ve kullanılan ısıl alan miktarı ile orantılı miktarda hareket etmektedir. Dizüstü bilgisayarlarda termoelektrik enerji üretimi uygulanabilirliği bu tezde gösterilmiştir.

Anahtar Kelimeler: Termoelektrik Enerji Geri Kazanımı, Termoelektrik Güç Üretimi, Dizüstü Bilgisayarlar, Sürdürülebilir Enerji

DEDICATION

I would like to dedicate this work to my mother, my father, my sister, Yağız and Ayşim; for their unconditional support and trust during my whole research and thesis writing process.

ACKNOWLEDGEMENTS

The author wishes to express his deepest gratitude to his advisor Assistant Professor Dr. Ali Muhtaroğlu for his guidance, advice, criticism, encouragements and insight throughout the research.

The author would like to thank Associate Professor Dr. Haluk Külah from Middle East Technical University MEMS Research Center, Mr. Rajiv Mongia from Intel and Assistant Professor Dr. Eray Uzgören from Middle East Technical University Northern Cyprus Campus for their contributions in reviewing different parts of this work, and to Hamburg Industries Co. Ltd. for donating a replacement for a damaged cable in the target system.

The technical assistance of Mr. Saim Seloğlu and Mr. İzzet Akmen are gratefully acknowledged.

This work is in part supported by MER, a partnership of the Intel Corporation to conduct and promote research in the Middle East and in part by TÜBİTAK, Turkey under grant number 109E220.

TABLE OF CONTENTS

LIST OF FIGURES

LIST OF TABLES

NOMENCLATURE

I_L	Loaded circuit current, (mA)
n	Number of TE couples
P	Power, (mW)
PF	Power factor, (W/ K m^2)
P_{max}	Maximum power, (mW)
R_L	Load resistance, (Ω)
R_S	Material resistance, (Ω)
T_C	Temperature of the cold surface, (°C)
T_H	Temperature of the hot surface, (°C)
V	Voltage, (mV)
V_L	Loaded circuit voltage, (mV)
V_{OC}	Open circuit voltage, (mV)
ZT	Dimensionless figure of merit
α	Seebeck coefficient, (mV/°C)
η_C	Carnot efficiency
κ	Thermal conductivity, (W/K m)
ρ	Electrical resistivity, (Ω m)
ψ	Thermal resistance, (°C/W)

CHAPTER 1

INTRODUCTION

1.1 Energy Harvesting

The power of energy acquisition has become a very important subject with the contributions of the acceleratingly growing economy and day-by-day decreasing amount of energy sources. On one hand, the continuing development of the technology increases the energy demand. On the other, hand the conventional fossil fuel sources grow scarcer. Therefore, more sustainable energy acquisition methods started to become a popular research topic. Energy acquisition has turned into a troublesome task especially for electrical and electronic devices, which keep becoming more prevalent, complex and small each passing day. The current miniaturization trend makes the former energy sources like batteries less functional, since their effectiveness also diminishes proportionally with their geometry. Therefore the improvement of the battery life highly depends on the reduction of the power consumption and battery dependency [1].

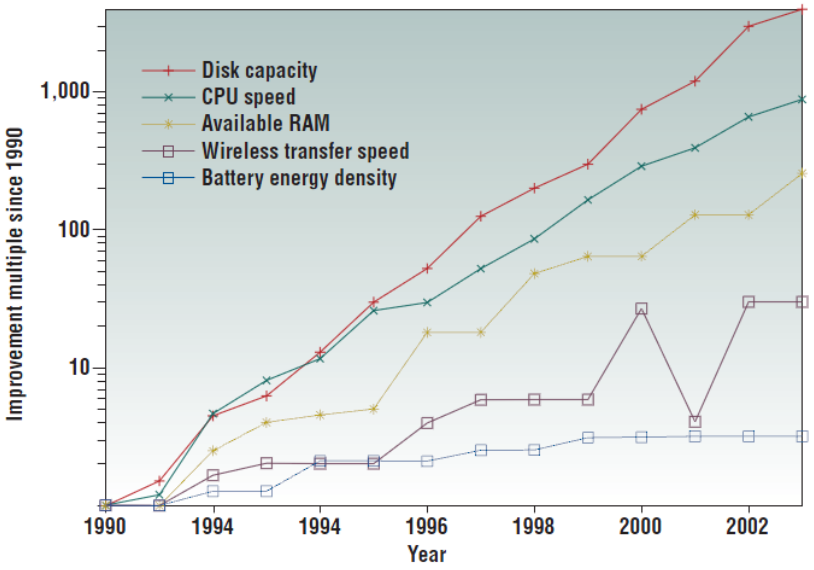

Figure 1.1 Relative improvements in notebook computing technology between 1990 – 2003. Note the wireless connectivity curve considers only cellular standards; not short-range 802.11 "hotspots" [1].

Figure 1.1 provides the recent development stages of different notebook components over the years. It is apparent that the battery energy density has developed over the years as well. However these improvements were quite small in comparison with the other parts. Empowering the electronic devices using chemical reactions is an ongoing research topic. Normal sized fuel cells seem to be too large to integrate into many models of electronic devices, while microcells are proven to be too small to provide enough energy for operating. There are additional options to solve the energy management problem in micro scale electronics such as microturbines and microengines. Although their efficiencies of power production are relatively high, they bring up additional problems like overheating, noise and safety. Their degree of sustainability is also open to discussion since they work on burning fuel [1]. A more detailed analysis in nanoscale energy harvesting has been carried out by Wang [2], who reviewed many different energy harvesting technologies with potential to power nano-systems.

As sustainability becomes an important part of the contemporary technological developments for environmental and economical reasons, the concept of energy scavenging offers a convenient solution. By definition, energy scavenging can be described as *the method to recover energy which was originally lost to the environment or unusable*. There are three major energy scavenging methods that utilize photovoltaic, vibration and thermal gradient [3, 4]. Photovoltaic systems are designated to collect and convert solar energy into electricity and can be applied to small electronic systems by placing small panels outside the chassis. This has been a very common practice used in many calculators for more than two decades, and recent developments in the photovoltaic technology enable extension of the same principle to notebooks as well [5, 6].

Vibration based scavenging is generally used with the assistance of micro-scale electromagnetic (EM) or piezoelectric (PZ) generators. EM generators have magnets on top, and convert the fluctuations in the electromagnetic field into electrical voltage. There are various applications like watches which have been developed to use the vibrations created by human body as an energy source. Consisting of a piezoelectric element with a resonantly matched transformer, piezoelectric generators can produce electricity under vibration. It is possible to harvest energy from a computer keyboard, for example, to supply the battery [1].

The third major method for energy scavenging is the thermal gradient method. This method is based upon using the heat difference between two surfaces as a power source in order to harvest this energy with thermoelectric (TE) materials.

1.2 Thesis Objective

This thesis will analyze the energy scavenging options in notebook systems through the utilization of thermoelectric materials. Notebooks are widespread technological devices which have a broad range of uses in the modern society. Like most of the modern devices, notebooks need electrical energy in order to operate and can only work for a limited time with the power supplied by their batteries. Although notebook batteries are rechargeable, it is a known fact that they have a limited lifespan and each time a battery has been recharged this life span is shortened by a small amount. Initiatives like Energy Star has caused a variety of power management features to be implemented in notebooks to reduce dependence of power from the electrical outlets during idle and active periods. In addition, dynamic control of the notebook features in a closed self-regulating loop required different kinds of sensors to be integrated into these systems.

The main purpose of this research is to reduce the dependence of notebooks on electrical outlets through thermoelectric generation without conceding from the operational performance and quality. It is expected that the current efficiency of the thermoelectric materials may result in modest power output [1, 3, 4, 5]. Yet, the present study focuses on developing the methodology for quantifying all thermoelectric energy scavenging opportunities in a spectrum of notebook platforms available today and tomorrow. It is expected that the generated energy can be used to increase battery life, or power up small distributed sensors around the system which only require modest power to operate.

The previous research and theoretical background is examined in Chapter 2 to establish the relevance to the topic at hand. Figure 1.2 depicts the identified steps which were followed throughout the research period for a healthy convergence to the system solution. The experimentally based methodology behind this flow has been developed as part of this thesis. Chapter 3 focuses on the TE characterization process including the experimental methodology developed for this purpose. Chapter 4 covers the experimental mechanical and thermal characterization of the target systems. After this point the research focuses on one of the pre-evaluated target systems and TE modules. In Chapter 5,

a partial and full CAD model of the selected system is presented. Chapter 6 focuses on the TE integration analysis and its validation. Finally the conclusions from the thesis are discussed in Chapter 7.

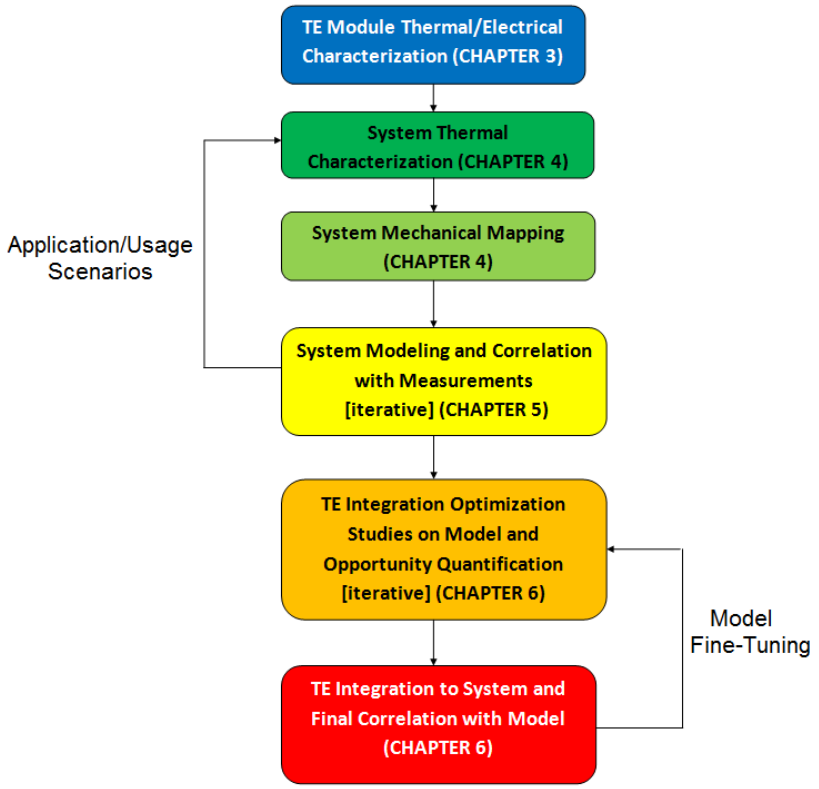

Figure 1.2 Steps in experimental development of TE generation in notebook systems

CHAPTER 2

BACKGROUND AND PREVIOUS WORK

2.1 Background Research

2.1.1 Thermoelectric Modules

Thermoelectric (TE) modules are specially designed systems used to convert the thermal gradient between two sides of a TE couple into a voltage difference by the Seebeck effect or vice versa (which is generally referred as Peltier effect.) This phenomenon is discovered in 1821 by Thomas Johann Seebeck, a German physicist, who had observed that a circuit built between two different metals with junctions at different temperatures, creates a voltage difference between those metals. The Seebeck effect can briefly be expressed with the following equation:

$$\Delta V = (\alpha_x - \alpha_y)(T_H - T_C) \quad (1)$$

Here T_H stands for the temperature of the hot surface and T_C at the cold surface. The Seebeck coefficient α (unit mV/K) is the conversion factor between the temperature gradient and the voltage. TE modules contain a pair of distinctly doped semi-conductors (x and y) each with a different Seebeck coefficient of opposite sign. These two coefficients can be combined as [7]:

$$\Delta V = \alpha_{xy}(T_H - T_C) \quad (2)$$

However one must keep in mind that this is a rather simplified definition, as the Seebeck coefficient itself is also temperature dependent and may vary according to the working condition. This situation may pose a problem especially for large temperature differences, thus rendering the equation less useful. However for cases, in which $\Delta T < 100°$, those changes are rather small, making a "constant α" assumption plausible.

A TE couple consists of an n-type material, negatively charged with electrons, and a p-type material, positively charged with holes. Figure 2.1 and Figure 2.2 show different schemes for possible TE application both as an energy generator and a cooler.

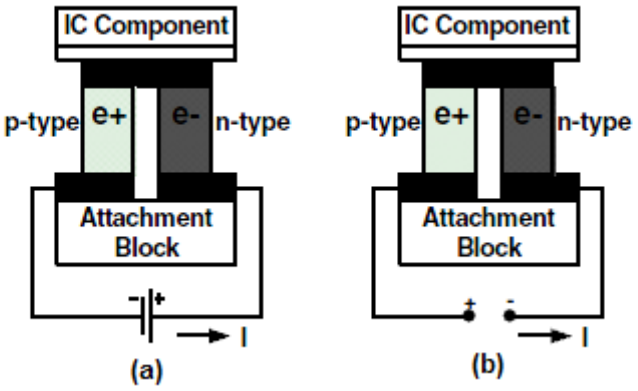

Figure 2.1 Thermoelectric couple in (a) cooler, and (b) generator configuration. [8]

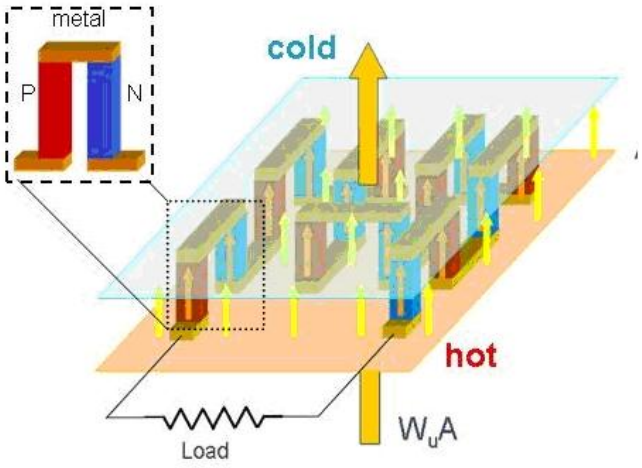

Figure 2.2 Schematics of a thermoelectric generator (approximately 6mm x 6mm) [9].

Another important parameter for the thermoelectric materials is the dimensionless figure of merit, *ZT*.

$$ZT = \frac{\alpha^2}{\rho\kappa}\, T \tag{3}$$

In Equation 3, ρ represents the electrical resistivity and κ stands for thermal conductivity. The actual figure of merit (Z) has been multiplied with the average temperature in order to obtain *the dimensionless figure of merit*, which is used as a parameter representing the effectiveness of the TE material. The maximum reported for the dimensionless figure of merit is 1.0 for the room temperature in the ideal case scenario [10], however ZT values 40-50% larger than this limit have been observed for temperature values 475-950 K.

Research in thermoelectric materials has shown that theoretical ZT values between 2.0-3.0 are possible [11].

This thesis deals with the internal temperatures of the mobile computers. As further documented in the following chapters, this application has an available temperature range of 25-110 °C under regular room conditions with 25 °C ambient. The most efficient Seebeck coefficient in this range has been observed between Bi_2Te_3 (bismuth telluride) as the n-type material and Sb_2Te_3 (antimony telluride) as the p-type material, which have practically provided Seebeck coefficient between 0.3-0.4 mV/K, and dimensionless figure of merit of 0.84-0.87 [10, 11, 12]. TE modules built using Bi_2Te_3 - Sb_2Te_3 couple is known for their relatively high power generation potential even with a temperature difference smaller than 10° C [13].

One of the reasons for this drop of efficiency in lower temperature difference can be explained with Carnot efficiency. Although solid state thermoelectric generators have many advantages like sustainability and being maintenance free, one must keep in mind that they are still thermal devices working with the principles of heat-work conversion. Therefore the laws of the thermodynamics have to be taken into consideration during the analysis of the TE materials.

$$\eta_C = 1 - \frac{T_C}{T_H} = \frac{\Delta T}{T_H} \tag{4}$$

Carnot cycle is accepted as the ideal case where the maximum possible heat can be converted into the work. Thus Carnot efficiency provides us with the maximum percentage of work attainable from any kind of heat transfer. As it has been shown in Equation 4, the temperature difference and the temperature of the hot surface play a dominant role in the determination of the Carnot efficiency [14].

$$PF = \frac{\alpha^2}{\rho} \tag{5}$$

The power factor *PF* is another important parameter after the figure of merit. PF is measured in Watts per Kelvin square per meter (W/K^2 m). It carries an important role for the thermoelectric converters because it shows the relationship between the Seebeck coefficient and the electrical resistivity of a material, thus determining the electrical performance of the thermoelectric materials [10].

Thermotunnel effect has also been an important thermal based energy scavenging method aside from the Seebeck effect. This phenomenon has been first observed in 1980's by an experiment in Al-PbBi tunnel-junctions and many experiments followed the first one especially in the cooling applications. In thermotunnel coolers, two metallic grades are being held separately with a vacuum in between and a bias voltage is applied to operate the device. Acting like a Schottky barrier, the bias voltage creates a barrier between the metals, thus disabling the electron transfer from the hot to the cold side, and enhancing the tunneling effect in the other direction (Figure 2.3). Depresse and Jager argued that thermotunneling devices have a much higher power density and thermal insulation capabilities, thus making them better coolers than TE devices. However, they are not so efficient for the energy scavenging opportunities due to weak voltage output and conversion efficiency. It has been stated that even if the difficulties in the development process can be overcome, the output voltage will be one magnitude lower than the thermoelectric devices, thus making them unsuitable for this project [15].

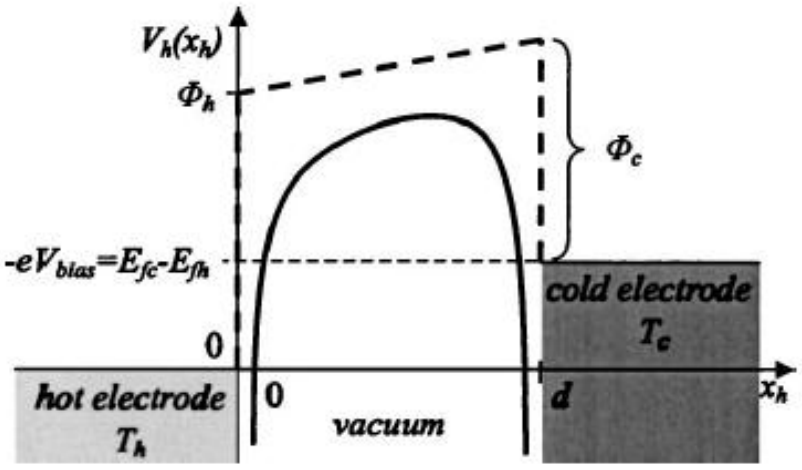

Figure 2.3 Potential barrier $V_h(x_h)$ profile between electrodes with different temperatures and electrode work functions. The solid line is the real potential profile taking into account the image charge correction, the dotted one is the trapezoidal approximation without correction [15].

2.1.2 Applications in Microelectronic Systems

The main topic of this thesis is the thermal energy scavenging opportunities in notebooks. Therefore, the thermal management of the notebooks and the location of the TE modules play a major role. There are certain thermoelectric applications to use *the bioheat* of the human body to empower small devices like watches and hearing aids. Figure 2.4 shows *Seiko Thermic* wristwatch as an example for this application. It uses 10 thermoelectric modules to generate the sufficient microwatts required to operate the mechanical motion in the watch [1].

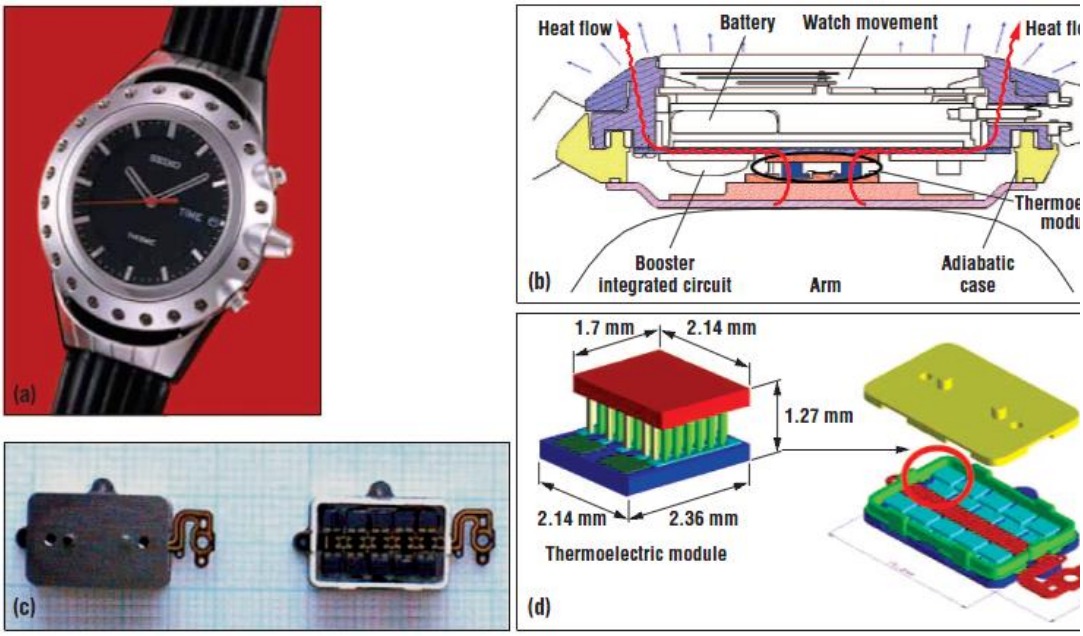

Figure 2.4 The Seiko Thermic wristwatch: (a) the product; (b) a cross-sectional diagram; (c) thermoelectric modules; (d) a thermopile array. Copyright by Seiko Instruments [1].

Naturally there are certain limitations in these practical applications. One of the major obstacles is that the thermoelectric materials provide an energy value measured in microwatts to milliwatts. If we build an open circuit, we would need more than 4000 junctions to obtain an output voltage of 10 V (without loads) which will be quite impractical since covering that much area on a human body will prevent the heat transfer between the human skin and the ambient temperature and thus it will be uncomfortable in daily usage [10]. The amount of thermal energy removed from the human body without compromising the comfort can be controlled by using a wearable thermal-generator. Yet

in most cases the thermoelectric generators are used as an additional source instead of replacing batteries.

This methodology becomes rather attractive especially in microsystems which rely on batteries with a limited life span. The continuously decreasing geometry of the new battery models have hard time catching up with the power density requirements of the current technology. In certain cases, replacing those batteries can also prove to be an expensive and laborious task. In order to address this problem, Carmo et al. came up with the idea of the integrated thin film rechargeable batteries to support the thermoelectric scavenging microsystems. The integrated thermoelectric material harvests the necessary energy from the heat difference between the environment and the surface. Therefore battery exchange will not be necessary until rechargeable battery expires [16] (Figure 2.5).

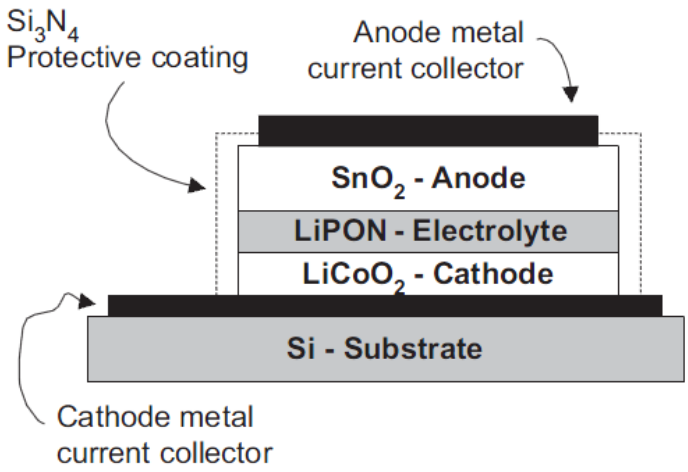

Figure 2.5 Cross-section of the thin film rechargeable battery [16]

By using cobaltate ($LiCoO_2$) as the cathode a micro-scaled version of the commercial type Lithium batteries can be structured. The main idea of the integrated battery is to aid the thermoelectric scavenging systems by broadening their usage capacity especially in biomedical applications.

There are several attachment concepts introduced by Solbrekken et al. [17] which should also be taken into consideration. Integrating TE modules directly on top of integrated circuit (IC) packages creates a risk of overheating. Therefore a “shunt attach” concept has been introduced. Unlike the direct attach concept, in which TE module is directly placed between the heat sink and the heat source (CPU), only a controllable part of the heat

energy is led to TE module while the rest of the heat is shunted to a different path. This path will be structured by a heat spreader, creating a need for an extra heat sink for the shunt path, while the original one is reserved for the TE module (Figure 2.6).

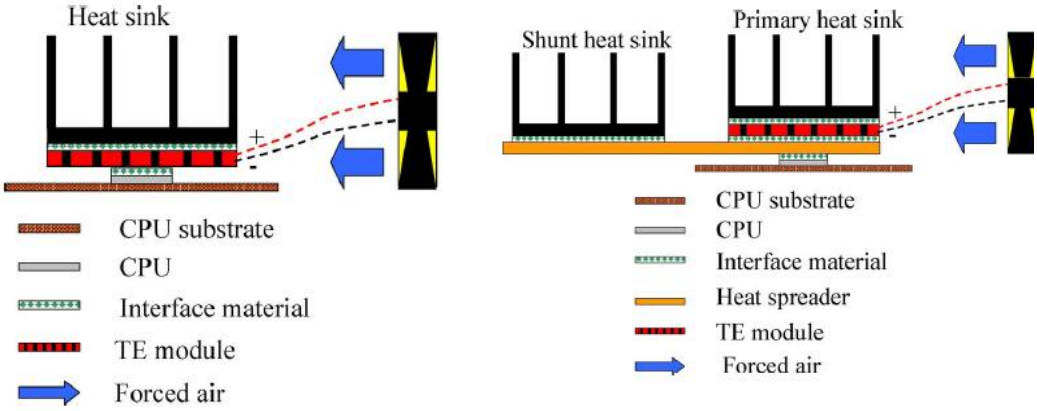

Figure 2.6 The schematics of a) direct attach, b) shunt attach [17].

Although this method seems very plausible in theory, a variety of arrangements needs to be done before it can be practically used. First of all, the configuration and the design of the shunt path should be compatible with the TE module and the fan. In their research, Solbrekken et al. assumed that the design and the optimization of the fan have already been completed so that the fan works with the energy harvested from the CPU to cool it down [17]. Even though advantageous, building such an alternative path inside the restricted notebook space may alter the heat dissipation paths radically. Because of the geometrical limitations, such an attempt may create a hindrance in the air flow and decrease the efficiency of the cooling solution, thus leading a possible scenario of performance drop for CPU due to the overheating.

Like Solbrekken et al., Freunek et al. [18] and Meng et al. [19] created very detailed numerical models for TE conversion. While Meng et al. did not have application focus, Freunek et al. created a demonstration setup which was adequate to compare their theoretical results with the calculated values. The work was not extended to a real target system, thus overheating (or performance loss) risk could not be evaluated. This thesis will focus on the experimental and application part of the thermoelectric modules rather than the analytical analysis performed by Freunek et al. and Meng et. al.

Hsu et al. [20] found a niche for TE harvesting in the exhaust system of the automobiles. They naturally dealt with much higher temperature and power levels in that particular application compared to what is available in a microelectronic system, but they have practically used an existing shunt path for heat dissipation, same concept as previously described.

The specifications and thermal characterization of TE modules also bear an important role in the energy scavenging systems. The paper by Niu et al. [21] includes a detailed analysis about how different commercially available TE generators act under various external conditions. However, the introduced experimental model seems too detailed for the scope of this research. Because it includes many different parameters on different scenarios which have no direct influence upon the system at hand. Thus a self-built TE characterization model inspired by the work of Muhtaroğlu et al. [8] will be used in this project.

Energy scavenging is an important part of sustainable energy technologies which can be utilized in computer and electronics branches. A study conducted by Mathuna et al. [22] shows the application possibilities for different energy scavenging methodologies in wireless sensor networks. This study is a good reference for a sequel research project to this thesis focusing on the utilization of the harvested energy in notebooks.

2.2 Previous Work

Some previously developed ideas about the thermoelectricity and heat management in microelectronic systems and other applications have been presented in the previous section. Although they were based on the same theories and principles they provided a general idea about the current condition of the state-of-the-art. In this section, however, the focus will be on two specific papers (Muhtaroğlu et al. [8] and Rocha et al. [12]) which followed the same or similar aim as this project, and therefore can be accepted as predecessors.

The first paper, written by Muhtaroğlu et al. [8], examined hybrid thermoelectric conversion. Two different cases were highlighted to focus on the average and maximum power usage in mobile computers. It was assumed that mobile computers spend 15% of their lifetime in maximum operation condition. This state is called thermal design power because the cooling solution is designed for this condition. The remaining 85% is assumed

to be working under average power. The pie charts in Figure 2.7 have been created in accordance with this assumption. The difference between the power distributions among the computer parts is rather prominent.

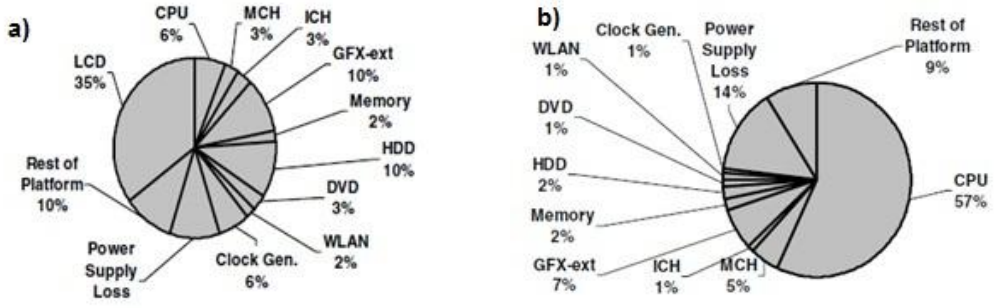

Figure 2.7 Mobile platform a) average power usage, and b) thermal design power [8].

The model described above has been named as *semi-realistic usage model* in the paper and the case studies of the TE modules have been done accordingly.

Since the aim of this thesis is using realistic situations, which are based upon applications and simulations, realistic models with TE modules will be utilized instead of such assumptions. The energy harvesting capacities of selected TE modules will be fully analyzed and TE modules will be integrated into the test system in order to obtain a clear view about the actual energy harvesting possibilities. A detailed mechanical analysis of the target system will indicate points, which are physically available for TE integration, and how much energy can be acquired from these selected points.

Unlike the first paper, the study of Rocha et al. [12] also included a 3D model which presents a more detailed approach and elaborates results closer to the actual scenario in notebook systems. Although the details of the presented data are limited, it can be understood that a system model aiming to improve the battery life in notebooks has been created by using semiconductor type TE modules made of Bi_2Te_3 and Sb_2Te_3. Yet the model of the whole system has been avoided in this paper as well and only the heat sink has been thoroughly analyzed. Also the model of Rocha et al. has an important disadvantage, rendering itself inappropriate for practical application in an actual notebook: In Figure 2.8, Rocha et al. have used a desktop type heat sink due to its higher thermal efficiency. However this type of heat sinks is unsuitable for notebooks due to their larger scales.

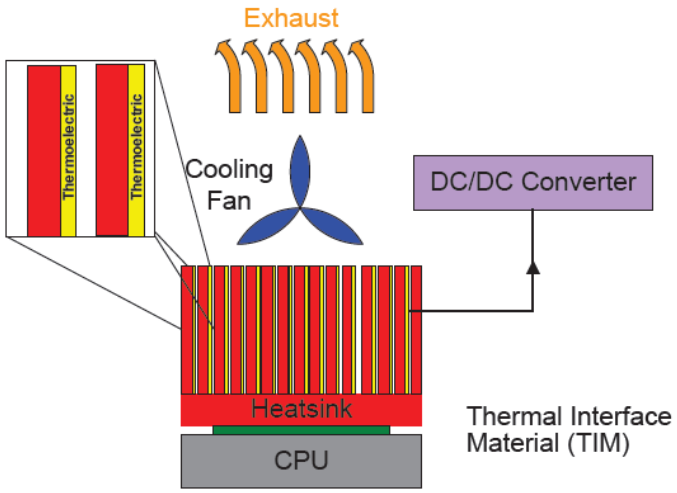

Figure 2.8 Illustration of the TE energy harvesting model, created by Rocha et al. [12].

In conclusion, it has been observed that TE modules can be applied to micro-scale setups like IC systems to harvest additional energy from the temperature difference between the heat source and the ambient temperature. The modeling for TE characterization done by Muhtaroğlu et al. [8] will be utilized for the measurements required to create a characteristics curve for the off-the-shelf TE modules. Rocha et al. [12] used a more detailed 3D custom model. By taking this approach one step further a CFD model has been prepared for the whole computer and the acquired results have been compared with actual measurements, which is a first in this subject to the author's knowledge. The details will be presented in the following chapters.

CHAPTER 3

CHARACTERIZATION OF THERMOELECTRIC MODULES

In this chapter the characterization steps of the TE modules will be explained. Two different off-the-shelf model TE modules have been selected for the characterization process. Off-the-shelf models were preferred for their superior quality and ease of availability. The selected TE modules are:

- *FerroTEC Peltier cooler model 9500/018/012 M P [23, 24]*
- *TETECH TE 17-0.6-1.0 Thermoelectric Module [25]*

These modules are originally designed to be small scaled Peltier coolers for a variety of uses. As explained in Chapter 2, TE materials can be used in both ways. Therefore they will be utilized as Seebeck generators.

For the characterization process a custom setup has been built which has been inspired from the work of Muhtaroğlu et al. [8]. The photograph and schematics of the experimental setup are presented in Figures 3.1 and 3.2.

Figure 3.1 TE model characterization setup prepared for this thesis

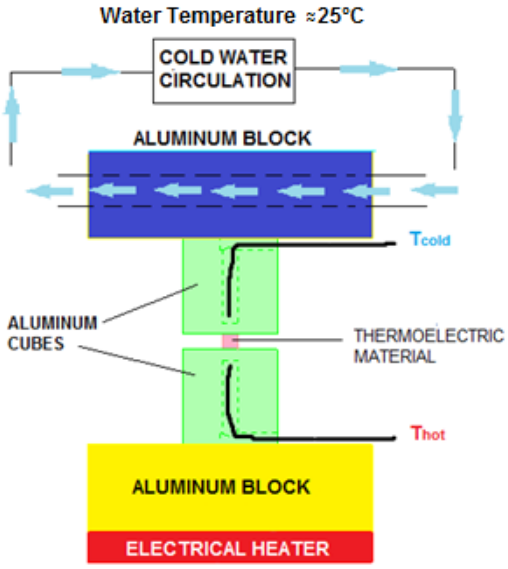

Figure 3.2 Schematics of TE module characterization setup

The experimental setup consists of the following elements:

- Two aluminum cubes (24 mm x 24 mm x 24 mm)
- Two aluminum blocks (75 mm x 75 mm x 23 mm)
- An ARE electrical heater
- A PolyScience Recirculator with cooler
- A Fluke 8846 Precision Multimeter
- An Omega HH506RA Multilogger Thermometer
- Two Omega K-type thermocouples
- TE materials to be measured
- A breadboard
- An electrical resistor (app. 1 Ω)

The objective of this experiment is to observe the relationship between the temperature difference between the upper and lower surfaces of the TE module and the voltage generated by the TE module. The TE module is placed between the aluminum cubes, which have channels with 3 mm diameter drilled inside. The depths of the channels have been adjusted accordingly so that the thermocouples put inside the cubes can touch the surface of the cubes from the inside. The small temperature difference between the contact points of the cube surface and the TE module surface has been neglected. In order to

ensure the homogeneity of temperature distribution, these channels were filled with thermal grease. The thermocouples inside the cubes are attached to the digital thermometer in order to acquire the necessary data.

These cubes are placed between two aluminum blocks. The lower aluminum block lies on an electrical heater to create a hot surface. Another channel with a 6-mm diameter has been drilled horizontally through the upper block and through two different hoses attached to each end the upper block is connected to the recirculator, which is filled with distilled water and serves as a cooler during the experiment. Once set to a certain temperature and activated, it simultaneously chills the water and starts a recirculation through the upper aluminum block, thus creating a cold surface with a constant temperature.

The (nearly) constant temperature of the upper block was rather useful because the electrical heater could only be set to certain values between the ambient temperature and 250°C. The following procedure was followed throughout the experiment:

1. The recirculator was set to 25°C. In this step, the thermocouple inside the upper cube was used in order to check the temperature of the aluminum block.
2. Once the upper block has reached to the steady state at a value near the preset temperature, the electrical heater was activated and its temperature was set to 100°C.
3. This time the lower thermocouple has been used to check the steady state.
4. Once the steady state of the lower block has been achieved, the first thermal and electrical measurement has been taken and the electrical heater has been turned off.
5. Without an active heat source, the temperature of the lower aluminum block starts to drop. So the data acquisition is repeated for each 3° C drop in the lower block till both of the blocks reach to a thermal equilibrium.

When the collected data has been analyzed, a temperature drop of 2° C has been observed in the upper block. Obviously, this is a side effect of the free convection created by the elevation of the hot air around the low lying hot block. This setup could have been inverted in order to increase the precision of the thermal points but this option has been evaded for two reasons: The electrical heater used for this experiment was not physically

suitable to operate upside down and the error is expected to be insignificant due to the present setup, thus it has been neglected.

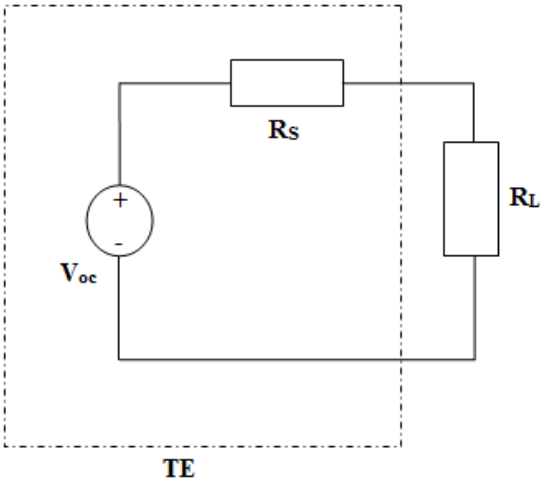

Figure 3.3 Thevenin circuit built for electrical data acquisition.

As depicted in Figure 3.3, the terminals of the TE module were connected to a basic resistor divider with an external load resistor in order to create a Thevenin circuit. The TE module served as the voltage source of the circuit with an intrinsic resistance R_s. The following electrical data has been acquired during the experiment in addition to the thermal data:

- Voltage of the open circuit (V_{OC})
- Voltage of the loaded circuit (V_L)

All other required data have been calculated using these two values for each step. The load resistance R_L has been placed in the circuit in order to calculate the intrinsic resistance of the material itself (R_S), which was required to calculate P_{max}, the maximum harvestable power from the TE material. The electrical and thermal measurements were also utilized to determine the Seebeck coefficient (α) of the TE module.

Once the data acquisition has been completed the following calculations have been commenced:

$$I_L = \frac{V_{OC}}{R_S + R_L} = \frac{V_L}{R_L} \tag{6}$$

$$R_S = \left(\frac{V_{OC}}{V_L} - 1\right) R_L \tag{7}$$

$$P = \frac{{V_L}^2}{R_L} \tag{8}$$

The power calculated here is the momentarily obtained power. However, the maximum power can only be achieved when the resistance of the material equals the resistance of the load.

$$R_L = R_S \tag{9}$$

$$I_{max} = \frac{V_{OC}}{2R_s} \tag{10}$$

$$P_{max} = \frac{{V_{OC}}^2}{4R_s} \tag{11}$$

In order to find the module Seebeck coefficient, the open circuit voltage has to be divided to the measured temperature difference. Considering there are a number of TE couples in one TE module, the result has to be normalized using the TE module number, *n.* This number equals to 18 for FerroTEC TE Module and 17 for TETECH.

$$\alpha = \left(\frac{1}{n}\right)\left(\frac{V_{OC}}{\Delta T}\right) \tag{12}$$

There are some fluctuations in the acquired results due to the slight dependency of the Seebeck coefficient on the temperature. By taking an arithmetic average, which would be a suitable approximation for this case, of the calculated results the Seebeck coefficients for Ferrotec and TETECH have been determined as 0.354 mV/K and 0.308 mV/K respectively, as seen in Figure 3.4 the variations in Seebeck coefficient values are negligibly small. The measured open voltage values and maximum available power curves for both TE modules have are given in Figures 3.5 and 3.6. Furthermore the data sheets including all of the measured and calculated data can be found in Appendix A.

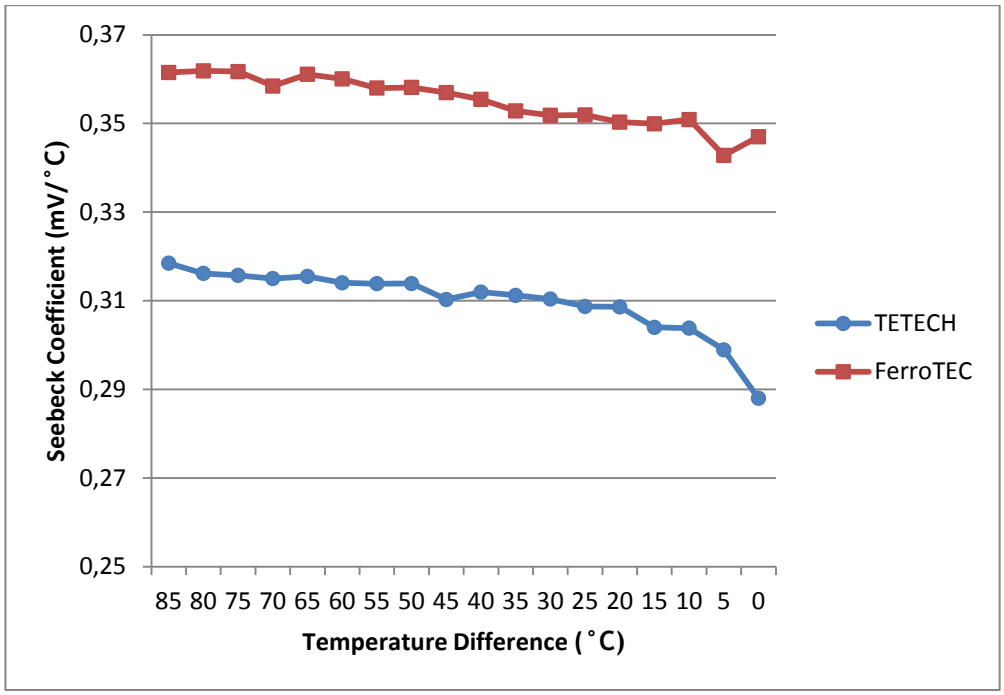

Figure 3.4 The Seebeck coefficients (mV/ °C) versus the temperature difference (Kelvin or degree Celsius) across the selected TE modules.

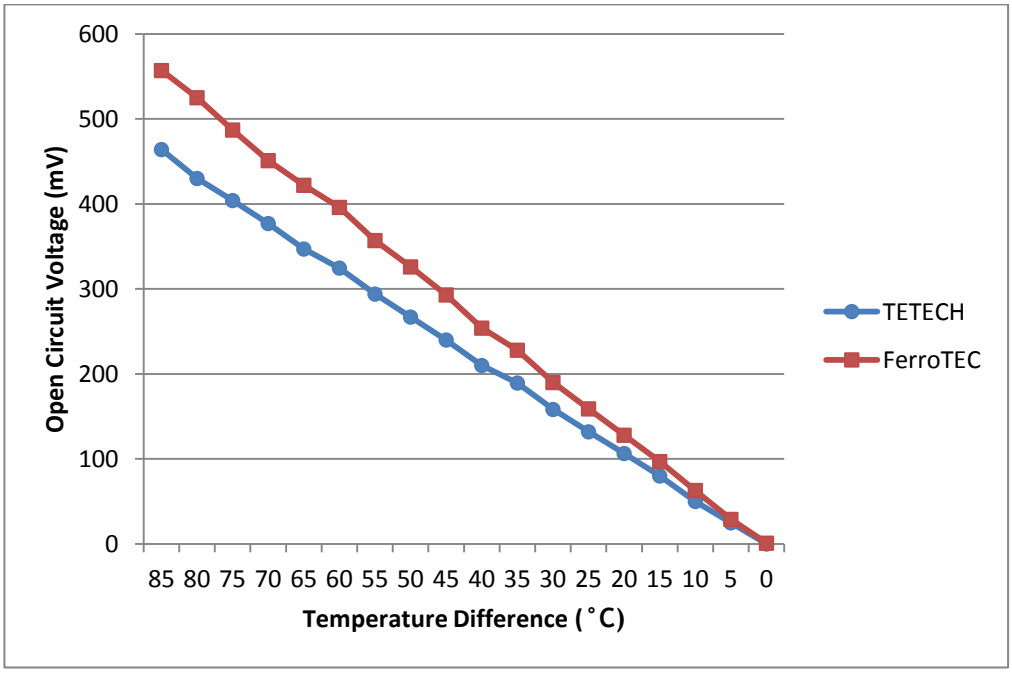

Figure 3.5 Measured open circuit voltage values (mV) versus the temperature difference (Kelvin or degree Celsius) across the selected TE modules.

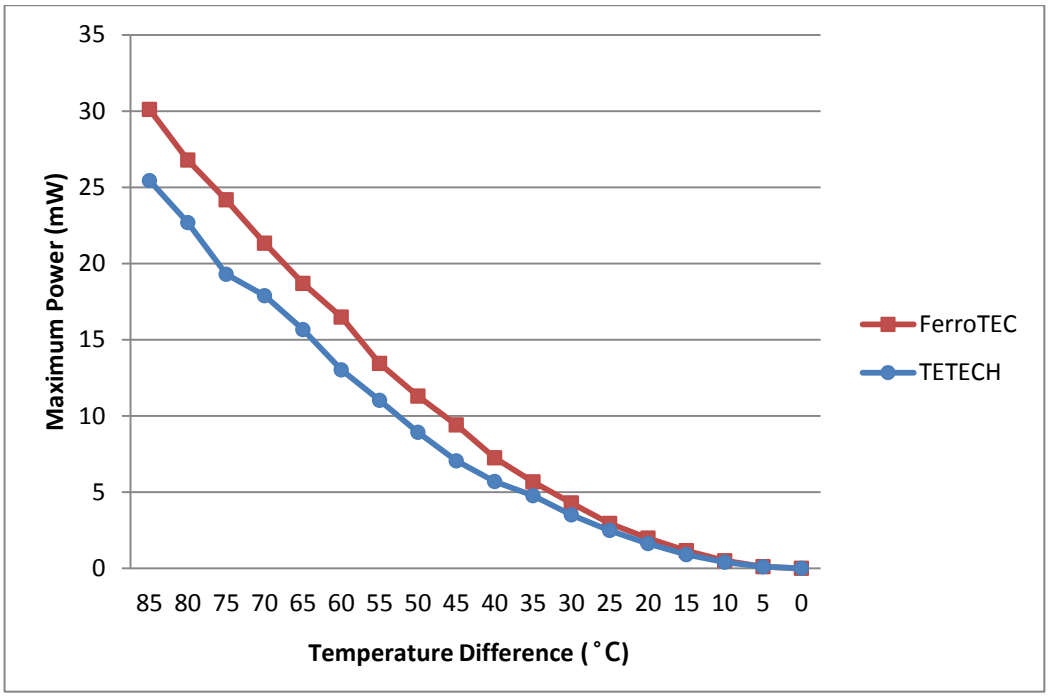

Figure 3.6 Maximum power (milli-Watt) curves versus the temperature difference (Kelvin or degree Celsius) across the selected TE modules.

CHAPTER 4

MECHANICAL AND THERMAL CHARACTERIZATION OF THE PLATFORMS

4.1 Selection and Basic Specifications of the Test Systems

By means of the recent advancements in the computer industry, the notebook usage became quite widespread nowadays. In order to respond to different demands of users, various new designs have been introduced, creating a wide variety of notebooks with different sizes and features. Today the term "notebook" does not correspond to a single object but a broad spectrum of designs, which vary in shape and mass. After consulting the project sponsor Intel, it has been decided to select one notebook from each extreme points of this spectrum to analyze in mechanical and thermal means. In this chapter the analysis and the obtained data will be presented. However, at the end of the chapter only one of the test systems will be selected for further investigation, and henceforth will be referred as the target system.

The first test system **Toshiba Portégé R705-P25** is an office type notebook that can easily be transported around due to its light weighted design. Since it has a small and thin geometry, this system can be classified as a "hot system" whose mechanical/thermal design is relatively more complicated.

The second test system **Dell Alienware M17xR2** has a large and heavy design. This notebook is accepted as a leading gaming system due to its high performance. Its large structure enables Alienware to operate in lower temperatures and it contains more reserve space for alternative thermal and mechanical applications.

The basic specifications of each system have been presented in Figure 4.1, Table 4.1, Figure 4.2 and Table 4.2.

Toshiba Portégé R705-P25:

Figure 4.1 Toshiba Portégé R705-P25 office type notebook

Table 4.1 Toshiba Portégé R705-P25 Specifications [26]

Operating System • Original Windows® 7 Home Premium 64-bit **Processor and Graphics** • Intel® Core™ i3-350M Processor o 2.26 GHz, 3MB Cache • Mobile Intel® HM55 Express Chipset • Mobile Intel® HD Graphics with dynamically allocated shared graphic memory. **Memory** • 4GB DDR3 **Storage Drive** • 500GB (5400 RPM); SATA hard disk drive • TOSHIBA Hard Drive Impact Sensor **Disk Drive** • CD/DVD **Display** • 13.3” diagonal widescreen HD TruBrite® TFT LED display at 1366x768 native resolution	**Communication** • Webcam and microphone • 10/100/1000 Ethernet • Intel® 802.11a/g/n wireless LAN **Dimensions** • Height (Front/Rear): 17-26 mm • Width: 316 mm • Depth: 227 mm • Weight: 1.4 kg **Adapter** • 65W (19V 3.42A) 100-240V/50-60Hz AC Adapter • Height: 47 mm • Width: 107 mm • Depth: 30 mm • Weight: 0.25 kg **Battery** • 6 cell/ 66Wh Lithium Ion battery pack **Input Devices** • Premium US keyboard • TouchPad™

Dell Alienware M17xR2:

Figure 4.2 Dell Alienware M17xR2 model high performance notebook

Table 4.2 Dell Alienware M17xR2 Specifications [27]

Operating System • Original Windows® 7 Home Premium 64-bit **Processor and System Chipset** • Intel® Core™ i5 M520 2.4 GHz • Mobile Intel® HM55 System Chipset **Memory** • 4GB DDR3 **Hard Drives** • Two 2.5-inch drive bays supporting SATA **Optical Drive** • SATA compliant DVD+RW **Display** • 17.0 inch, dual-CCFL, WXGA+ (1440 x 900) **Input** • US Keyboard (backlit) • TouchPad™ **Graphics Card** • ATI Mobility Radeon HD 5870 model graphics card	**Communications** • WLAN Mini-Card (half Mini-Card slot) • WPAN, Bluetooth card (full Mini-Card slot) **Dimensions** • Height (Front to Back): 51.31-53.59 mm • Width: 405.89 mm • Depth: 321.31 mm • Weight: 5.3 kg **AC Adapter** • Type: 240 W/150 W • Output current: 12.31 A (240 W) 7.7 A (150 W) **Battery** • 9-cell "smart" lithium ion (86 W/s) • Height: 41.40 mm • Width: 292.61 mm • Depth: 52.32 mm • Weight: 0.52 kg

4.2 Characterization of the First Test System: Toshiba Portégé R705-P25

In the analysis of Toshiba system the first step taken was creating a mechanical mapping. Once the chassis of the test system has been opened, the dimensional measurements for the major components have been completed in order to create the schematics in Figures 4.3 and 4.4. These schematics bear an important role in the determination of the thermal measurement points inside and outside of the chassis. These measurement points have been shown in Figure 4.4 in detail.

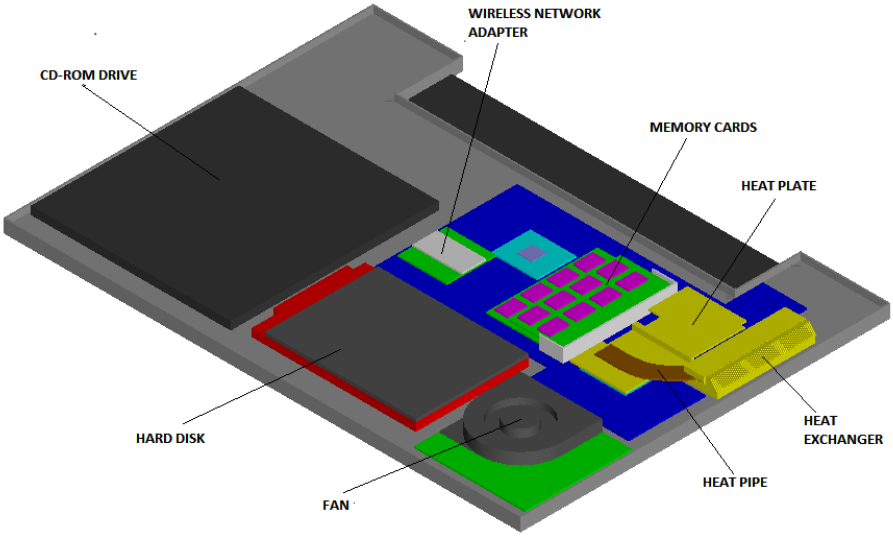

Figure 4.3 Toshiba internal schematics

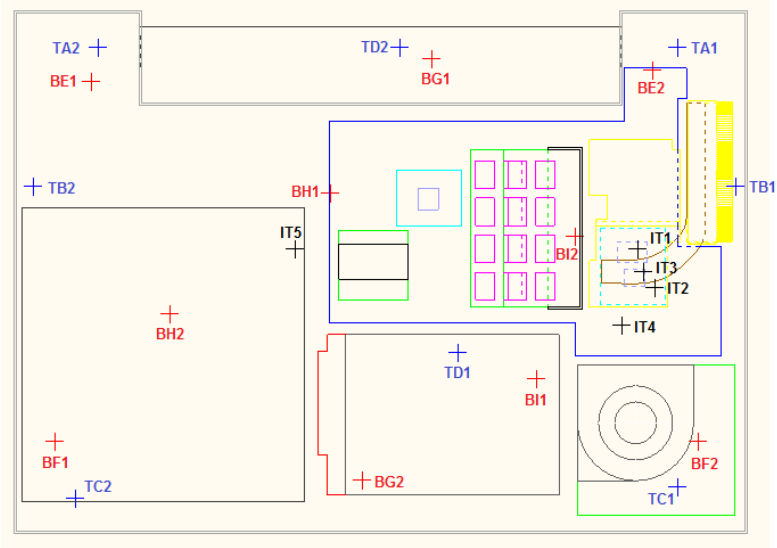

*Figure 4.4 Toshiba temperature measurements (Prefix **T** stands for top layer, prefix **B** stands for bottom layer and prefix **I** stands for internal layers)*

After the completion of the mechanical mapping, the thermal phase of the characterization has been initiated. The thermal measurements were taken by using thermocouples and software controlled sensors while the system was operational. The **Thermal Analysis Tools (TAT)** software has been utilized during the measurements. TAT is a software developed by Intel in order to operate the CPU of the computers under a variety of workloads. In this project, the measurements were taken when TAT was running under 80% and 100%workloads.

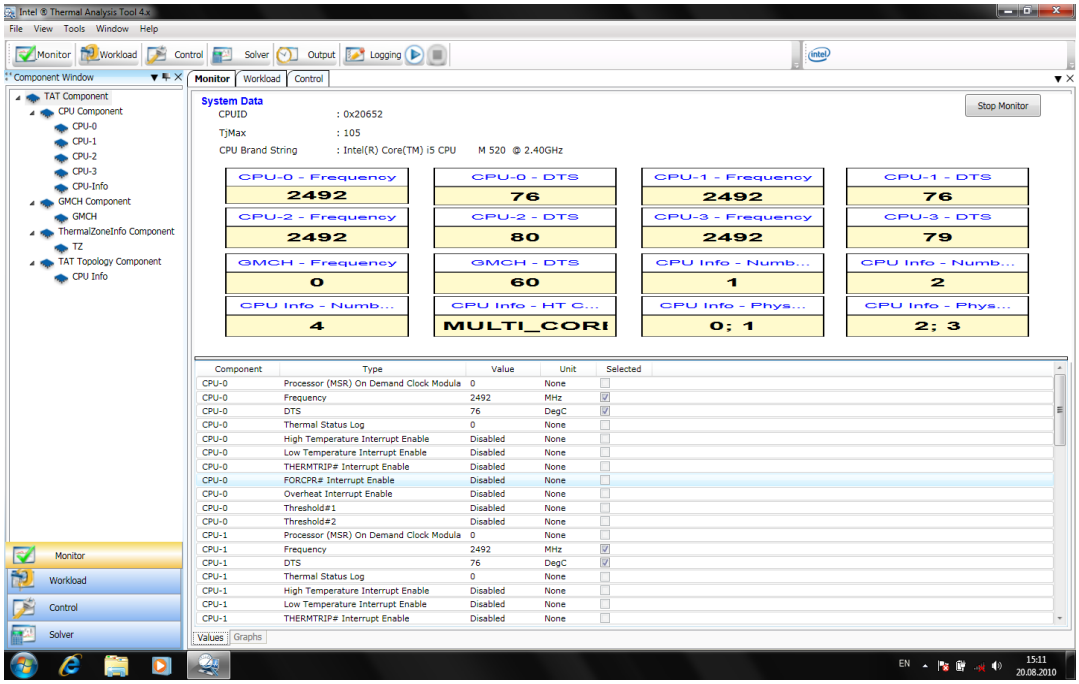

Figure 4.5 Thermal Analysis Tools (TAT) Screenshot

At the first step 18 different measurement points have been selected from the upper and lower layers of the chassis. These measurements were taken in pairs therefore they have been named with a character and a number (A1 and A2, etc.). The photos taken from both of the layers can be seen in Figures 4.6 and 4.7. The characters between A and D indicate to the points taken from the upper layer while the characters between E and I represent the lower measurement points. Data collected from some of the selected points are given in Figures 4.8 and 4.9. For the graphics including full data please see Appendix B.

Figure 4.6 Toshiba external measurement points (top layer)

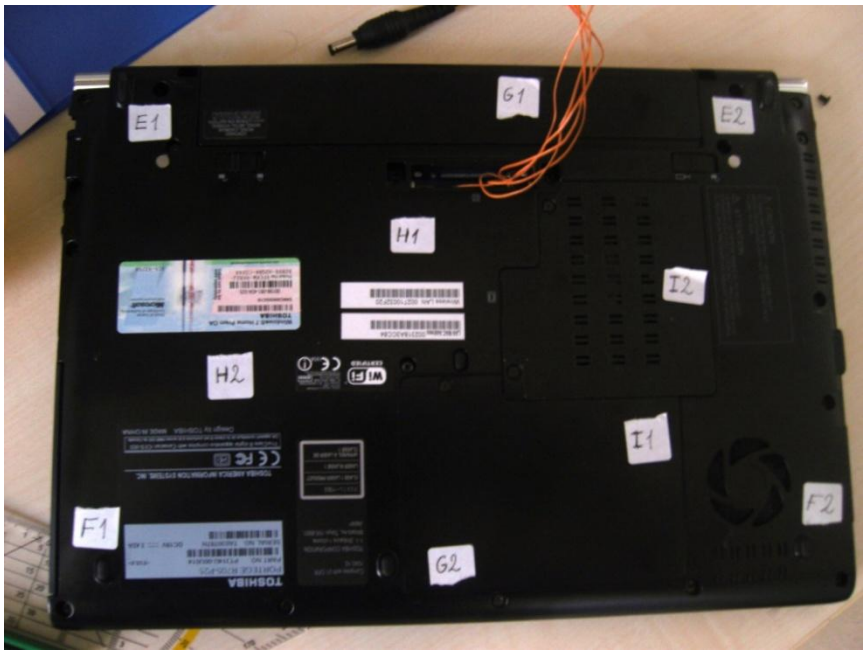

Figure 4.7 Toshiba external measurement points (bottom layer)

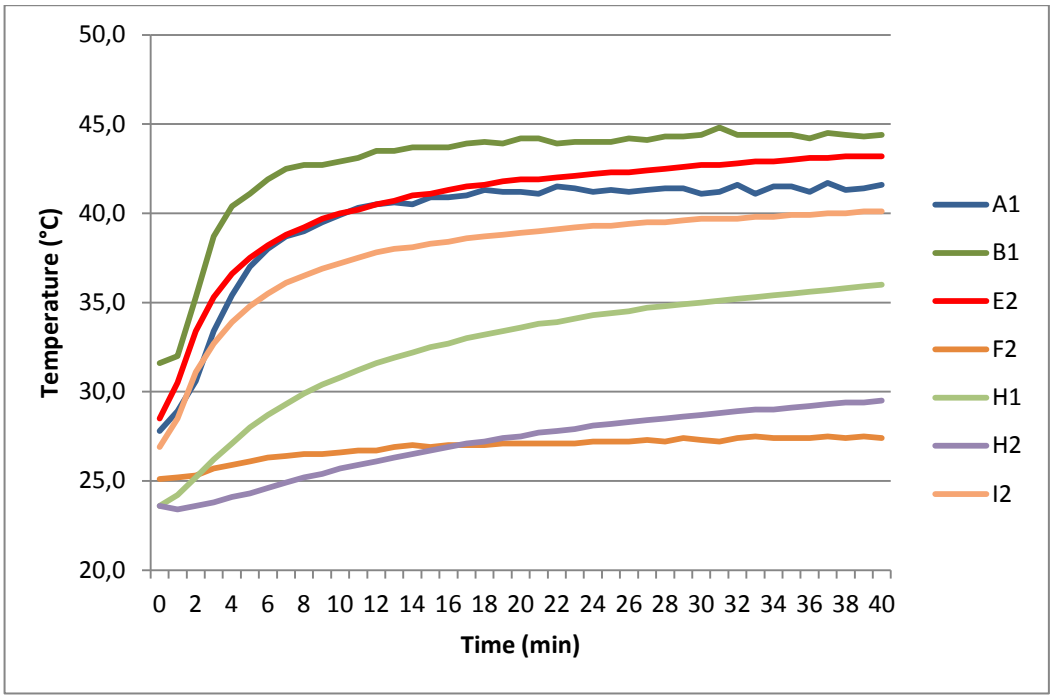

Figure 4.8 Selected measurement data from the chassis of Toshiba (under 80% workload)

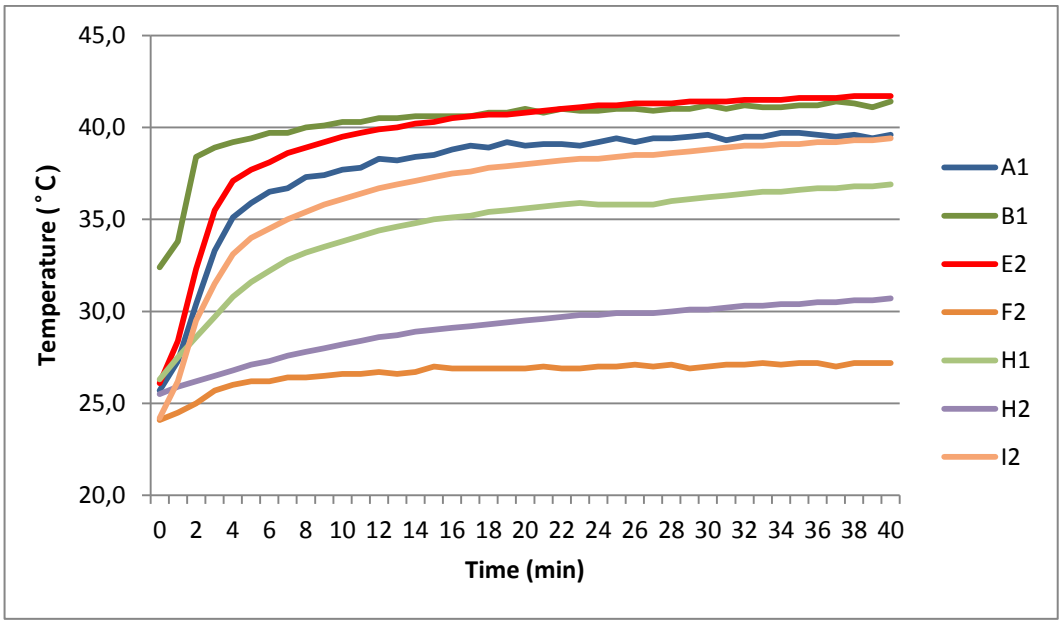

Figure 4.9 Selected measurement data from the chassis of Toshiba (under 100% workload)

The charts in Figures 4.8 and 4.9 show two important results:

- The temperature distribution on different parts of the chassis varies between the ambient temperature ($\approx 25^{\circ}C$)and $45^{\circ}C$ while the system is operational.
- The system obtains larger temperature values while operating under 80% workload. This result is an outcome of the fan efficiency. It has been observed that the fan of the notebook runs faster under 100% workload, thus creating a stronger air flow to cool down the system.

Based upon these results the internal temperature measurements were taken only for 80% workload. For the internal measurements of Toshiba, 5 different points are selected. These points are located on:

1. Heat plate (rear)
2. Heat plate (front)
3. Heat pipe
4. Motherboard
5. A random place on the metallic surface under keyboard (for reference)

The selected surfaces were attached with Omega T-type thermocouples (Figure 4.10).

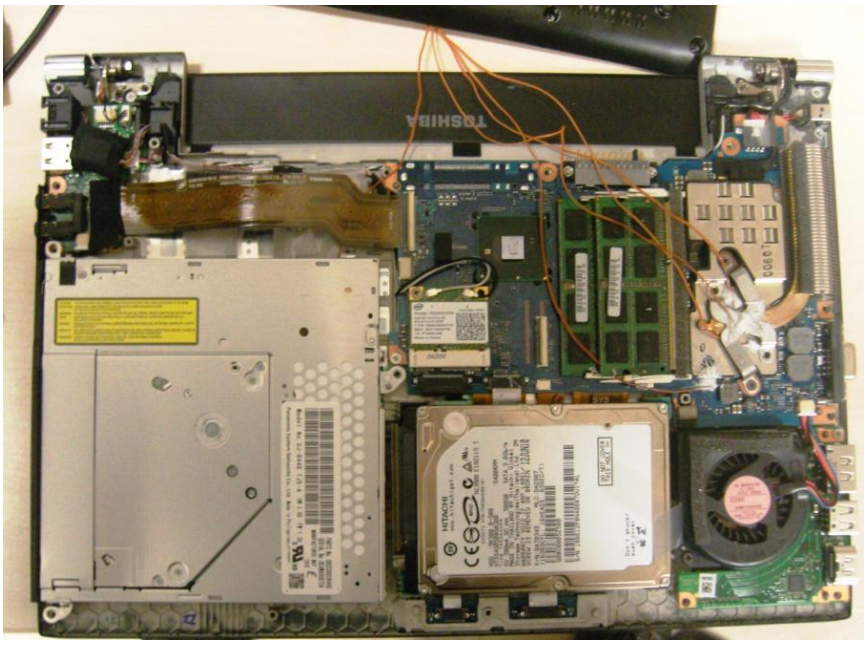

Figure 4.10 Toshiba internal photo (with thermocouples connected)

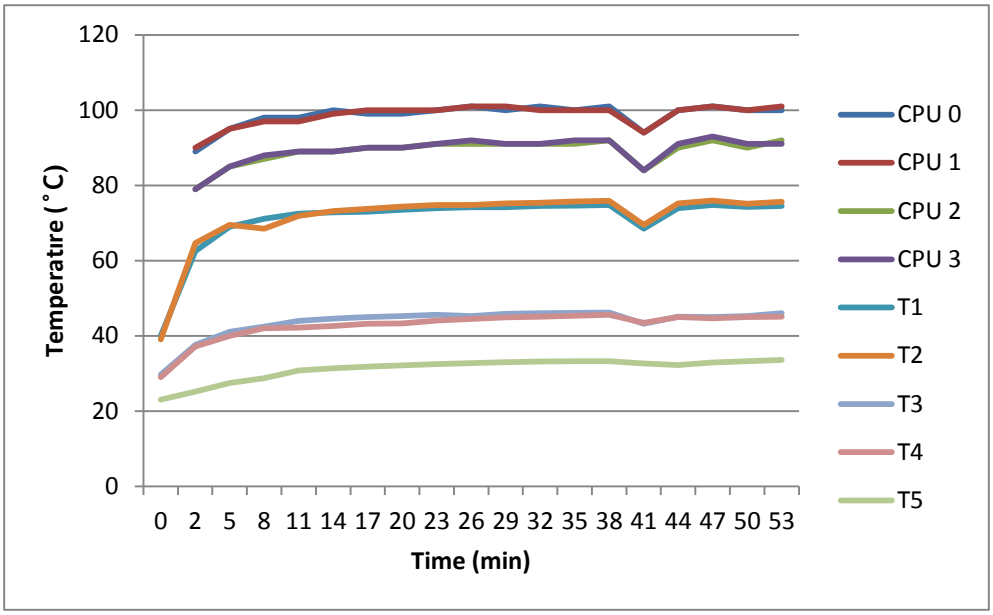

Figure 4.11 Toshiba internal data (T1-T5) and data acquired from TAT with 80% workload.

The internal data collected from Toshiba notebook has been presented in Figure 4.11. Here, the thermocouples connected to the selected points have been named after the thermocouple type and their number (T1 – T5). As mentioned in Section 4.1, this notebook has a dual core CPU and each core consists of 2 different threads. While operating TAT software, the user can get data from each thread separately. By combining both of these sources the internal temperature distribution of the Toshiba has been acquired. During these measurements the ambient temperature inside the laboratory was around 25˚C. The fifth measurement point can be taken as a reference point for the internal ambient temperature as well. A general table combining both the internal and the external measurements can be found in Appendix B.

At the last step of the characterization process, a quantitative methodology for power analysis has been developed in order to attain a firsthand insight into the energy conversion opportunities in the system. After mapping the mechanical and thermal characteristics of the system, possible locations with medium to high temperature differences have been selected in order to convert the temperature difference into electrical power by using the Seebeck effect. The heat dissipation paths in these locations were picked to represent shunt paths for cooling and not the mainstream cooling paths.

This method has been followed on purpose to avoid significant performance impact. The maximum power generation potential has been calculated by using the maximum power curve for both of the TE modules, which were presented in Figure 3.4. During these calculations, it has been assumed that the temperature differences between the selected points are constant and available for the geometrical space between the points. Also instead of placing a standard TE module, which has surface dimensions of 6.3 mm x 6.3 mm for TETECH and 6.05 mm x 6.05 mm for FerroTEC, the whole area given for each location was assumed to be filled with TE couples. In the end the results were summed up and a power discount of 50% has been applied to the end result in order to represent possible power losses.

As it can be seen from Table 4.3, the major elements affecting the power acquisition are the temperature difference and the surface area of the TE materials. Among the selected regions the maximum power can be harvested from region 4 where both of these elements are significantly high. This table will be used as a representation for the ideal case scenario of the first test system.

Table 4.3 Energy scavenging opportunities using FerroTEC and TETECH modules in different locations of Toshiba test system

Region	Description of vertical heat path	ΔT	x (mm)	y (mm)	z (mm)	Ferro P_{max} (mW)	TETECH P_{max} (mW)
1	From top of heat spreader (IT2) to metal each above it (IT3)	29	5	7	3	3.96	2.91
2	Metal attach above heat spreader (IT3) to bottom surface (BI2)	6	29	22	4	2.63	2.53
3	Main PCB card (IT4) to top surface (TD1)	11	50	12	8	9.85	7.55
4	Main PCB card (IT4) to bottom surface (BI2)	13	38	20	7	17.94	13.32
5	Bottom metal cage (IT5) to bottom surface (BH1)	5	8	8	9	0.19	0.16
				Sum		34.57	26.46
				50% Power Electronics Discount		**17.28**	**13.23**

4.3 Characterization of the Second Test System: Dell Alienware M17xR2

In this section the second test system, Alienware, is examined. There are some major differences between Alienware and Toshiba and some of these differences will also be reflected to the experimentation procedure. First of all Alienware has a much bigger geometry in comparison to Toshiba and has very good thermal insulation on its outer chassis, which renders the external temperature measurements unimportant. Therefore the experimental procedure of AW will directly start with interior mechanical mapping.

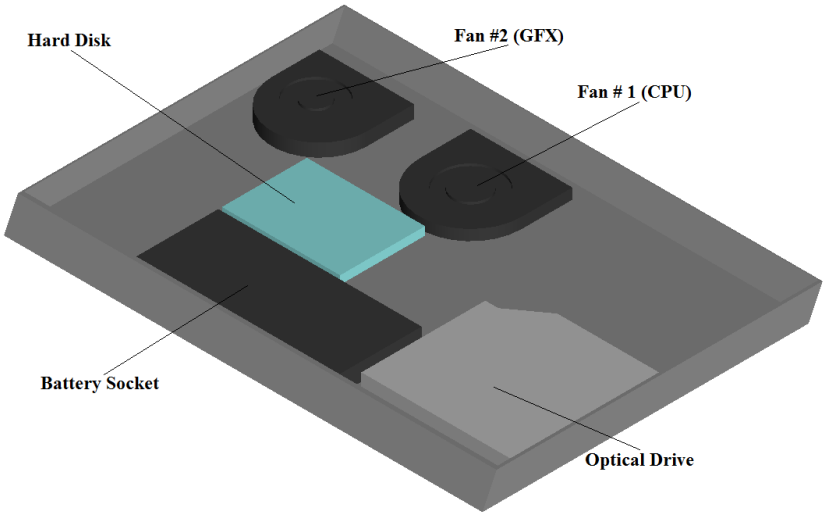

Figure 4.12. Alienware mechanical schematics (first layer)

Alienware's design is more advanced and complicated compared to Toshiba. Therefore its schematics will be given in two layers. Figure 4.12 shows the first layer of the system. This layer focuses on the chassis in general. The fans, optical drive and hard disk drive have been shown on this drawing. The grilles and small objects are neglected for the sake of simplicity. Most of these hardware parts cannot be seen in the second layer due to the printed circuit boards (PCB) placed upon them. Figures 4.13 and 4.14 show the second layer which focuses on the integrated cards and their cooling systems. The eight points marked on the drawing refer to the inner temperature measurement points.

A thermal shield has been placed upon the second layer in order to create thermal insulation between the second layer and the keyboard. This "third layer" (Figure 4.15) has not been added to the model and the schematics because it was constructed from an insulating material and thus reduces the temperature difference between the inner and the outer parts of the computer.

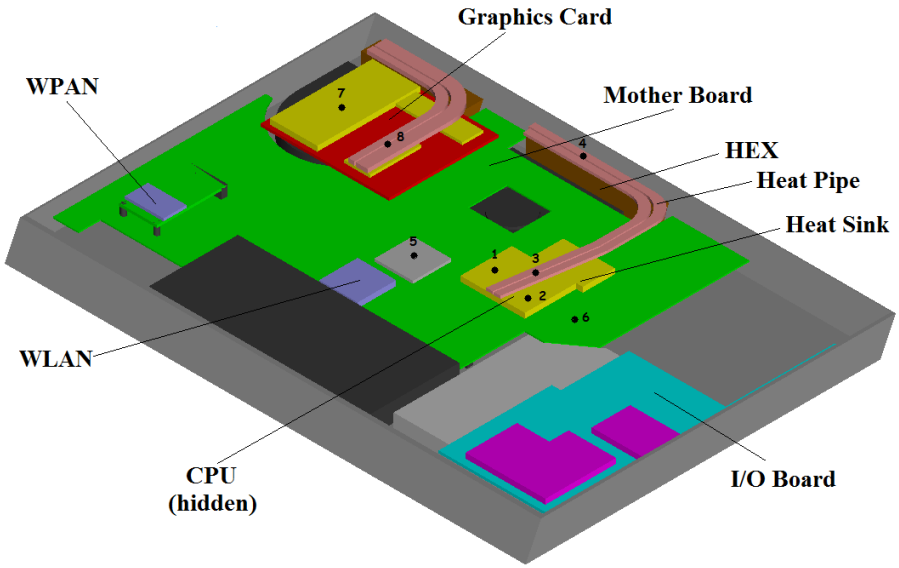

Figure 4.13 Alienware mechanical schematics (second layer) and the thermal measurement points

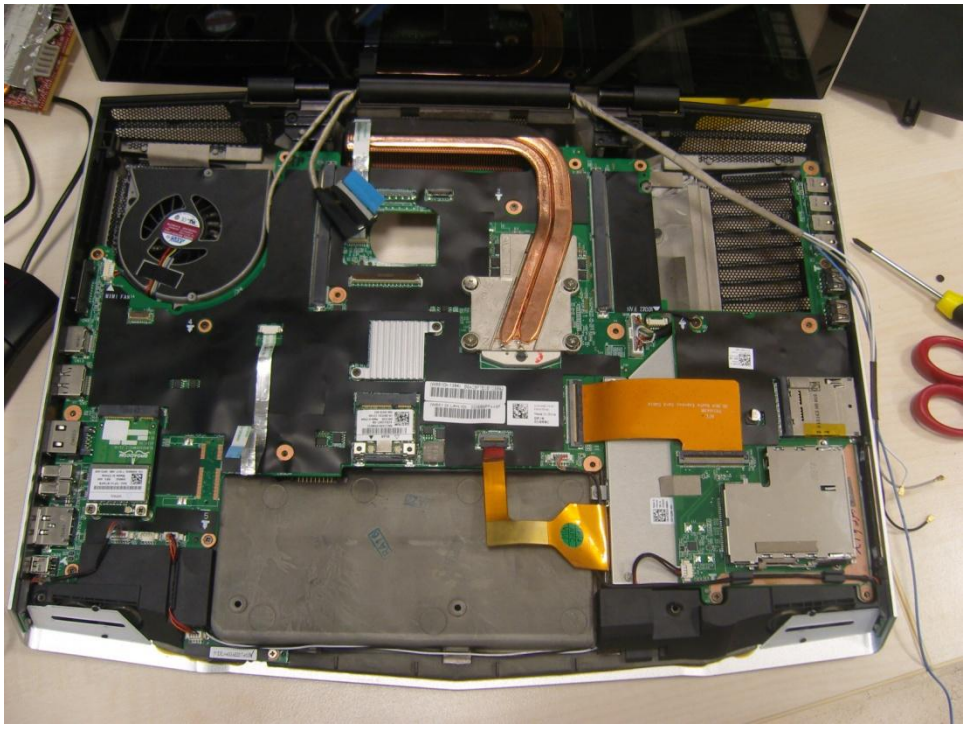

Figure 4.14 Alienware, photo of the second layer (graphics card removed)

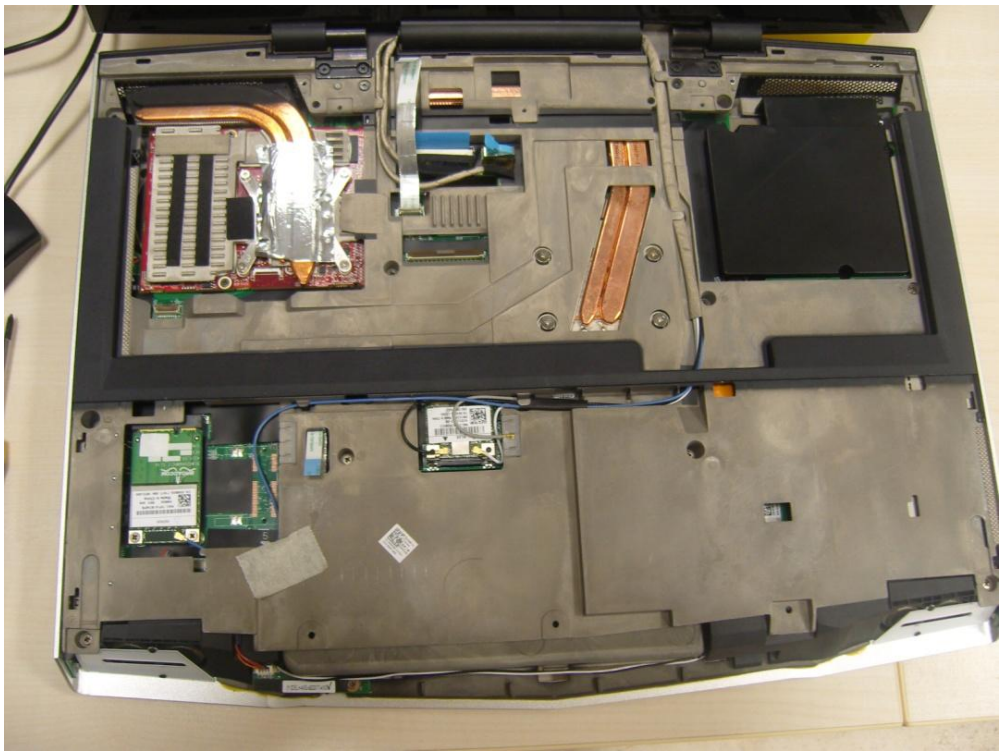

Figure 4.15 Alienware third layer (with the thermal shield)

Once the mechanical mapping has been prepared, the thermal characterization of the test system has begun. The first step of the thermal characterization was determining the hot spots to focus on. For this purpose a thermal camera has been used to take thermal pictures of the system while it was operating and its keyboard and thermal shield was removed.

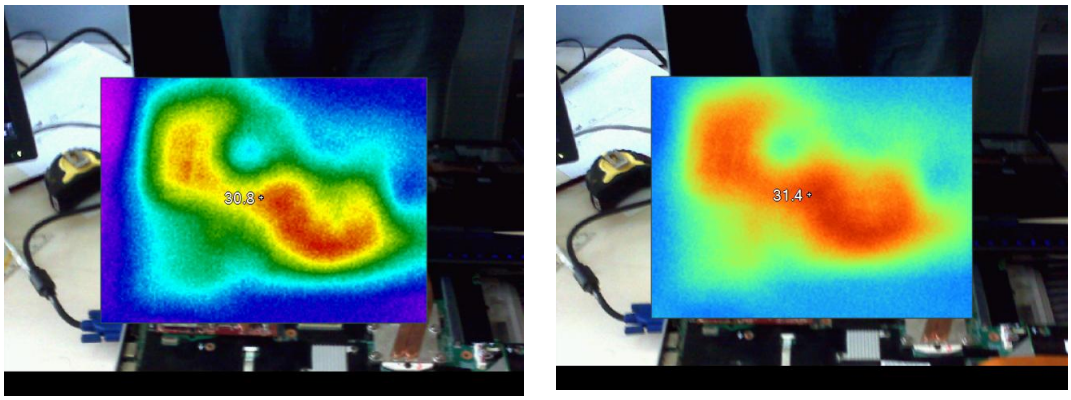

(a) *(b)*

Figure 4.16 Alienware thermal photos ((a) with high contrast, (b) with normal contrast)

Due to the absence of the aforementioned elements the system became an open system which is affected by the air circulation within the laboratory room as well. The absolute temperature values cannot be utilized from this exercise since this operation is performed while the upper layer of the computer is open. Hence the overall system is cooler than what would be expected in a closed system. However the acquired images provide a clear view of the relative thermal dissipation. The details of the thermal map dissipation are apparent in Figures 4.16 and 4.17.

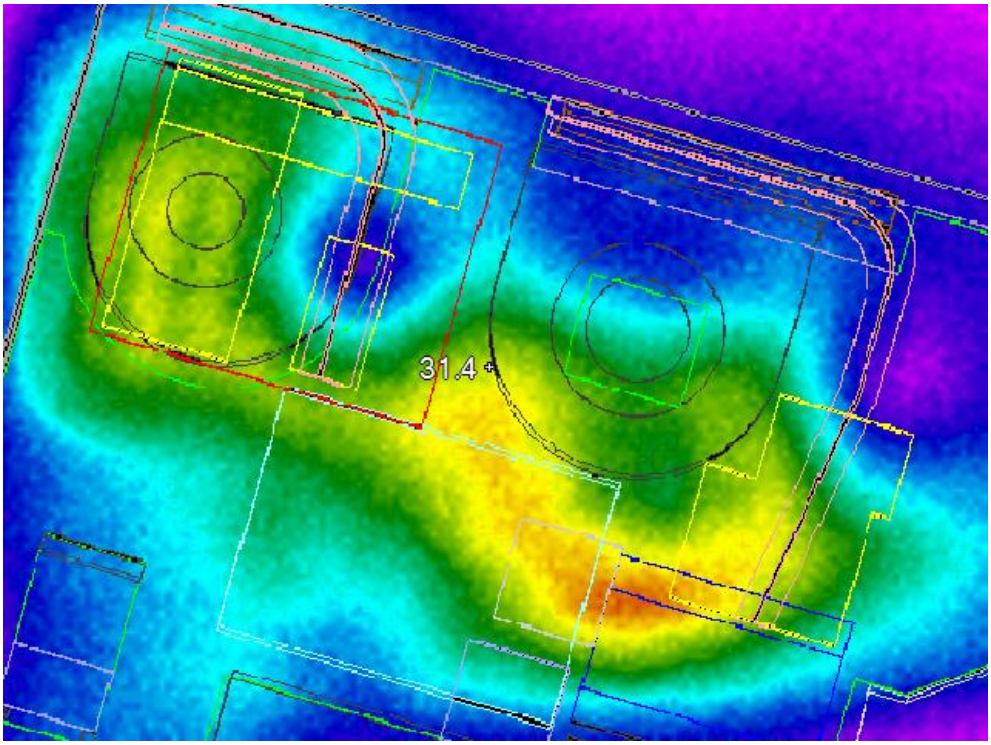

Figure 4.17 Thermal photo overlaid on the mechanical map

As it can clearly be seen from Figure 4.17 the heat dissipation originates from a certain area of the laptop including the areas around the CPU and graphics card which are the main heat sources in this system. Additionally a certain rise in the temperature of a heat exchanger has also been observed (point 5 in Figure 4.12). In the guidance of these thermal images 8 temperature measurement points have been selected to collect data under different scenarios. The data acquisition process has been achieved by attaching thermocouples to the selected points and connecting them to a *Omega OM-SQ2040 Portable data logger* through the grilles at the back of the notebook system. These selected internal points (Figure 4.12) are as follows:

1. Heatsink on CPU (left side)
2. Heatsink on CPU (right side)
3. Heatpipe hot side (on CPU)
4. Heatpipe cold side (on heat exchanger)
5. Other heat exchanger on the motherboard
6. A random reference point on surface of the motherboard
7. Heatsink on GFX
8. Heatpipe on GFX

Similarly thermocouples have been attached to the selected locations around the keyboard and at the bottom of the notebook for thermal characterization of the chassis. Ambient temperature has been also been monitored through another thermocouple (Figure 4.18).

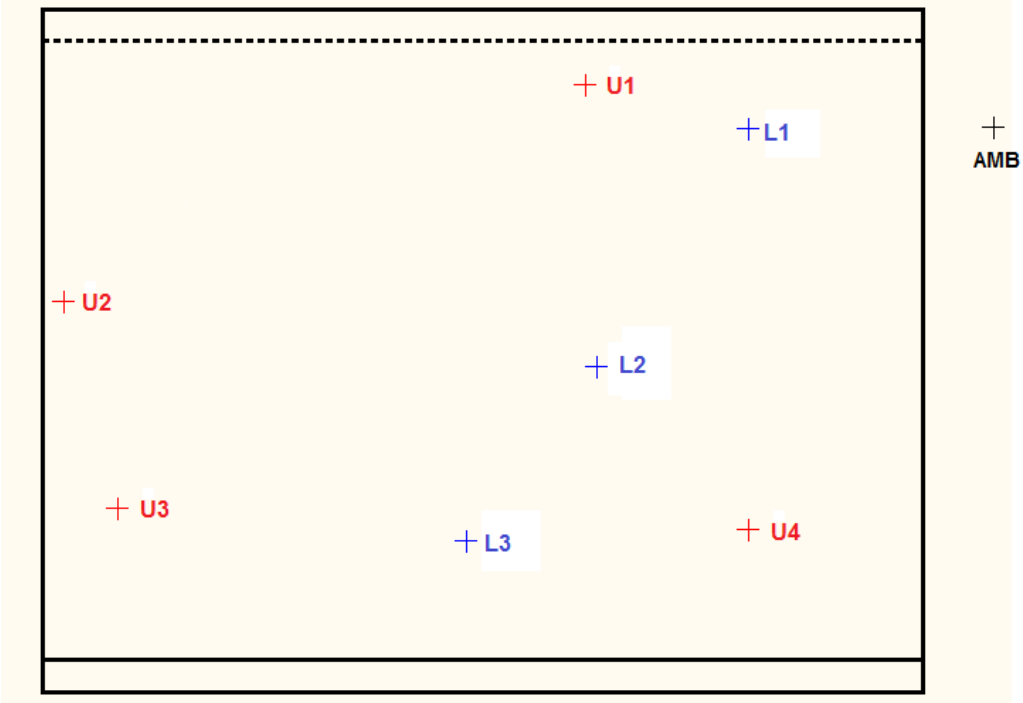

Figure 4.18 Measurement points on the notebook chassis – 'L' denotes bottom surface or points under the box, 'U' denotes top surface or points around the keyboard.

Intel-developed software *TAT* and the freeware *GPU-Z* has been used to collect the temperature data from GFX and CPU. By adjusting the workloads of the CPU threads, the test system was characterized using 80% and 100% activity to represent different conditions. The workloads provided by the demo version of *3D Mark Vantage* have been

operated to exercise graphics during the experimentation which consists of two independent animations:

1. **Jane Nash** (lasts 1:40 min) is an animation focusing on the details of the large objects. The number of the objects is relatively low while their geometries are bigger and more detailed.
2. **New Calico** (lasts 2:40 min) has a lot of small objects. The detail of the objects are lower than the previous animation, however the number of independent objects are rather high.

Including their loading screens, one animation cycle lasts between 8-9 minutes. Sample results of the thermal characterization experiments are summarized in Figures 4.19 and 4.20. The detailed versions of these graphs and their data tables can be found in Appendix C.

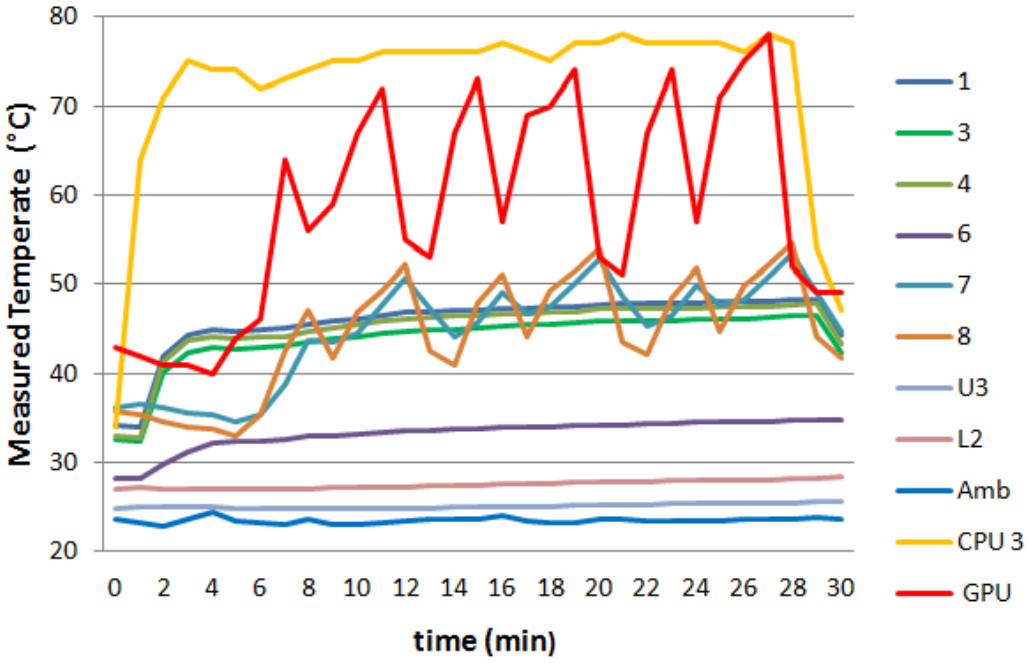

Figure 4.19 Temperature measurements of the selected points inside the test system while operating with 80% CPU workload.

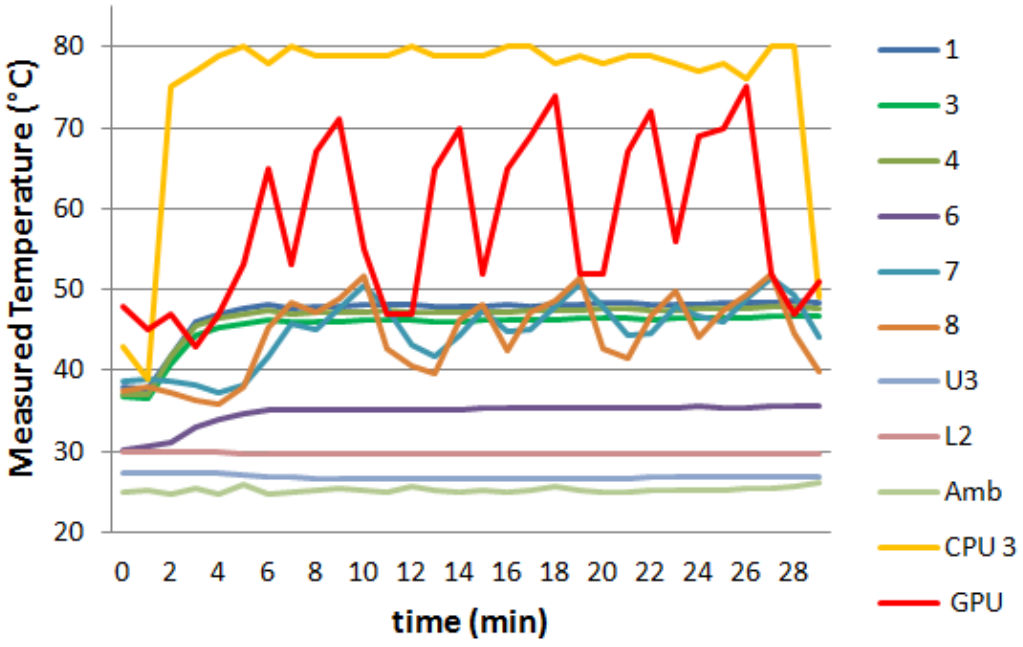

Figure 4.20 Temperature measurements of the selected points inside the test system while operating with 100% CPU workload.

The double-peaks measured at GFX and its cooling system (points 7 and 8) indicate the three time periods when the animation cycles are running. The observations from thermal characterization data can be summarized as follows:

- CPU and GFX temperatures are effectively independent of each other in this particular notebook system, allowing independent TE placement optimizations around each of the two main heat sources.
- Although there is a minor difference between the upper and the lower surfaces of the chassis, their temperatures remain almost constant during the runs.
- Monitored points around the CPU are a couple of degrees Celsius' higher with 100% workload, but in general CPU temperature does not significantly increase when the activity is increased from 80% (Figure 4.19) to 100% (Figure 4.20). This is due to the fact that the notebook has control mechanisms to ensure thermal design power, which is close to 80% workload, is not exceeded. For example, the speed of the fan dedicated to cooling the CPU is increased with the workload. 80% CPU activity can be used as a more realistic worst case usage scenario that represents the thermal design power scenario.

- The maximum operating condition for the CPU is specified as 105˚C [28] in the datasheet. Yet the temperature is regulated to stay under 82˚C in this notebook. This approach potentially leaves headroom in the platform for TE integration closer to CPU. This additional temperature margin will not be utilized in this thesis, since its main approach is addressing the tougher case of a thermally limited system.

Based upon the mechanical and thermal characterizations of the system, a quantitative analysis has been made in order to derive a theoretical best case TE generation potential, assuming mainly the surroundings of the main hot spots are utilized and instead of the standard geometry of the TE materials, custom designs are used to fill all of the geometrical gaps. An electrical conversion (power electronics) loss about 50% was conservatively assumed based on previous studies. The results of the analysis are provided in Table 4.4.

Table 4.4 Energy scavenging opportunities using FerroTEC and TETECH module in different locations of Alienware test system

Region	**Description of vertical heat path**	**ΔT**	**x (mm)**	**y (mm)**	**FerroTEC P_{max} (mW)**	**TETECH P_{max} (mW)**
1	Motherboard (6) and upper chassis (U2)	4	110	102	26.30	16.96
2	Motherboard (6) and upper chassis (U4)	9	7	116	9.24	6.26
3	Heat spreader (4) and upper chassis (U2)	16	207	10	74.74	52.68
4	Heat spreader on CPU (4) and upper chassis (U2)	21	27	118	189.16	142.08
			Sum		299.44	217.98
	50% Power Electronics Efficiency				**149.72**	**108.99**

Like Table 4.3, this table has also been prepared under the assumption that the selected temperature points represent homogenous heat dissipation in their vicinities. Under this circumstance and the absence of any physical obstacles, filling the selected regions with the TE materials would have provided us with the shown wattage values, which represent the ideal case scenario for the second test system.

4.4 Selection of the Target System

In this chapter both of the test systems have been analyzed on thermal, mechanical and power production basis. Although the thermal conditions of Toshiba system seem better at the first glance, Alienware has a much larger chassis enabling a larger amount of TE integration possibilities, which affects the quantitative power production model as well. By comparing Tables 4.3 and 4.4, it can be clearly seen that Alienware is much more advantageous in the power production branch. Since it is not classified as a hot system, the danger of overheating or heat related performance losses are also more difficult to occur in comparison to the Toshiba system. In conclusion Dell Alienware M17xR2 has been selected as the target system of this thesis. For a more detailed study, computer simulations of its major parts and the whole system will be made in the following chapters.

4.5 Effects of the TE Module Integration on the Carbon Footprints

A small model may be helpful to estimate the environmental effects of the TE module integration on the notebook computers. Based upon the results shown in Table 4.4, it may be assumed that a TE integrated notebook computer would require 0.15 Whr less energy per hour. (The size variations among different notebook computer models have been neglected.) The researches show that there were around 1.2 billion mobile computers in the world in 2008 [29]. It is estimated that the number will be 2 billion by around 2015. If all of these computers would have TE modules integrated inside them, providing an energy of 0.15 Whr in each, this would decrease the hourly energy need by an amount of:

$$\Delta E = (0.15 Whr)(2 \times 10^9) = 0.3\ GWhr \tag{13}$$

In a thermic power plant around 250 g of oil needs to be consumed to produce 1 kWhr electricity [30].

$$\begin{aligned} Fuel\ Consumption &= (0.3 \times 10^6\ kWhr)(250 \times 10^{-6}\ t\ oil\ per\ kWhr) \\ &= 75\ t\ of\ oil \end{aligned} \tag{14}$$

It follows that global TE integration in computers would create a decrease of 75 tons of oil consumption per hour by year 2015. This would correspond to a yearly drop of 657,000 tons in the oil consumption. In order to calculate the carbon footprint of this amount, the stoichiometric equation of the fuel burning must be taken into consideration:

$$4C_2H_3 + 11O_2 \rightarrow 8CO_2 + 6H_2O \quad (15)$$

Equation (15) indicates that 108 g fuel exhausts 352 g CO_2 while burning.

$$(657{,}000\ t)\frac{352}{108} = 2{,}141{,}333\ t \quad (16)$$

This simple model presents that globalizing the TE module integration would cause a drop of nearly 2 million tons of annual CO_2 dissipation by year 2015. The model ignores the CO_2 emissions during the manufacturing and distribution or transportation of the TE modules. It also ignores the transmission, distribution, and conversion electricity losses from the thermic power station to the computer load. On the other hand, the result is sufficient to demonstrate that every mW saving counts when it comes to one of the fastest growing industries.

CHAPTER 5

TARGET SYSTEM MODELING

The characterization processes of the target system and the TE modules have been completed in the previous chapters. This chapter focuses on the phases of the computer simulation process of the target system. In Chapter 4, it has been noted that Alienware has two major heat sources: CPU and GFX. Since CPU, its surroundings and its cooling solution can be considered independently from GFX, its surroundings and cooling solution in the target notebook system, the initial model has only been constructed for the CPU subsystem shown in Figure 5.1. The thermal and mechanical data were used to create a consistent model for CPU [27].

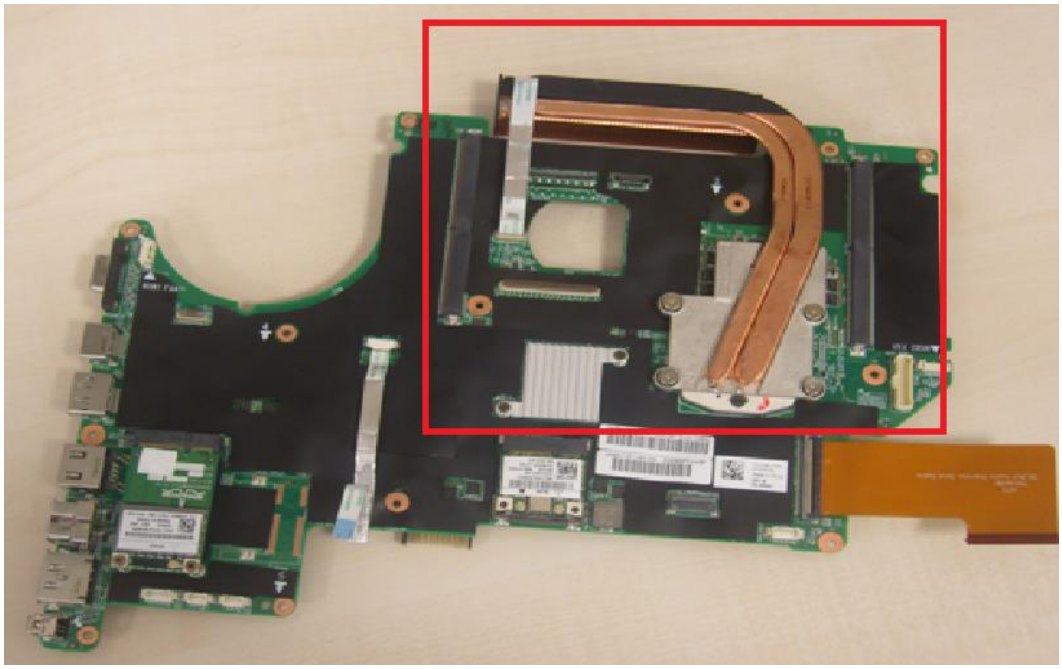

Figure 5.1 Motherboard of the target system (CPU and its cooling system is shown inside the red box)

For the simulation of the target system *ANSYS Icepak 13.0.2* has been utilized. ICEPAK is a specific software designed for thermal and fluid applications of the electronic components. Icepak uses the engine of *FLUENT* (a CFD software developed by the same company for general purpose) to compute the flow rate and heat transfer calculations and has a vast library for electronic and hardware parts in its database. These features were the main reasons for this tool choice.

The operation principle of Icepak is relatively simple. It is based upon creating bodies of different sizes and assigning them the necessary material properties either from the database or manually. The mechanical characterization of the system was completed beforehand. The data acquired from the mechanical model was useful in the geometrical part of the simulation. For the material parts, however, a more detailed resource was necessary. Research on commercial parts, and communication with experienced mentors from Intel helped to determine the material properties.

The heat source was assigned to be 35 W inside the CPU Die according to the specs [28]. The ambient temperature inside the laboratory varied between 22-27° Celsius throughout the year. Since the notebook is a closed system, the ambient temperature inside its chassis was expected to be a little higher. As it can be seen from the readings of the 6th measurement point, this temperature was around 30°C.

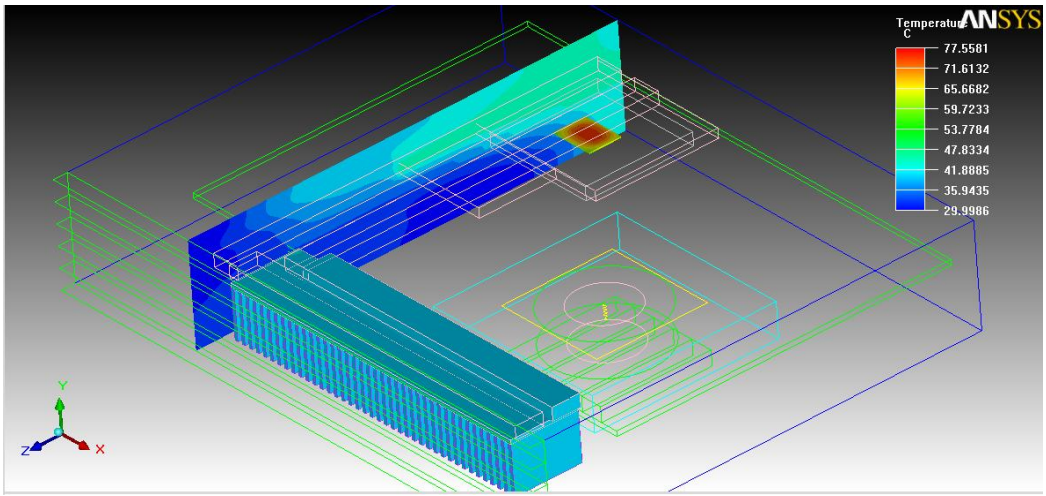

Figure 5.2 A screenshot representing the results of the CPU simulation

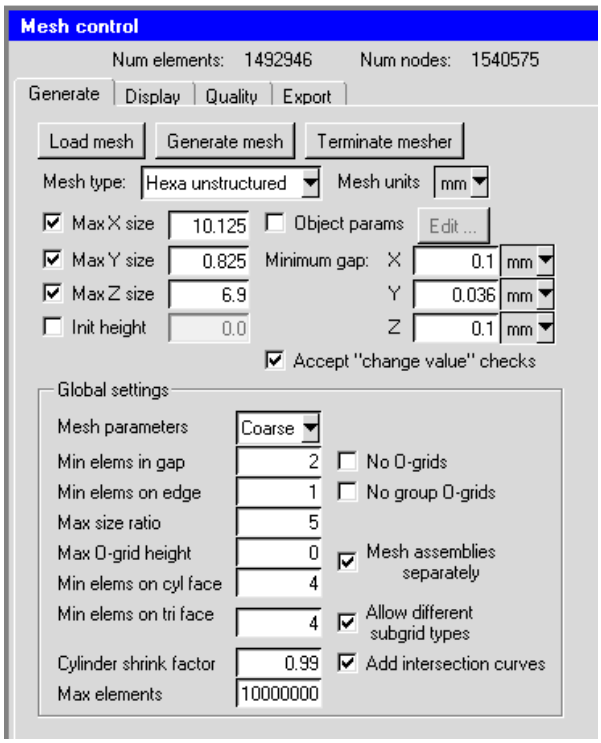

Figure 5.3 Utilized mesh control settings of Icepak

Once the simulation is completed, Icepak presents a solution overview file with numerical results. It is also possible to have a visual presentation of results for temperature distribution in a contour map or for the air flow in a colored vector field. Such a presentation of temperature distribution is depicted in Figure 5.2. In this simulation all of the heat transfer modes (conduction, convection and radiation) were enabled, while the ambient temperature was set to 30˚C. The details of the meshing settings can be seen in Figure 5.3.

Table 5.1 Measured and simulated values for CPU simulation

	Measured		***Simulated (Max. Temp.)***
Microprocessor	*CPU-0*	*72 °C*	*79.0 °C*
	CPU-1	*71 °C*	
	CPU-2	*79 °C*	
	CPU-3	*79 °C*	
Heat Sink	*1*	*48.3 °C*	*49.2 – 51.9°C*
	2	*48.3 °C*	
Heat Pipes and HEX	*3*	*46.4 °C*	*49.7 °C*
	4	*47.6 °C*	*48.7 °C*
PCB	*6*	*35.5 °C*	*31.5 °C*

Also a small comparison between the numerical values and the measurements is provided in Table 5.1. As shown in the table, the initial results are very close to the measured values and the minor differences are within the limits of tolerance. Henceforth the first version of the simulation was accepted to be successful. This simulation and its values will be utilized in the next chapter for the selection of a plausible location for the TE module.

Although this version of the simulation was successful, it only covers geometrically 1/6 of the whole system and excludes a secondary thermal source, the GFX area, which has a certain (small) degree of thermal interdependency with CPU. Since the aim of this thesis was to create a model for the whole system the simulation was upgraded several times. The most important step was creating the simulation of the GFX area and merging it with the CPU simulation.

Figure 5.4 ATI Mobility Radeon HD 5870 model graphics card

The first problem about the simulation of the GFX was determining the wattage of the graphics card. Generally the graphics cards would be motherboard integrated in the notebooks and carry a small about of wattage. However Alienware is a specifically gamer oriented notebook. Therefore it has an independent ATI Mobility Radeon HD 5870 model graphics card with a separate cooling solution including a fan, a heatsink, a couple of heatpipes and two separate heat exchangers as seen in Figure 5.4.

It is difficult to say the exact wattage of this graphics card; however it has been stated in a semi-official source to be around 50 W [31]. There is another important point which has a mild impact on the results. As stated in the previous chapters the measurement period for the GFX is based upon the demo version of 3D Mark Vantage. Unlike its counterpart in CPU measurements, 3D Mark only remains operational for a short amount of time and keeps repeating the same cycle. Thus the graphics card of the system can reach neither its maximum condition, nor steady state as shown in Figures 4.19 and 4.20. Unfortunately the power sources in Icepak cannot be adjusted to be time dependent. A power source can be either constant or temperature dependent. Since the power measurements of GFX are out of the scope of this thesis, the first option has been selected, fixing the power of GFX at 50 W. Therefore the results involving the measurement points on the graphics card would be higher than the collected data, representing a semi-realistic scenario where the GFX reaches its maximum value and remains at a steady state.

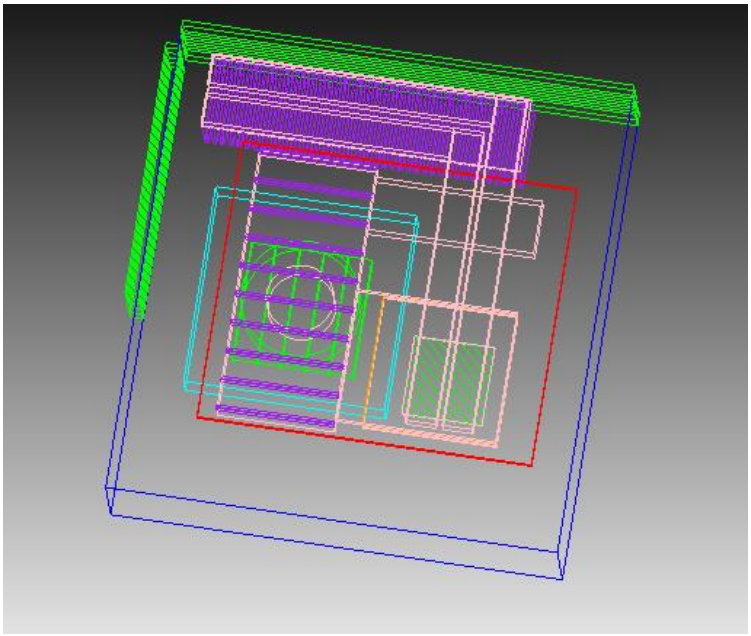

Figure 5.5 A screenshot from the simulation of GFX

After the merger of the simulations of CPU and GFX, the last step for completing the simulation was increasing the cabinet size to the size of the chassis and placing additional bodies representing major objects shown in the schematics (Figure 4.13). Table 5.2 has been prepared for the comparison of the measured and simulated data. The actual

overview and a detailed version of the simulation report are placed in Appendix E. A screenshot from ***Full Simulation without TE*** can be seen in Figure 5.6.

Table 5.2 Measured and simulated values for the whole simulation (in °C)

	Measured		***Simulated (Max. Temp.)***
Microprocessor	*CPU-0*	*73*	*78.4*
	CPU-1	*71*	
	CPU-2	*79*	
	CPU-3	*78*	
Heat Sink on CPU	*1*	*48.2*	*46.5-51.6*
	2	*48.2*	
Hear Pipes and HEX on CPU	*3*	*46.4*	*46.6*
	4	*47.5*	*45.9*
HEX on the motherboard	*5*	*40.7*	*43.7*
PCB	*6*	*35.4*	*31.3*
Heatsink on GFX	*7*	*44.7*	*56.6*
Heatpipe on GFX	*8*	*46.8*	*56.5*
GFX Source	*GPU*	*72*	*77.2*

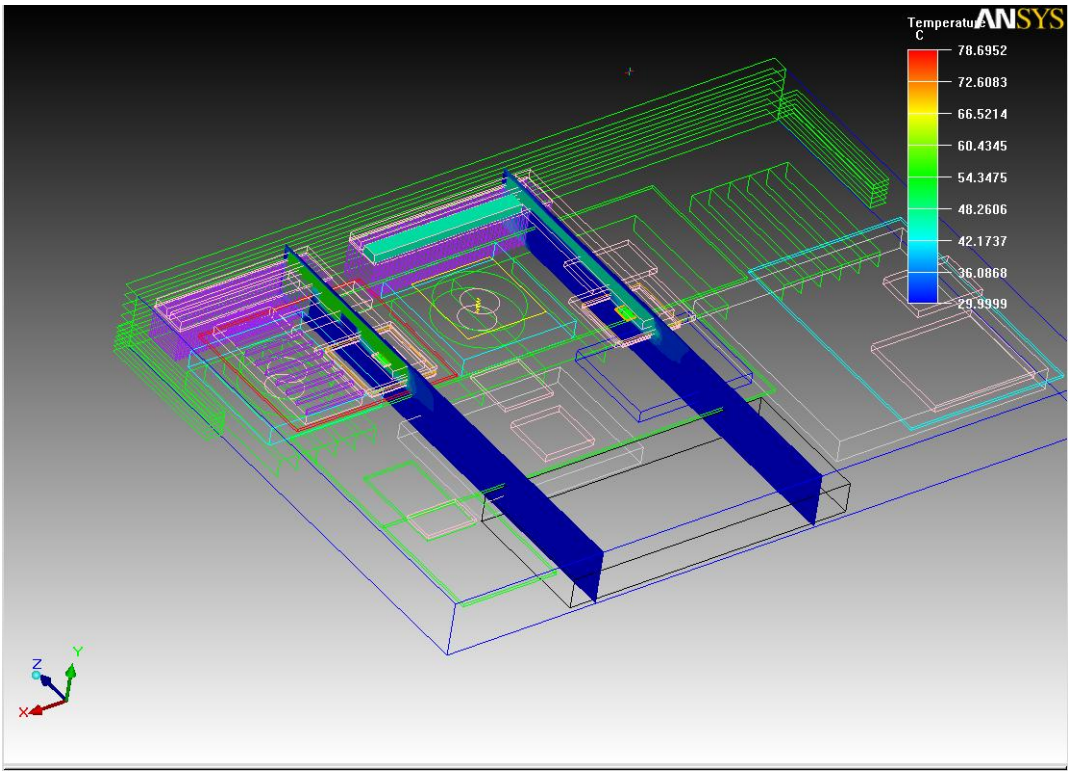

Figure 5.6 A screenshot from the Final Simulation without TE

CHAPTER 6

THERMOELECTRIC MODULE INTEGRATION ANALYSIS AND VALIDATION

This chapter is split into four sections. The first section describes the simulations performed for selecting a feasible location for the TE module. In the second section, the TE module is physically attached to the selected coordinates in the actual target system, and thermal impact of the TE module on the system is characterized. The results obtained from TE integration is compared to the simulation predictions in the third section. The last section discusses results, and power production possibilities based on physical validation experiments.

6.1 Selecting a Feasible Integration Point for TE Module

The selection of a correct spot is an important, but also difficult step of this project. Because the selected spot needs to be close to the heat source in order to harvest enough heat to create a plausible amount of temperature difference between the surfaces of the TE module. But picking a shunt path location that has a minimum or no impact to the CPU temperature in order to preserve performance is also essential. As stated previously there are only two major heat sources in the target system. Since the CPU is more consistent than GFX, the selection process will be carried out within the CPU simulation.

The first steps of the selection procedure are methodologically empirical. Therefore only some of the preliminary selections will be presented (Figure 6.1). At the first step a small model of the TE module has been prepared and has been placed:

1. On CPU die (red)
2. Inside the heat sink (blue)
3. Under the heat sink (green)
4. On top of the heat spreader (purple)
5. On top of the heat exchanger (grey)
6. Under the heat pipe (yellow)

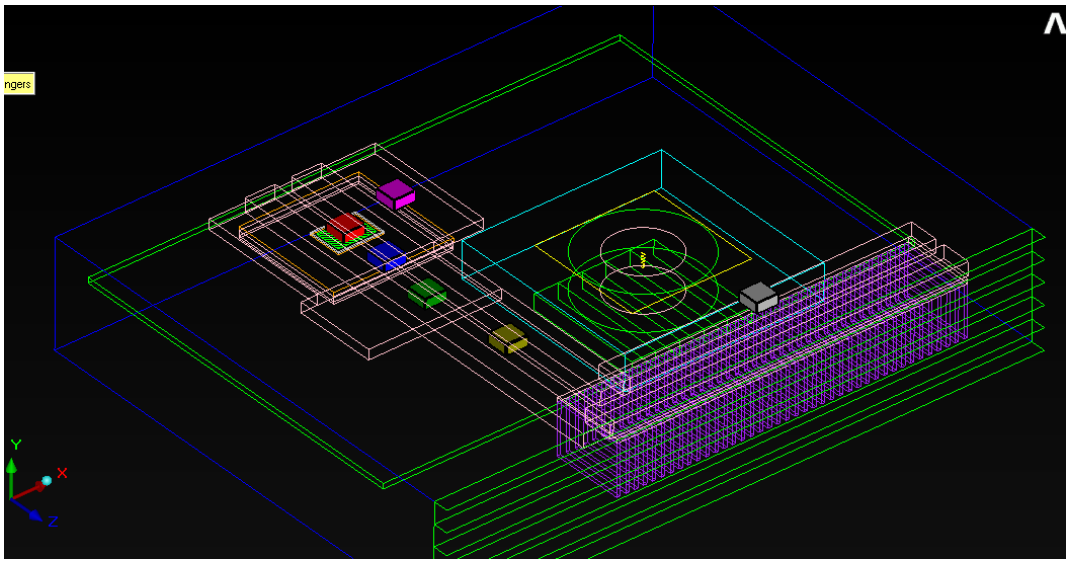

Figure 6.1 The locations of the preliminarily selected points for TE module

Table 6.1 Integration results in the simulation

		Ref.	**1**	**2**	**3**	**4**	**5**	**6**
Coordinates (mm)	x	-	0	0	0	15	50	0
	y	-	0	0.2	-2.7	3.2	8.5	0.3
	z	-	0	15	30	0	91	60
Power Source (˚C)	**CPU_Source**	**79.0**	**100.2**	**74.6**	**78.3**	**85.7**	**84.9**	**76.3**
Heat Sink (˚C)	CPU_Block	51.9	63.5	47.5	51.3	58.2	57.9	49.2
	CPU_Block.1	49.2	49.8	44.8	48.5	55.4	55.2	46.5
Heat Pipes (˚C)	block.1	49.1	49.8	44.7	48.4	55.3	55.1	46.3
	block.2	49.7	50.2	45.2	49.0	55.9	55.7	46.9
	block.3	48.7	49.3	44.3	48.0	54.9	54.7	46.0
	block.4	48.7	49.3	44.3	48.0	54.9	54.7	45.9
BGA (˚C)	BGA	52.6	55.9	49.4	52.0	57.3	57.1	50.7
Die (˚C)	Die	78.9	100.2	74.5	78.2	85.6	84.8	76.2
Sockets and pins (˚C)	Socket and Pins	53.7	57.3	50.3	53.0	58.6	58.2	51.6
Thermoelectric Module (˚C)	BiTe.1	-	88.9	44.9	48.0	54.5	52.5	46.2
	TE bottom.1	-	89.9	44.9	36.4	54.5	52.6	33.8
	TE top.1	-	51.7	44.9	48.4	43.4	34.4	46.2
	Temperature Difference	-	**38.2**	**0.04**	**12.0**	**11.2**	**18.1**	**12.3**

The temperature difference between the faces of the TE model has been taken as the primary parameter in these attempts. Table 6.1 shows the data obtained from these simulations. In order to create a geometrical understanding, the first spot, which has been selected exactly on the CPU die, has been set as the origin and the other locations have been given coordinates relatively. Also a reference column has been given in order to highlight the heating or performance effects of the integration attempts on the system.

This initial integration attempts provided essential information about possible effects of the TE integration on different spots around CPU. However none of the above selections qualify as a correct selection. Capturing a decent temperature difference may have been the initial purpose; however any selection triggering an overheating may cause the system performance loss. Therefore points 1, 4 and 5 have been eliminated at the first step. Among the others the factor of physical obstacles kicks in, because there is a thermal shield on the actual system rendering most selections like point 6 impossible and points like 2 and 3 need some machining work in order to be integrated which may be harmful to the cooling solution or create short circuits in the PCB area.

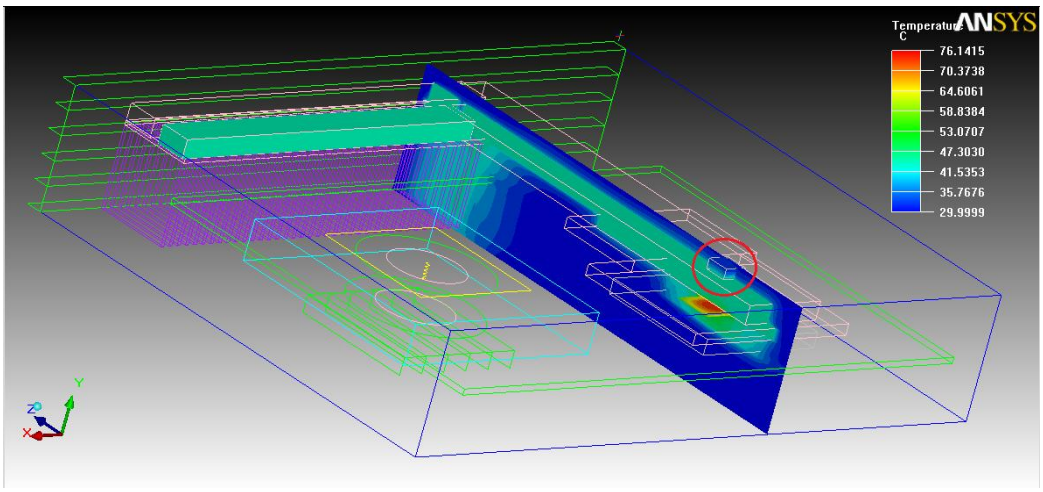

Figure 6.2 The virtual results of the TE integration on the 7th point. (TE module has been highlighted in the red circle)

All those reasons considered, a seventh point has been selected as the appropriate spot for the TE integration which has been close to the 1st point in the previous attempts. A slight relocation in the assigned coordinate system *(0; 0; 8.1)* has enabled the TE module to fit into a gap on the thermal shield (Figure 6.3). Also the TE module has been placed on one of the heat pipes instead of the CPU Die to overcome the heating problem. Therefore the

seventh point has been selected to be the integration point for the TE module. The results of the CPU simulation including the TE module have been given in Figure 6.2 and Table 6.2.

Table 6.2 A comparison for the results obtained before and after the TE integration on point 7

	Temperature results without TE integration			*Temperature results for 7th point*		
	Measured		***Simulated (Max. Temp.)***	***Measured***		***Simulated (Max. Temp.)***
Microprocessor	*CPU-0*	*72*	*79.0*	*CPU-0*	*72*	*76.1*
	CPU-1	*71*		*CPU-1*	*73*	
	CPU-2	*79*		*CPU-2*	*79*	
	CPU-3	*79*		*CPU-3*	*79*	
Heat Sink	*1*	*48.3*	*49.2 - 51.9*	*1*	*47.9*	*45.7 - 48.6*
	2	*48.3*		*2*	*47.9*	
Heat Pipes and HEX	*3*	*46.4*	*49.7*	*3*	*47.0*	*45.6*
	4	*47.6*	*48.7*	*4*	*47.3*	*45.3*
TE lower surface		-	-		*48.7*	*41.4*
TE upper surface		-	-		*40.3*	*29.1*

Figure 6.3 The TE integration on the actual system (with the keyboard removed)

As it can clearly be seen from these results, the selected point does not create any unrequited heat loads and also it seems to have discharged some of the heat around to CPU area creating a minor cooling effect. This cooling may be more apparent in the simulations due to the idealized conditions and the minor temperature drop in the measured data might have been caused by externalities as well. Yet the data exhibited in this table proves that implementing the TE module on this point composes no danger of overheating in the system..

6.2 TE Module Integration and Analysis

The integration process has begun after selecting a suitable spot for TE module. Due to its higher efficiency the TE module of FerroTEC has been selected to be used in application parts. Most of the thermocouples have been preserved from the system characterization in Chapter 4. Yet due to the number limitations in the data logger two of the exterior thermocouples (U1 and U2 from Figure 4.18) had to be replaced and attached to the both sides of TE module in order to observe the temperature differences as well. A thermal paste has been put between the selected spot (Figure 6.3) and the lower surface of the TE module, in order to reduce the contact resistance. Due to the unavailability of any conducting type adhesives, celluloid bands were utilized in the attachment process which also contributed to nonideal contact. The attached thermocouples were led through the rear grills as explained in Chapter 4.

In order to create a connection between the TE module and the multimeter the original leads were extended with long wires. Since this process was done with soldering, some additional electrical resistance was expected. The TE module terminals were externally wired to a Thevenin circuit (Figure 3.3) in order to acquire open circuit and loaded voltage values.

After the integration process was completed, the system was closed again with the TE module and the thermocouples attached to its two surfaces. The first thermocouple is compressed between the lower surface of the TE material and the heat pipe, while the second one is placed between the upper surface and the lower metallic surface of the keyboard. Six scenarios were created for in system characterization of the TE module performance. The measurements of the first two scenarios were done before the integration process in order to create a reference point. These scenarios were:

1. TAT set to 80% workload, without TE in the system.
2. TAT set to 100% workload, without TE in the system.
3. TAT set to 80% workload, with TE in the system.
4. TAT set to 100% workload, with TE in the system.
5. TAT set to 80% workload, 3D Mark running with TE in the system.
6. TAT set to 100% workload, 3D Mark running with TE in the system.

The experiments were commenced according to the following procedures:

- All runs were designed for 40 minute time spans.
- After the end of the first minute the TAT software was executed setting the CPU to the required workload.
- The TAT was disabled after 35th minute in order to collect data during cooling down.
- When used, 3D Mark was activated at 5th, 14th and 23th minutes to create a load on the GFX.
- All of the thermal data was collected by the data logger through the attached thermocouples, excluding the data referring to CPU die, which was acquired through TAT software.
- For the scenarios 3-6, the open circuit and loaded voltage were measured by using a multimeter.

The charts in Figures 6.4 – 6.8 present a summary of the data obtained from these experiments. Appendix D contains the complete data set.

Figure 6.4 and 6.5 highlight the observed temperature differences between the first and second pair of scenarios, comparing the temperature differences of selected critical points before and after the TE integration. Although the same workloads and scenarios were used in both pre- and post-integration runs, minor delays in the operation sequences may result in a bit larger temperature differences than actual due to lack of perfect synchronization between runs. This explains the peaks at the boundary of activities, especially at the starting and ending points of the experimental runs. However these peaks do not create any potential danger of overheating since they have been regulated right away. Even in these conditions any temperature difference exceeding 6.4˚ C has not been observed in either of the cases.

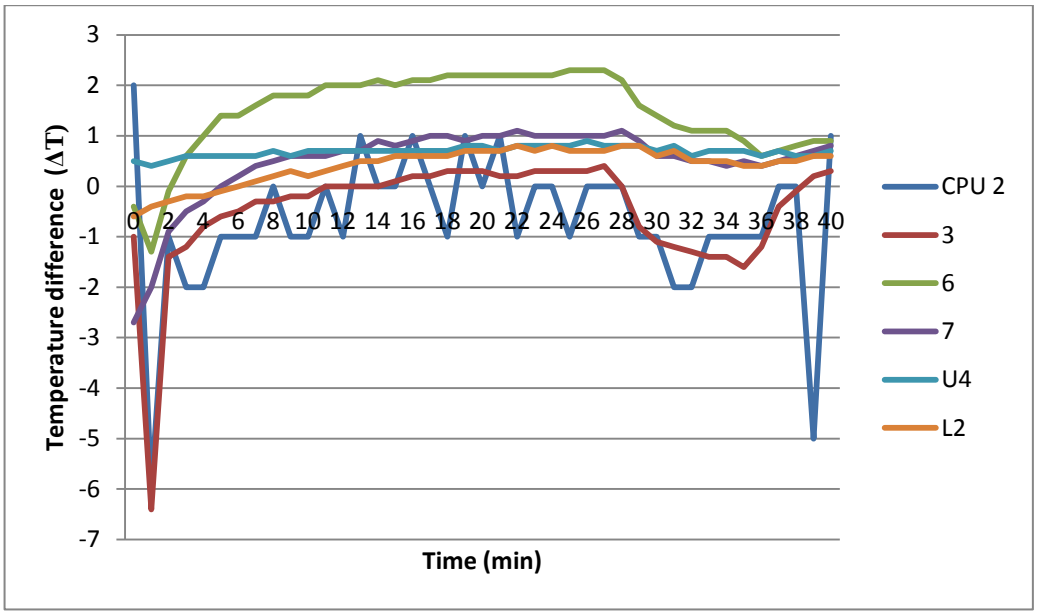

Figure 6.4 Temperature differences between the pre- and post TE integration cases for some selected points when CPU operates in 80% workload. (This graph serves as a comparison between 1st and 3rd scenarios)

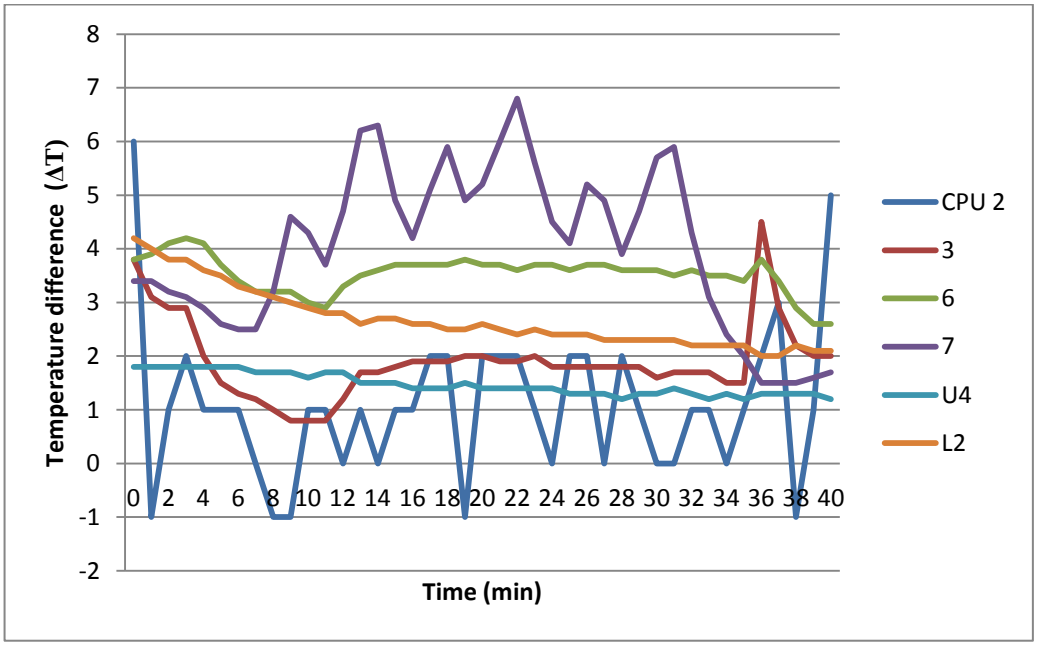

Figure 6.5 Temperature differences between the pre- and post TE integration cases for some selected points when CPU operates in 100% workload. (This graph serves as a comparison between 2nd and 4th scenarios)

As it has been stated in Chapter 4, any significant CPU heat-up results in performance loss. Figure 6.6 shows the thermal behavior of the CPU under different conditions from scenarios 3-6. As observed, the temperature of CPU never exceeds 82˚C even in the extreme conditions indicating that this application poses no danger of overheating for the CPU. Table 6.3 includes the average CPU values from the selected thread (CPU-2) from the first 4 scenarios in order to emphasize the effects of TE presence on the CPU temperature. As it can clearly be seen from these measurements the difference is barely noticeable.

Table 6.3 Average Temperature of CPU in different scenarios

	without TE	with TE
CPU Temperature with 80% workload	73.6˚ C	72.2˚ C
CPU Temperature with 100% workload	73.6˚ C	74.9˚ C

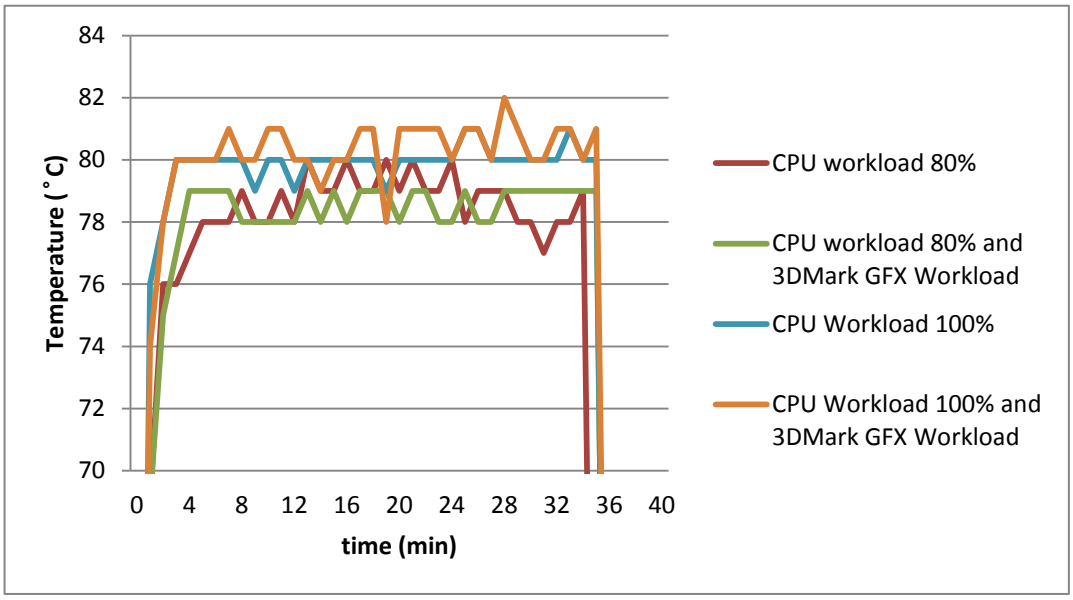

Figure 6.6 CPU temperatures from scenarios 3, 4, 5 and 6.

The aforementioned observations on the data proved that TE integration created no significant negative effects on the cooling solution of the system. Therefore, electrical gains will be reviewed next. The load voltage generated in the Thevenin circuit is depicted in Figure 6.7 for all the scenarios where TE module is present. Similarly, the open circuit voltage data is shown in Figure 6.8. A graph indicating the maximum power production

(Figure 6.11) is presented in Section 6.4. The fluctuations in Figure 6.7 are likely due to instantaneous temperature variations and resulting changes in generated TE current.

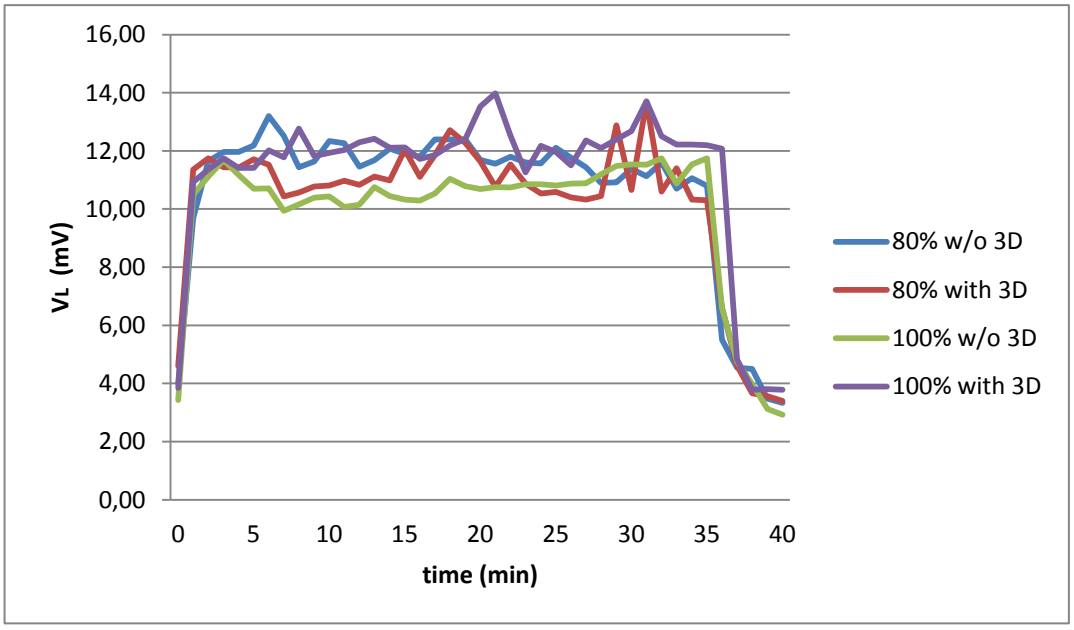

Figure 6.7 Loaded voltage values harvested by TE module for different scenarios

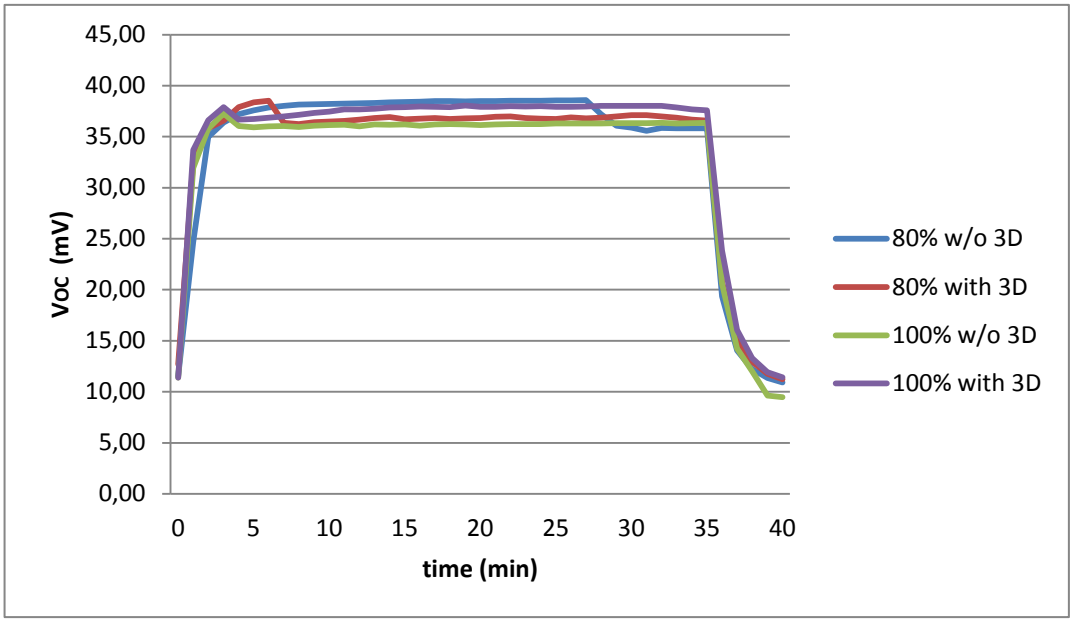

Figure 6.8 Open circuit voltage values harvested by TE module for different scenarios

In summary, system experiments have proven that inserting a TE module in a carefully picked spot of the target system has not significantly disturbed the cooling solution of the system, and offered gains in terms of power generation from waste heat. The verification of the electrical gain will be revisited in Section 6.4.

6.3 Full Simulation with TE Module

After the data acquisition was completed, a comparison of the full system simulations could be performed against full measurements. Figures 6.9, 6.10 and Table 6.3 demonstrate the visual and numerical results of this simulation.

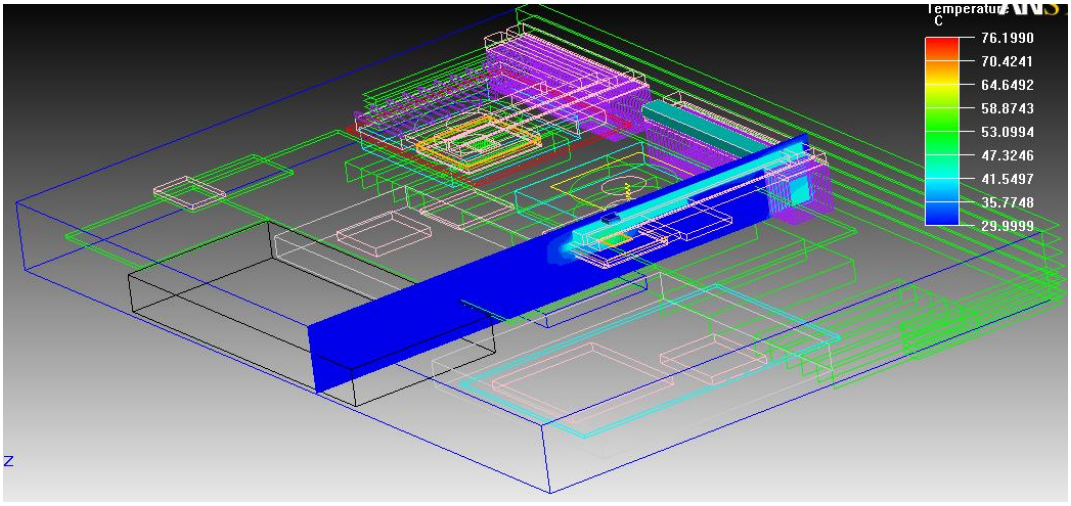

Figure 6.9 Full Simulation with TE results (general view)

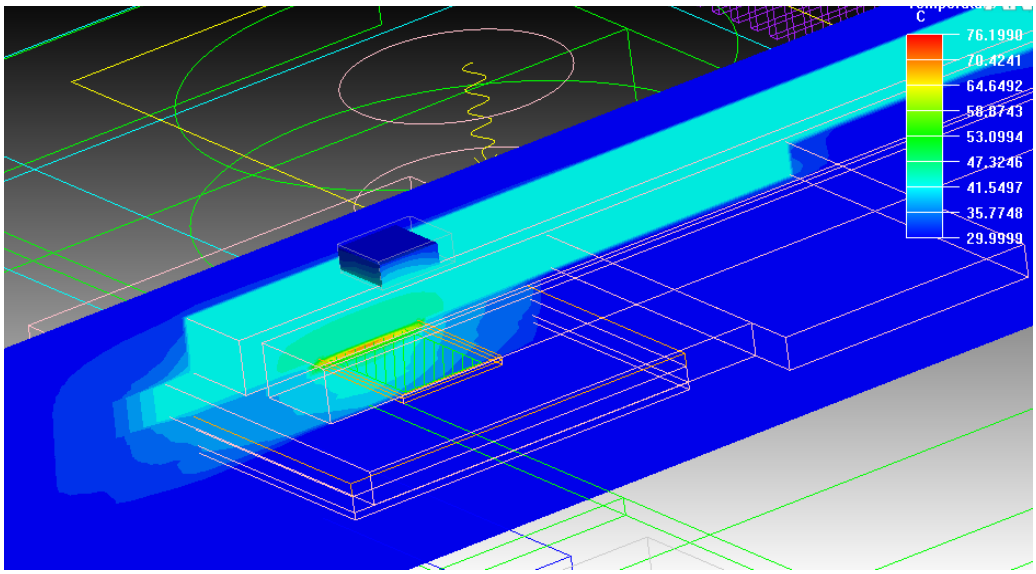

Figure 6.10 Full Simulation with TE results (zoomed on TE module)

Table 6.4 Measured and simulated values for the whole simulation including TE module (in °C)			
	Measured		***Simulated (Max. Temp.)***
Microprocessor	*CPU-0*	*74*	*75.9*
	CPU-1	*73*	
	CPU-2	*79*	
	CPU-3	*80*	
Heat Sink on CPU	*1*	*49.5*	*44.3-49.4*
	2	*49.5*	
Heat Pipes and HEX on CPU	*3*	*48.4*	*44.4*
	4	*49.0*	*43.8*
HEX on the motherboard	*5*	*39.7*	*42.7*
PCB	*6*	*40.4*	*45.9*
Heatsink on GFX	*7*	*41.7*	*48.1*
Heatpipe on GFX	*8*	*39.4*	*50.2*
TE bottom. 1	T_H	*50.4*	*44.5*
TE top. 1	T_C	*41.7*	*33.7*
Temperature Difference	***ΔT***	***8.4***	***10.7***

As observed in Table 6.4, the measured and simulated results are reasonably close to each other. The differences for GFX areas have already been indicated in the previous chapter. The temperature difference in the last row may be considered a little higher than expected. However, non-uniform temperature distributions around the thermocouples sandwiched between surfaces of TE and heatpipe could explain some of the difference. Appendix E contains a more elaborate report on the full system simulations used for correlation to system measurements with integrated TE module.

6.4 Verification of the Results

The electrical results in Section 6.2 are significant. However, the voltage measurements need to be converted to generated power before the benefits can be quantified. As in Chapter 3 the maximum power formula was:

$$P_{max} = \frac{{V_{OC}}^2}{4R_s} \tag{17}$$

V_{OC} values were previously presented. The load resistance of the circuit was measured as 1.42Ω. The missing variable, the resistance of the source, can be determined from:

$$R_S = \left(\frac{V_{OC}}{V_L} - 1\right) R_L \tag{18}$$

A maximum power curve can be created using the last two formulas. The average of these values can be seen for each scenario in Table 6.5. The inconsistencies in the results originate from the variables like fan speed and other externalities, which could not be directly controlled during the experiment. However the acquired results are close to each other, which indicate accuracy.

Table 6.5 Maximum generated power by the TE module (6.05 mm x 6.05 mm x 2.59 mm) for different scenarios

	P_{max} (μW)
80% CPU workload	111.98
80% CPU workload with 3DMark GFX workload	104.82
100% CPU workload	98.54
100% CPU workload with 3DMark GFX workload	119.19

The differences are due to workload activity and temperature fluctuations. The generated power value is expected to scale mainly with CPU activity. Figure 6.11 shows the maximum power curve for the last scenario. A CPU temperature graph is also included in order to show the relationship between the notebook performance impact and the power production of the TE module.

A thermal characterization curve for the FerroTEC TE module (Figure 3.4) was presented in Chapter 3. However, the terminal wiring done to the TE module (wire extensions at the legs etc.) increased TE output electrical resistance. Therefore, the need arose to make a secondary TE characterization table which uses the same circuitry and same cables to examine the efficiency of the TE module under the same conditions used in system validation. The relevant part of the new TE characterization data is depicted in Table 6.6. The full data can be found in Appendix A.

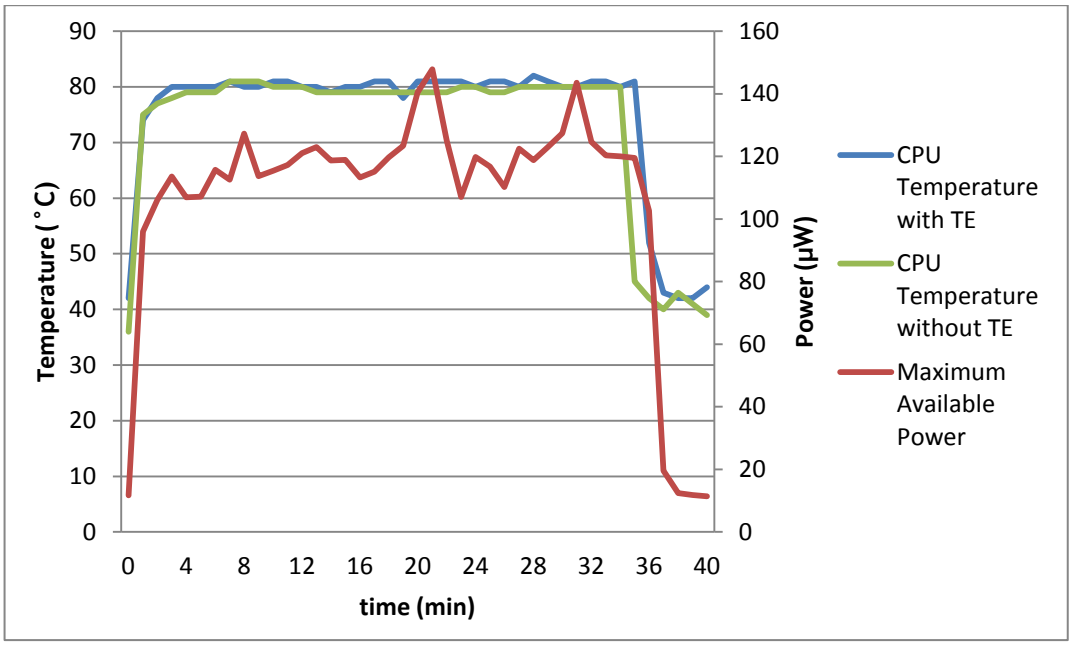

Figure 6.11 Temperature of CPU operating with 100% workload and the maximum power generation possibilities by the TE module (6.05 mm 6.05mm x 2.59 mm) over time

Table 6.6 Revised FerroTEC characterization values

° C	°C	°C	mV	mV	mA	Ω	mW	mW	mV/°C
T_H	T_C	ΔT	V_{OC}	V_L	I_L	R_S	P	P_{max}	Seebeck
32	21.6	10.4	63.2	19.8	12.375	3.507	0.245	0.285	0.338
31	21.6	9.4	57.6	18	11.250	3.520	0.203	0.236	0.340
30	**21.4**	**8.6**	**52.5**	**16.1**	**10.063**	**3.617**	**0.162**	**0.190**	**0.339**
29	21.3	7.7	46.8	14.5	9.063	3.564	0.131	0.154	0.338
28	21.5	6.5	39.8	12.4	7.750	3.535	0.096	0.112	0.340

As Table 6.6 shows, the maximum power generation for the temperature difference acquired in the system experiments should have been around 190 µW instead of 119 µW, indicating a loss of 37 % in the maximum power generation scenario. This loss can be explained by the additional thermal resistance at the surfaces of the TE module in the system experiment.

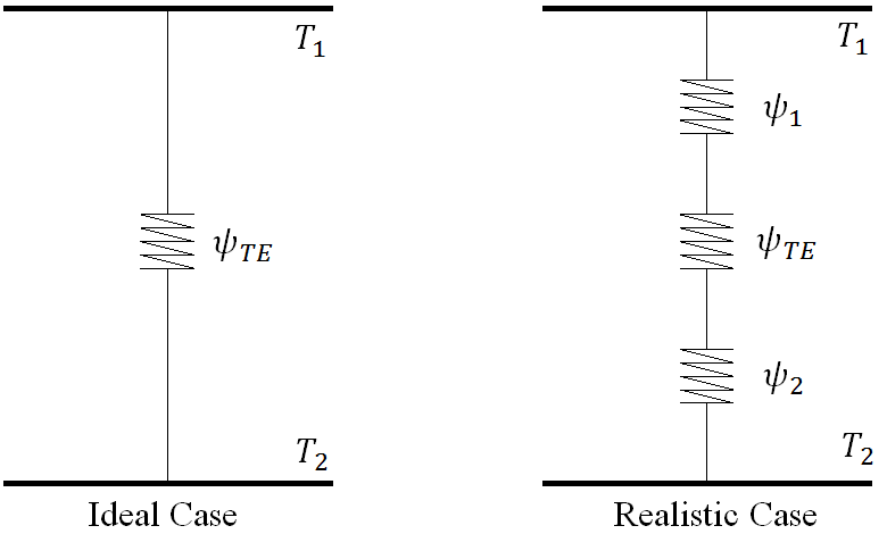

Figure 6.12 Thermal resistance cases

Figure 6.12 shows two diagrams as an example to this case where ψ_{TE} stands for the thermal resistance of the TE module. The total thermal resistance can be defined as:

$$\psi_{Total} = \frac{\Delta T}{P} \tag{19}$$

Here ΔT stands for the temperature difference and P stands for the power. In an ideal case the total thermal resistance would be equal to the thermal resistance of the TE material as shown in Equation (20). However in the real case two important factors as:

1. Contact roughness
2. Non-uniform temperature distribution

appear, which reduce the total power.

$$\psi_{ideal} = \psi_{TE} \tag{20}$$

$$\psi_{real} = \psi_1 + \psi_{TE} + \psi_2 \tag{21}$$

Non-uniform heat distribution is a common problem which can be seen on any thermal area. However, it may have the same effect as additional thermal resistance, causing temperature drops. Normally surface roughness could have also been addressed as a minor problem. However, in the particular experimental setup used, the presence of the thermocouples on both ends creates a major obstacle, since their relative thickness compared the surface area of the TE module cannot be overlooked. Attaching a thermocouple with a 36 AWG width (approximately 0.127 mm) longitudinally on the surface may break the contact of some of the TE couples with the hot surface while reducing the heat conduction to others due to the air gap.

When all above factors are considered, an effectiveness ratio of 62.73% in the experimental application platform is an encouraging outcome. This ratio is expected to improve using special adhesive materials instead of celluloid bands without the temperature sensors, better quality thermal paste, and custom designed electrical circuitry.

CHAPTER 7

CONCLUSION

7.1 Thesis Conclusion

This study was based upon the investigation of energy scavenging opportunity in notebook computers using off-the-shelf thermoelectric modules. Two test platforms were selected for analysis from different extremes of the notebook spectrum. A small office type notebook (Toshiba Portégé R705-P25) and a large gaming type notebook (Dell Alienware M17xR2) were mechanically and thermally characterized, and the later was utilized for the detailed analysis. Similarly two different TE modules (FerroTEC Peltier cooler model 9500/018/012 MP and TETECH TE 17-0.6-1.0 Thermoelectric Module) were validated. Although these modules were originally designed to serve as Peltier coolers, the direct relationship between Seebeck-Peltier effects enabled them to be used as thermoelectric generators as well. A computer simulation model of the selected platform was built using ANSYS Icepak software, which created the opportunity to analyze potential locations for integrating the TE modules into the notebook platform beyond experimental measurements. After developing a healthy model using system measurements for verification, a suitable slot was selected for the TE module placement in the notebook. It was then experimentally proven that energy harvesting in notebook computers is possible without significantly disturbing the thermal balance of the computer. The experimental validation results indicate that up to 1.26 mW/cm^3 of thermoelectric power can safely be harvested using off-the-shelf TE technology in the carefully selected region of the heat pipe in a large notebook under realistic high activity scenarios. The harvested energy can be increased by using more efficient TE couples, larger surface area, and better attachment to the heat pipe that excludes the thermocouples used to monitor TE surface temperatures. Although the scavenged total power with today's technology is bound to remain at most milli-Watts in order of magnitude, this can be stored on a small energy storage component, and used to power battery-independent electronic subsystems and autonomous devices. Also integrating TE module into computers may help in reducing the yearly CO_2 emissions by decreasing the energy

acquisition from the grid. This study is the first of its kind to conclusively demonstrate the feasibility of thermoelectric harvesting within microelectronic systems.

7.2 Future Work

The acquired results show that a portion of the waste heat dissipated by the notebooks can be converted back to the electricity through thermoelectric materials, which can be used as a sustainable energy generation method. The harvested energy can be increased by using more efficient thermoelectric couples to cover more of the opportunistic system volume. Even a custom computer design can be created as a future study to utilize the thermoelectric modules more efficiently.

A future study, which will be conducted in the power circuitry and electronics, may improve the energy efficiency of the TE module drastically. Although the reclaimed energy is bound to remain at milliwatts at most in today's technology, it can still be used to empower battery-independent sub-systems and autonomous devices.

Ambient intelligent systems which are using smart wireless sensors are becoming more wide spread nowadays. These systems are generally used to improve the quality of devices via additional feedback involving education, health, security and entertainment. Especially the "deploy and forget" types of sensors are being preferred for micro and nano systems for their ease of use. These kinds of sensors do not require battery replacements thus can be used for a very long time. Since they only activate themselves for short time intervals and stay in the SLEEP mode for more than 99% of their operation time, they require a very small amount of energy to operate and can be recharged by energy scavenging [22]. These devices may also be utilized in biomedical platforms so that they can be implemented to the human body and empowered by the body heat [2].

REFERENCES

[1] J. A. Paradiso and T. Starner, “Energy Scavenging for mobile and wireless electronics”, IEEE, Pervasive Computing, Vol. 4, Issue 1, pp 18-27, 2005.

[2] Z.L. Wang, "Energy harvesting for self-powered nanosystems”, Nano Research, Vol. 1, Number 1, pp 1-8, 2008.

[3] J.P. Carmo, R.P. Rocha, A.F. Silva, L.M. Gonçalves and J.H. Correria, “Integrated thin-film rechargeable battery in a thermoelectric scavenging microsystem”, Power Engineering, Energy and Electrical Drives, International Conference on POWERENG ’09, pp 359-362, 2009.

[4] A. Harb, “Energy Harvesting: State-of-the-art”, Renewable Energy, Vol. 36, Isuue 10, pp 2641-2654, 2011.

[5] A. Muhtaroğlu, A. Yokochi and A. von Jouanne, “Integration of thermoelectric and photovoltaics as auxiliary power sources in mobile computing applications”, Journal of Power Sources; Vol. 177, Issue 1, pp 239-246, 2008.

[6] A. Muhtaroğlu, “Sustainable power management of microelectronic systems”, VDM Verlag, Dr. Müller, pp 1-67, 2004.

[7] T. Huesgen, P. Woias and N. Kockmann, “Design and fabrication of MEMS thermoelectric generators with high temperature efficiency”, Sensors and Actuators A: Physical, Vol. 145-146, pp 423-429, 2008.

[8] A. Muhtaroğlu, A. von Jouanne and A. Yokochi, “Hybrid thermoelectric conversion for enhanced efficiency in mobile platforms”, Journal of Micromechanics and Microengineering, Vol. 17, Issue 9, pp 1767-1172, 2007.

[9] IMEC [Online], “Micropower generation and storage”, Available at: http://www.imec.be/ScientificReport/SR2007/html/1384267.html, (2012, July 15)

[10] J.P. Carmo, L.M. Gonçalves and J.H. Correia, “Thermoelectric microconverter for energy harvesting systems”, IEEE Transactions of Industrial Electronics, Vol. 57, Issue 3, pp 861-867, 2010.

[11] J.P. Fleurial, A. Borschchevsky, T. Caillat and R. Ewell, “New materials and devices for thermoelectric applications”, Proceedings of the 32nd Intersociety Energy Conversion Engineering Converence (IECEC-97), pp 1080-1085, 1997.

[12] R.P. Rocha, J.P. Carmo, L.M. Golçanves and J.H. Correria, “An energy scavenging microsystem based on thermoelectricity for the battery life extension in laptops”. 35th Annual Conference of IEEE Industrial Electronics, pp. 1813-1816, 2009.

[13] L.M. Gonçalves, C. Vouto, P. Alpium and J.H. Correria, "Thermoelectric micro converters for cooling and energy scavenging systems", Journal of Micromechanics and Microengineering, Vol. 18, Number 6, pp 1-5, 2008.

[14] G. Savelli, M. Plissonnier, J. Bablet, C. Salvi and J.M. Fournier, "Realization and optimization of thermoelectric devices using bismuth and antimony materials", 25th International Conference on Thermoelectrics, pp 394-398, 2006.

[15] G. Depresse and T. Jager, "Explotation of the thermotunnel effect for energy scavenging", Journal of Applied Physics, Vol. 96, Issue 9, pp 5026-5031, 2004.

[16] J.P. Carmo, R.P Rocha, A.F. Silva, L.M Gonçalves and J.H. Correria, "Integrated thin-film rechargeable battery in thermoelectric scavenging microsystem", International Conference on Power Engineering (POWERENG '09), Energy and Electrical Drives, pp. 359-362, 2009.

[17] G.L. Solbrekken, K. Yazawa and A. Bar-Cohen, "Heat driven cooling of portable electronics using thermoelectric technology", IEEE Transactions on Advanced Pacakging, Vol. 31, No. 2, pp 429-437, 2008.

[18] M. Freunek, M. Müller, T. Ungan, W. Walker and L.M. Reindi, "New physical model for thermoelectric generator", Journal of Electronic materials, Vol. 38, Number 7, pp 1214-1220, 2009.

[19] F. Meng, L. Chen and F. Sun, "A numerical model and comparative investigation of a thermoelectric generator with multi-irreversibilities", Energy, Vol. 36, Issue 5, pp 3513-3522, 2011.

[20] C. Hsu, G. Huang, H. Chu, B. Yu and D. Yao, "Experiments and simulations on low temperature waste heat harvesting system by thermoelectric power generators", Applied Energy, Vol. 88, Issue 4, pp 1291-1297, 2011.

[21] X. Niu, J. Yu and S. Wang, "Experimental study on low-temperature waste heat thermoelectric generator", Journal of Power Sources, Vol. 188, Issue 2, pp 661-626, 2009.

[22] C. Mathuna, T. O'Donell, R.V. Martinez-Catala, J. Rohan and B. O'Flynn, "Energy scavenging for long-term deployable wireless sensor networks", Talanta, Vol. 75, Issue 3, pp 613-623, 2008.

[23] Ferrotec [Online], "Ferrotec Thermoelectric Modules". Available at: http://thermal.ferrotec.com/index.php?id=module_detail&mod_id=6, (July 17, 2012)

[24] Ferrotec [Online], "Ferrotec Global Thermoelectric Module Catalogue", Available at: http://www.ferrotec.com/downloads/FerrotecGlobalTECatalog0507.pdf, pp 7, (July 17, 2012)

[25] TETECH [Online], "TETECH Peltier Cooler Model TE-17-0.6-1.0 specs" Available at: http://www.tetech.com/temodules/graphs/TE-17-0.6-1.0.pdf (July 17, 2012)

[26] TOSHIBA [Online], "TOSHIBA Portégé R705 Detailed Product Specification", Available at: http://cdgenp01.csd.toshiba.com/content/product/pdf_files/detailed_specs/portege_R705-P25.pdf , (July 18, 2012)

[27] DELL [Online], "DELL Alienware M17x Mobile Manual ", Available at: http://support.dell.com/support/edocs/systems/M17x/en/mm/mm_en.pdf , (July 18, 2012)

[28] CPU-World [Online], "CPU World Intel® Core™ i5-520M mobile processor specs", Available at: http://www.cpu-world.com/CPUs/Core_i5/Intel-Core%20i5%20Mobile%20I5-520M%20CP80617004119AE%20(BX80617I5520M).html (July 23, 2012)

[29] Euractive [Online], "EU warns of digital gap as IP numbers dry up", Available at: http://www.euractiv.com/infosociety/eu-warns-digital-gap-ip-numbers-dry/article-176127 (August 23, 2012)

[30] W. P. M. R. Pathirana and A. Muhtaroğlu, "PV solar technology status and feasibility in Northern Cyprus.", Global Conference of Global Warming (GCGW) 2012 , pp 1-12, 2012.

[31] Notebook Check [Online], "ATI Mobility Radeon 5870", Available at: http://www.notebookcheck.net/ATI-Mobility-Radeon-HD-5870.23073.0.html (July 24, 2012)

[32] R. Denker, A. Muhtaroğlu and H. Külah, "Quantification of thermoelectric energy scavenging opportunity for a compact notebook", PowerMEMS 2011 Technical Digest, pp. 371-374, 2011.

[33] R. Denker, A. Muhtaroğlu and H. Külah, "Empirically based methodology for thermoelectric generation in notebook systems", International Conference on Energy Aware Computing (ICEAC) 2011, pp 1-5, 2011.

APPENDIX A

DATA SHEETS OF TE CHARACTERIZATION EXPERIMENT

Table A.1 FerroTEC Peltier cooler model 9500/018/012 M P data (with R_L = 1.2 Ω)

	° C	° C	° C	mV	mA	mV	mA	Ohm	mW	mW	mV/C
	T_C	**T_H**	**ΔT**	**V_{OC}**	**I_{SC}**	**V_L**	**I_L**	**R_S**	**P**	**P_{max}**	**SEEBECK**
1	26.8	121	94.2	617	119	202	168.33	2.465	34.003	38.604	0.364
2	26.6	118	91.4	595	117	184	153.33	2.680	28.213	33.019	0.362
3	26.6	116	89.4	582	124	182	151.67	2.637	27.603	32.108	0.362
4	26.4	112	85.6	557	119	177	147.50	2.576	26.108	30.106	0.362
5	26.5	109	82.5	539	114	173	144.17	2.539	24.941	28.609	0.363
6	26.4	107	80.6	525	112	167	139.17	2.572	23.241	26.786	0.362
7	26.3	104	77.7	505	109	163	135.83	2.518	22.141	25.322	0.361
8	26.2	101	74.8	487	104	160	133.33	2.453	21.333	24.176	0.362
9	26.1	99	72.9	470	102	158	131.67	2.370	20.803	23.305	0.358
10	26.1	96	69.9	451	99	151	125.83	2.384	19.001	21.329	0.358
11	26	93	67	434	96	146	121.67	2.367	17.763	19.893	0.360
12	26	90	64	416	92	139	115.83	2.391	16.101	18.092	0.361
13	25.9	87	61.1	396	88	137	114.17	2.269	15.641	17.281	0.360
14	25.8	85	59.2	382	85	130	108.33	2.326	14.083	15.683	0.358
15	25.7	83	57.3	371	82	125	104.17	2.362	13.021	14.571	0.360
16	25.6	81	55.4	357	79	120	100.00	2.370	12.000	13.444	0.358
17	25.6	79	53.4	344	76	117	97.500	2.328	11.408	12.707	0.358
18	25.5	77	51.5	332	74	113	94.167	2.326	10.641	11.849	0.358
19	25.5	75	49.5	320	72	109	90.833	2.323	9.901	11.021	0.359
20	25.5	73	47.5	305	69	105	87.500	2.286	9.188	10.175	0.357
21	25.4	71	45.6	293	66	101	84.167	2.281	8.501	9.408	0.357
22	25.4	69	43.6	280	63	98	81.667	2.229	8.003	8.795	0.357
23	25.3	67	41.7	267	60	93	77.500	2.245	7.208	7.938	0.356
24	25.3	65	39.7	254	58	89	74.167	2.225	6.601	7.250	0.355
25	25.2	63	37.8	241	54	86	71.667	2.163	6.163	6.714	0.354
26	25.1	61	35.9	228	52	81	67.500	2.178	5.468	5.968	0.353
27	25.1	59	33.9	215	49	77	64.167	2.151	4.941	5.373	0.352
28	25	57	32	204	46	73	60.833	2.153	4.441	4.831	0.354
29	25	55	30	190	43	69	57.500	2.104	3.968	4.289	0.352
30	25	53	28	178	41	67	55.833	1.988	3.741	3.984	0.353

31	24.9	51	26.1	166	38	60	50.000	2.120	3.000	3.250	0.353
32	24.9	50	25.1	159	37	57	47.500	2.147	2.708	2.943	0.352
33	24.8	49	24.2	153	35	55	45.833	2.138	2.521	2.737	0.351
34	24.8	48	23.2	147	34	53	44.167	2.128	2.341	2.538	0.352
35	24.8	47	22.2	141	32	51	42.500	2.118	2.168	2.347	0.353
36	24.8	46	21.2	135	31	49	40.833	2.106	2.001	2.163	0.354
37	24.7	45	20.3	128	30	47	39.167	2.068	1.841	1.981	0.350
38	24.7	44	19.3	122	28	45	37.500	2.053	1.688	1.812	0.351
39	24.7	43	18.3	116	1.1	42	35.000	2.114	1.470	1.591	0.352
40	24.6	42	17.4	109	1.05	41	34.167	1.990	1.401	1.492	0.348
41	24.6	41	16.4	104	0.99	38	31.667	2.084	1.203	1.297	0.352
42	24.6	40	15.4	97	0.92	36	30.000	2.033	1.080	1.157	0.350
43	24.6	39	14.4	91	0.87	33	27.500	2.109	0.908	0.982	0.351
44	24.6	38	13.4	85	0.81	31	25.833	2.090	0.801	0.864	0.352
45	24.6	37	12.4	78	0.75	29	24.167	2.028	0.701	0.750	0.349
46	24.5	36	11.5	72	0.69	27	22.500	2.000	0.608	0.648	0.348
47	24.5	35	10.5	66	0.63	25	20.833	1.968	0.521	0.553	0.349
48	24.5	34	9.5	60	0.57	22	18.333	2.073	0.403	0.434	0.351
49	24.4	33	8.6	54	0.51	20	16.667	2.040	0.333	0.357	0.349
50	24.4	32	7.6	48	0.45	18	15.000	2.000	0.270	0.288	0.351
51	24.4	31	6.6	41	0.39	15	12.500	2.080	0.188	0.202	0.345
52	24.4	30	5.6	35	0.33	13	10.833	2.031	0.141	0.151	0.347
53	24.3	29	4.7	29	0.28	11	9.167	1.964	0.101	0.107	0.343
54	24.3	28	3.7	23	0.22	8.6	7.167	2.009	0.062	0.066	0.345
55	24.3	27.5	3.2	20	0.19	7.5	6.250	2.000	0.047	0.050	0.347
56	24.3	27	2.7	17	0.16	6.2	5.167	2.090	0.032	0.035	0.350
57	24.4	26.5	2.1	13	0.13	4.8	4.000	2.050	0.019	0.021	0.344
58	24.4	26	1.6	10	0.1	3.8	3.167	1.958	0.012	0.013	0.347
59	24.4	25.5	1.1	7	0.07	2.8	2.333	1.800	0.007	0.007	0.354
60	24.4	25	0.6	4	0.04	1.8	1.500	1.467	0.003	0.003	0.370
61	24.4	24.5	0.1	1	0.01	0.8	0.667	0.300	0.001	0.001	0.556

Table A.2 TETECH Peltier Cooler Model TE-17-0.6-1.0 data (with R_L = 1.36 Ω)

	° C	° C	° C	mV	mA	mV	mA	Ohm	mW	mW	mV/C
	T_C	**T_H**	**ΔT**	**V_{OC}**	**I_{SC}**	**V_L**	**I_L**	**R_S**	**P**	**P_{max}**	**SEEBECK**
1	32.3	118	85.7	464	95	183	134.559	2.088	24.624	25.774	0.318
2	32.2	116	83.8	452	92	180	132.353	2.055	23.824	24.853	0.317
3	32.1	114	81.9	441.7	90	176	129.412	2.053	22.776	23.756	0.317
4	32	112	80	430	91	172.1	126.544	2.038	21.778	22.681	0.316
5	31.8	110	78.2	420	89	169	124.265	2.020	21.001	21.833	0.316
6	31.8	108	76.2	409	86	164.7	121.103	2.017	19.946	20.731	0.316
7	31.7	106	74.3	399	85	160.8	118.235	2.015	19.012	19.756	0.316
8	31.6	104	72.4	388	83	157.1	115.515	1.999	18.147	18.829	0.315
9	31.6	102	70.4	377	81	153.2	112.647	1.987	17.258	17.885	0.315
10	31.5	100	68.5	367.4	79	149.4	109.853	1.984	16.412	17.005	0.316
11	31.4	98	66.6	357	77	145.3	106.838	1.982	15.524	16.080	0.315
12	31.3	96	64.7	347	75	141.5	104.044	1.975	14.722	15.241	0.315
13	31.2	94	62.8	336	71	137.7	101.250	1.959	13.942	14.411	0.315
14	31.2	92	60.8	324.6	68	133.3	98.015	1.952	13.065	13.496	0.314
15	31	90	59	315.7	66	128.3	94.338	1.986	12.104	12.543	0.315
16	31	88	57	305	65	125.1	91.985	1.956	11.507	11.891	0.315
17	30.9	86	55.1	294	63	120.4	88.529	1.961	10.659	11.020	0.314
18	30.9	84	53.1	283.6	60	115.4	84.853	1.982	9.792	10.144	0.314
19	30.8	82	51.2	273.2	57	111.5	81.985	1.972	9.141	9.461	0.314
20	30.7	80	49.3	262	55	104.6	76.912	2.047	8.045	8.386	0.313
21	30.7	78	47.3	252	54	101.6	74.706	2.013	7.590	7.886	0.313
22	30.5	76	45.5	240	51	97	71.324	2.005	6.918	7.182	0.310
23	30.5	74	43.5	231.1	49	93.3	68.603	2.009	6.401	6.647	0.313
24	30.5	72	41.5	220.6	47	89.5	65.809	1.992	5.890	6.107	0.313
25	30.4	70	39.6	210	45	85.4	62.794	1.984	5.363	5.556	0.312
26	30.3	68	37.7	199	44	84.4	62.059	1.847	5.238	5.361	0.311
27	30.2	66	35.8	189.4	42	81.7	60.074	1.793	4.908	5.002	0.311
28	30.1	64	33.9	178.3	39	76.9	56.544	1.793	4.348	4.432	0.309
29	30.1	62	31.9	168	37	72.5	53.309	1.791	3.865	3.939	0.310
30	30	60	30	158.3	35	68.4	50.294	1.787	3.440	3.505	0.310
31	29.9	58	28.1	147.7	33	64.3	47.279	1.764	3.040	3.092	0.309
32	29.9	56	26.1	137.4	31	59.8	43.971	1.765	2.629	2.674	0.310
33	29.8	54	24.2	127	28	55.4	40.735	1.758	2.257	2.294	0.309
34	29.7	52	22.3	116.3	26	50.8	37.353	1.754	1.898	1.928	0.307
35	29.7	50	20.3	106.5	1.01	46.6	34.265	1.748	1.597	1.622	0.309
36	29.6	48	18.4	96	0.91	42.1	30.956	1.741	1.303	1.323	0.307

37	29.6	47	17.4	90.7	0.86	40	29.412	1.724	1.176	1.193	0.307
38	29.5	46	16.5	85.9	0.82	38	27.941	1.714	1.062	1.076	0.306
39	29.5	45	15.5	80.1	0.77	35.6	26.176	1.700	0.932	0.944	0.304
40	29.5	44	14.5	75.6	0.72	33.6	24.706	1.700	0.830	0.840	0.307
41	29.4	43	13.6	70.45	0.67	31.4	23.088	1.691	0.725	0.734	0.305
42	29.4	42	12.6	65.1	0.62	29.2	21.471	1.672	0.627	0.634	0.304
43	29.4	41	11.6	60.3	0.57	27	19.853	1.677	0.536	0.542	0.306
44	29.3	40	10.7	55.4	0.53	24.9	18.309	1.666	0.456	0.461	0.305
45	29.3	39	9.7	50.1	0.48	22.5	16.544	1.668	0.372	0.376	0.304
46	29.2	38	8.8	44.9	0.43	20.3	14.926	1.648	0.303	0.306	0.300
47	29.2	37	7.8	40	0.38	18.3	13.456	1.613	0.246	0.248	0.302
48	29.2	36	6.8	34.6	0.33	15.8	11.618	1.618	0.184	0.185	0.299
49	29.2	35	5.8	29.7	0.28	13.6	10.000	1.610	0.136	0.137	0.301
50	29.1	34	4.9	24.9	0.24	11.4	8.382	1.611	0.096	0.096	0.299
51	29.1	33	3.9	19.8	0.19	9	6.618	1.632	0.060	0.060	0.299
52	29	32	3	14.7	0.14	6.7	4.926	1.624	0.033	0.033	0.288
53	29	31	2	9.8	0.09	4.6	3.382	1.537	0.016	0.016	0.288
54	29	30.5	1.5	7.3	0.07	3.4	2.500	1.560	0.009	0.009	0.286
55	29	30	1	4.9	0.04	2.3	1.691	1.537	0.004	0.004	0.288
56	28.9	29.5	0.6	2.2	0.02	1.1	0.809	1.360	0.001	0.001	0.216
57	28.9	29.1	0.2	0.12	0.001	0.1	0.074	0.272	0.000	0.000	0.035

Table A.3 FerroTEC Peltier cooler model 9500/018/012 M P data acquired after alteration of TE module

	° C	° C	° C	mV	mV	mA	Ohm	mW	mW	mV/° C
	T_H	**T_C**	**ΔT**	**V_{OC}**	**V_L**	**I_L**	**R_S**	**P**	**P_{max}**	**Seebeck**
1	72.1	25.3	46.8	291	87.8	54.875	3.703	4.818	5.717	0.345
2	71.4	24.7	46.7	290	87.3	54.563	3.715	4.763	5.659	0.345
3	70.3	24.6	45.7	285	82.3	51.438	3.941	4.233	5.153	0.346
4	69	24.4	44.6	276.6	81.7	51.063	3.817	4.172	5.011	0.345
5	67	24.2	42.8	266.8	79.5	49.688	3.770	3.950	4.721	0.346
6	65	24.1	40.9	253.5	75.9	47.438	3.744	3.601	4.291	0.344
7	63	23.8	39.2	244.2	73.4	45.875	3.723	3.367	4.004	0.346
8	61	23.6	37.4	232	70.9	44.313	3.636	3.142	3.701	0.345
9	59	23.6	35.4	219	69.3	43.313	3.456	3.002	3.469	0.344
10	57	23.6	33.4	207.1	65.7	41.063	3.444	2.698	3.114	0.344
11	55	23.5	31.5	195.5	63.5	39.688	3.326	2.520	2.873	0.345
12	53	23.4	29.6	182.9	61.2	38.250	3.182	2.341	2.629	0.343
13	51	22.7	28.3	173.3	56.7	35.438	3.290	2.009	2.282	0.340
14	49	22.9	26.1	162.4	55.1	34.438	3.116	1.898	2.116	0.346
15	47	22.6	24.4	148.1	48.5	30.313	3.286	1.470	1.669	0.337
16	45	22.3	22.7	138.2	45.5	28.438	3.260	1.294	1.465	0.338
17	43	22.2	20.8	127.5	55	34.375	2.109	1.891	1.927	0.341
18	41	22.1	18.9	115.4	50.5	31.563	2.056	1.594	1.619	0.339
19	39	21.8	17.2	103.9	45.5	28.438	2.054	1.294	1.314	0.336
20	37	21.8	15.2	92.5	39.9	24.938	2.109	0.995	1.014	0.338
21	35	22	13	79.9	33.8	21.125	2.182	0.714	0.731	0.341
22	33	21.9	11.1	68.4	21.6	13.500	3.467	0.292	0.337	0.342
23	32	21.6	10.4	63.2	19.8	12.375	3.507	0.245	0.285	0.338
24	31	21.6	9.4	57.6	18.0	11.250	3.520	0.203	0.236	0.340
25	30	21.4	8.6	52.5	16.1	10.063	3.617	0.162	0.190	0.339
26	29	21.3	7.7	46.8	14.5	9.063	3.564	0.131	0.154	0.338
27	28	21.5	6.5	39.8	12.4	7.750	3.535	0.096	0.112	0.340

APPENDIX B

DATA COLLECTED FROM TOSHIBA PORTÉGÉ R705-P25

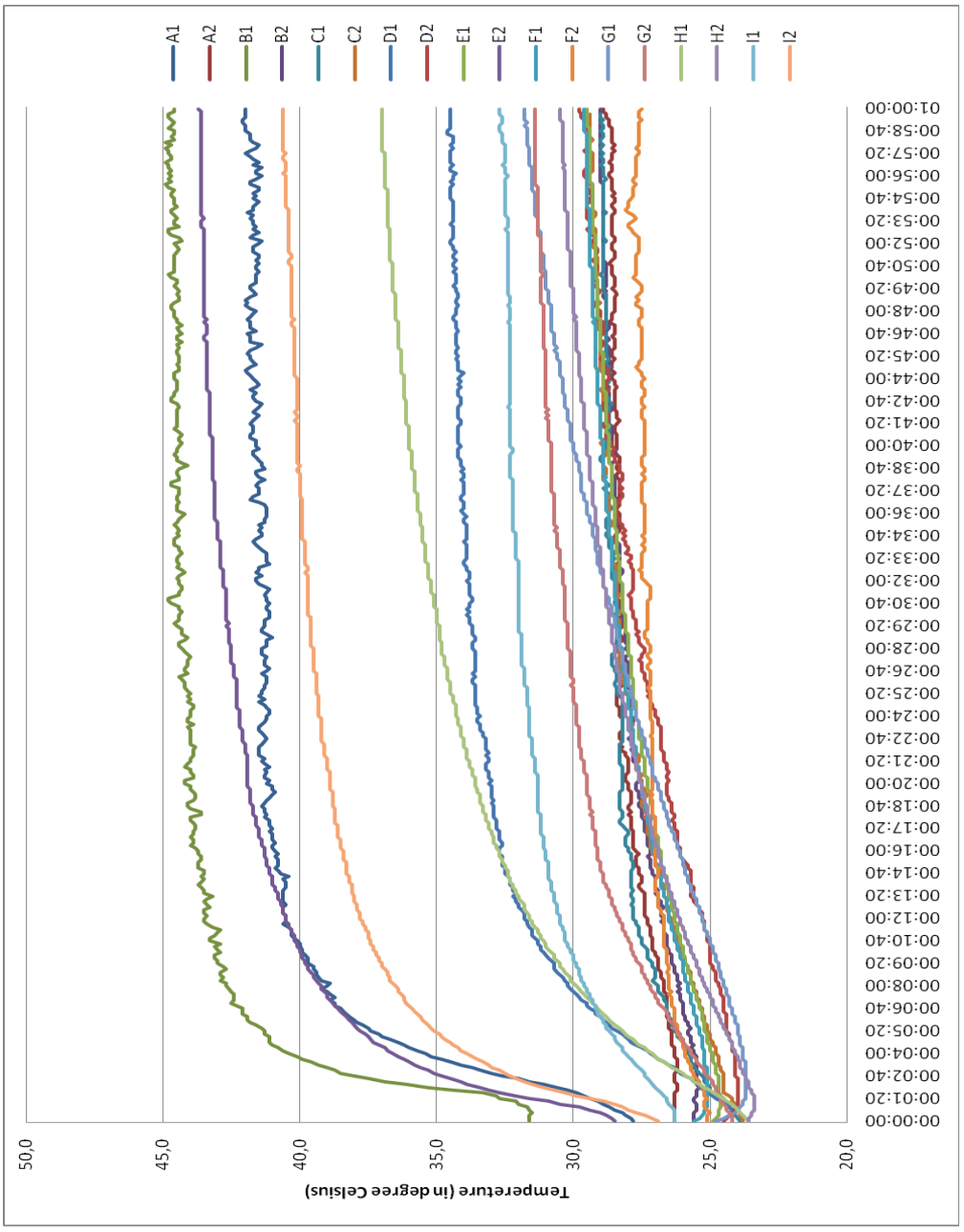

Figure B.1 Temperature measurements taken from the external layer of Toshiba with 80% workload (full data)

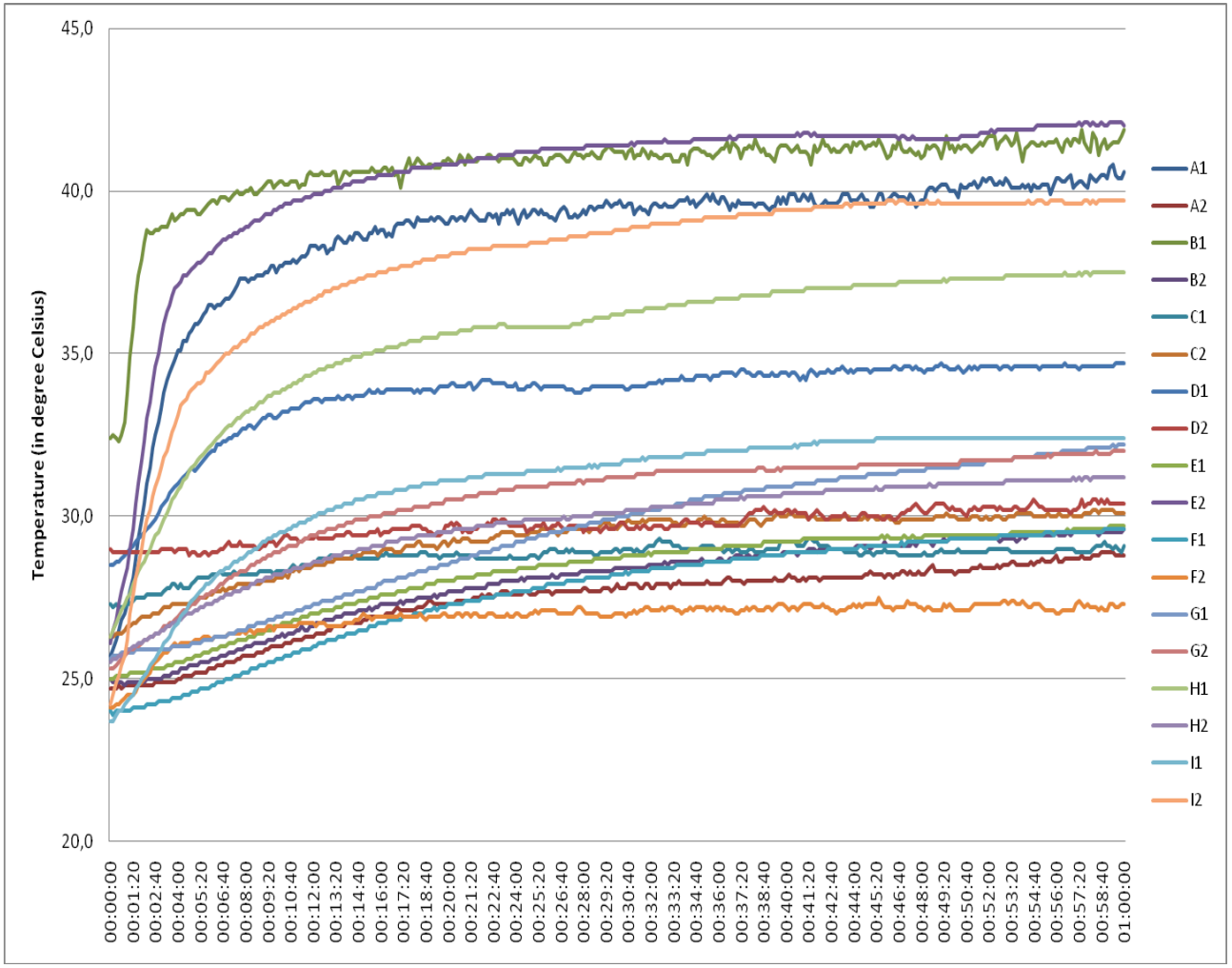

Figure B.2 Temperature measurements taken from the external layer of Toshiba with100% workload (full data)

Table B.1 Complete set of temperature measurements for Toshiba with 80 % workload (°C)

		TAT Processor Measurements by TAT- Tools				Internal Measurements (T type Thermocouple)					External Measurements from Top Layer (K type Thermocouple)								External Measurements from Bottom Layer (K type Thermocouple)									
	Time	CPU 0	CPU 1	CPU 2	CPU 3	T1	T2	T3	T4	T5	A1	A2	B1	B2	C1	C2	D1	D2	E1	E2	F1	F2	G1	G2	H1	H2	I1	I2
1	Pre -op	-	-	-	-	22.6	22.6	22.6	22.6	22.4	-	-	-	-	-	-	-	-	-	-	-	-	-	-	-	-	-	-
2	Op	-	-	-	-	40.0	39.1	29.7	29.0	23.1	-	-	-	-	-	-	-	-	-	-	-	-	-	-	-	-	-	-
3	60-120 sec	89	90	79	79	62.5	64.7	37.6	37.2	25.2	29.6	26.3	32.8	25.5	24.6	24.3	24.9	24.0	24.6	32.1	25.1	25.2	23.7	24.7	24.7	23.4	26.7	29.9
4	5 min	95	95	85	85	69.0	69.5	41.1	40.0	27.5	37.0	26.4	41.1	25.7	26.2	25.0	28.1	24.3	25.1	37.5	25.3	26.1	23.9	26.1	28.0	24.3	28.5	34.8
5	8 min	98	97	87	88	71.1	68.5	42.5	42.0	28.8	39.0	26.7	42.7	26.2	26.9	25.6	30.2	24.7	25.6	39.2	25.8	26.5	24.5	27.2	29.9	25.2	29.6	36.5
6	11 min	98	97	89	89	72.5	71.9	44.0	42.2	30.8	40.3	27.2	43.1	26.6	27.6	26.2	31.5	25.1	26.1	40.2	26.3	26.7	25.1	28.1	31.2	25.9	30.3	37.5
7	14 min	100	99	89	89	72.8	73.2	44.6	42.6	31.4	40.5	27.6	43.7	27.0	27.9	26.7	32.3	25.7	26.6	41.0	26.8	27.0	25.7	28.8	32.2	26.5	30.8	38.1
8	17 min	99	100	90	90	73.0	73.8	45.0	43.2	31.8	41.0	27.8	43.9	27.3	28.0	27.3	32.7	26.2	27.0	41.5	27.2	27.0	26.3	29.2	33.0	27.1	31.2	38.6
9	20 min	99	100	90	90	73.5	74.4	45.3	43.3	32.2	41.2	28.0	44.2	27.7	28.2	27.5	33.1	26.6	27.3	41.9	27.5	27.1	26.9	29.5	33.6	27.5	31.3	38.9
10	23 min	100	100	91	91	73.9	74.8	45.6	44.1	32.5	41.4	28.3	44.0	27.9	28.2	27.8	33.3	26.8	27.6	42.1	27.8	27.1	27.5	29.8	34.1	27.9	31.6	39.2
11	26 min	101	101	91	92	74.2	74.8	45.3	44.5	32.8	41.2	28.2	44.2	28.0	28.5	28.2	33.7	27.3	27.8	42.3	28.1	27.2	28.0	30.0	34.5	28.3	31.8	39.4
12	29 min	100	101	91	91	74.2	75.2	45.9	44.9	33.0	41.4	28.3	44.3	28.1	28.4	28.3	33.7	27.6	28.1	42.6	28.3	27.4	28.4	30.2	34.9	28.6	32.0	39.6
13	32 min	101	100	91	91	74.5	75.4	46.0	45.1	33.2	41.6	28.3	44.4	28.3	28.5	28.4	33.9	27.8	28.3	42.8	28.5	27.4	28.9	30.4	35.2	28.9	32.0	39.7
14	35 min	100	100	91	92	74.6	75.7	46.1	45.4	33.3	41.5	28.3	44.4	28.4	28.7	28.7	33.9	28.1	28.4	43.0	28.7	27.4	29.3	30.7	35.5	29.1	32.2	39.9
15	38 min	101	100	92	92	74.8	75.9	46.2	45.6	33.3	41.3	28.3	44.4	28.5	28.9	28.9	34.1	28.2	28.6	43.2	28.9	27.4	29.7	30.8	35.8	29.4	32.2	40.0
16	41 min	94	94	84	84	68.5	69.5	43.2	43.5	32.7	41.7	28.5	44.6	28.6	28.7	28.8	34.2	28.8	28.8	43.3	29.0	27.4	30.1	30.9	36.0	29.6	32.3	40.1
17	44 min	100	100	90	91	73.9	75.2	45.1	45.0	32.3	41.7	28.6	44.6	28.7	28.7	28.9	34.2	28.7	28.9	43.4	29.1	27.4	30.4	31.0	36.2	29.7	32.3	40.1
18	47 min	101	101	92	93	74.8	76.0	45.0	44.7	32.9	41.8	28.5	44.5	28.7	28.8	29.1	34.3	28.9	29.0	43.4	29.2	27.5	30.8	31.1	36.4	29.9	32.3	40.2
19	48 min	93	93	85	85	69.0	70.7	44.0	44.0	32.8	41.6	28.5	44.6	28.8	28.8	29.1	34.3	29.0	29.1	43.5	29.3	27.5	30.8	31.1	36.5	30.0	32.3	40.3
20	50 min	100	100	90	91	74.3	75.1	45.3	45.0	33.3	41.6	28.5	44.7	28.8	28.9	29.2	34.3	29.3	29.2	43.5	29.3	27.8	31.0	31.2	36.6	30.1	32.4	40.3
21	53 min	100	101	92	91	74.5	75.6	46.0	45.1	33.6	41.6	28.6	44.4	28.9	28.9	29.3	34.4	29.4	29.3	43.6	29.4	28.0	31.3	31.3	36.8	30.2	32.4	40.4

APPENDIX C

DATA COLLECTED FROM DELL ALIENWARE M17xR2

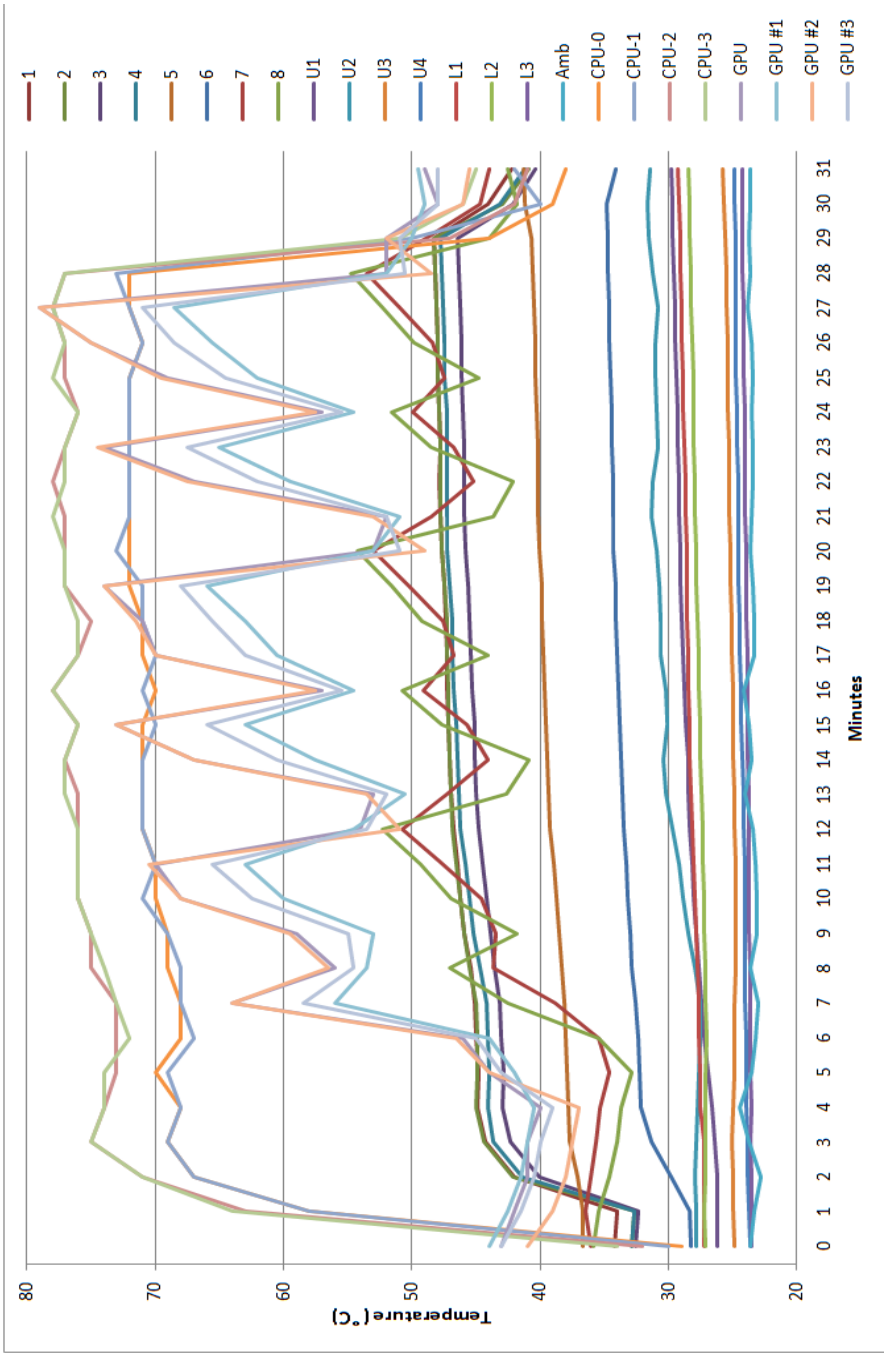

Figure C.1 Alienware temperature measurements with 80% workload (full data)

Table C.1 Thermal data collected with 80% workload

	DATA LOGGER																TAT TOOLS				GPU-Z			
Minute	1	2	3	4	5	6	7	8	U1	U2	U3	U4	L1	L2	L3	Amb	CPU-0	CPU-1	CPU-2	CPU-3	GPU	GPU #1	GPU #2	GPU #3
0	34.2	32.9	32.6	32.9	36.7	28.2	36.1	35.8	26.2	27.8	24.9	23.6	27.2	27.1	23.5	23.6	29	30	32	34	43	44	41	43
1	34.0	32.7	32.4	32.7	36.7	28.3	36.5	35.4	26.2	27.8	25.0	23.7	27.2	27.2	23.5	23.3	58	58	63	64	42	42.5	39	41.5
2	42.0	42.1	40.1	41.4	37.1	29.8	36.1	34.6	26.2	27.9	25.0	23.8	27.2	27.1	23.5	22.8	67	67	71	71	41	41.5	38	40.5
3	44.3	44.4	42.3	43.7	37.7	31.3	35.6	34.0	26.4	27.8	25.1	23.8	27.2	27.1	23.6	23.7	69	69	75	75	41	41	37.5	40
4	44.9	45.0	42.9	44.1	37.8	32.1	35.3	33.7	26.6	27.7	25.0	23.9	27.5	27.1	23.5	24.4	68	68	74	74	40	40.5	37	39
5	44.8	44.9	42.8	44.0	37.9	32.3	34.6	32.9	26.9	27.6	24.9	23.9	27.5	27.1	23.6	23.5	70	69	73	74	44	42	44	43
6	45.0	44.9	43.0	44.1	38.0	32.4	35.4	35.4	27.2	27.5	24.9	23.9	27.6	27.0	23.6	23.2	68	67	73	72	46	44	46.5	45
7	45.1	45.0	43.1	44.2	38.1	32.6	38.8	42.5	27.4	27.5	24.9	24.0	27.6	27.1	23.6	23.0	68	68	73	73	64	56	64	58.5
8	45.4	45.5	43.6	44.7	38.3	32.9	43.7	47.0	27.6	27.9	24.8	24.0	27.7	27.1	23.6	23.6	69	68	75	74	56	53.5	56.5	54.5
9	45.9	45.9	43.9	45.2	38.5	33.0	43.5	41.8	27.8	28.5	24.8	24.0	27.8	27.2	23.7	23.1	69	69	75	75	59	53	59.5	55
10	46.2	46.2	44.2	45.5	38.7	33.2	44.6	46.9	28.0	28.9	24.8	24.0	27.9	27.2	23.7	23.1	70	71	76	76	68	60	68	62.5
11	46.4	46.5	44.5	45.8	38.9	33.3	47.6	49.3	28.1	29.2	24.8	24.0	28.0	27.3	23.7	23.2	70	70	76	76	70	63	70.5	65.5
12	46.7	46.8	44.8	46.2	39.2	33.5	50.7	52.3	28.3	29.7	24.9	24.1	28.1	27.3	23.7	23.4	71	71	76	76	54	54.5	51	53.5
13	46.9	46.9	45.0	46.3	39.3	33.6	47.3	42.6	28.4	30.2	24.9	24.1	28.2	27.4	23.7	24.0	71	71	76	77	53	50.5	53.5	52
14	47.0	47.0	45.1	46.4	39.4	33.7	44.1	40.9	28.5	30.4	25.0	24.2	28.3	27.5	23.8	23.5	71	71	77	77	67	57.5	67	60.5
15	47.1	47.1	45.1	46.5	39.5	33.8	45.7	47.7	28.7	30.1	25.0	24.3	28.3	27.5	23.8	23.7	71	70	76	76	73	63	73	66
16	47.2	47.1	45.3	46.7	39.6	33.9	49.1	50.7	28.8	30.2	25.0	24.3	28.4	27.6	23.8	24.1	70	71	78	78	57	54.5	57.5	55.5
17	47.3	47.3	45.4	46.8	39.8	34.0	46.7	44.1	28.9	30.6	25.1	24.4	28.4	27.6	23.8	23.3	71	70	76	76	70	60.5	70	63
18	47.4	47.3	45.5	46.8	39.9	34.1	47.6	49.2	29.0	30.6	25.1	24.4	28.6	27.7	23.9	23.3	71	71	75	76	71	63	71.5	65.5
19	47.5	47.5	45.6	47.0	39.9	34.1	50.2	51.6	29.1	30.7	25.2	24.5	28.6	27.8	23.9	23.4	72	71	77	77	74	66	74	68
20	47.7	47.7	45.8	47.2	40.1	34.3	53.0	54.2	29.1	30.9	25.2	24.5	28.6	27.8	23.9	23.6	72	73	77	77	53	53	49	51
21	47.8	47.8	45.9	47.3	40.2	34.3	48.5	43.7	29.2	31.3	25.3	24.5	28.7	27.9	24.0	23.5	72	72	77	78	52	51	53	52
22	47.9	47.8	45.9	47.3	40.2	34.3	45.2	42.1	29.2	31.2	25.3	24.5	28.7	27.9	24.0	23.4	72	72	78	77	67	59.5	67.5	62
23	47.8	47.8	45.9	47.2	40.2	34.4	46.7	48.5	29.3	30.8	25.3	24.6	28.8	28.0	24.0	23.4	72	72	77	77	74	65	74.5	67.5
24	47.9	47.9	46.0	47.3	40.3	34.4	49.9	51.6	29.3	30.9	25.4	24.6	28.9	28.0	24.0	23.5	72	72	76	76	57	54.5	57.5	55.5
25	48.0	48.0	46.1	47.5	40.4	34.5	47.5	44.8	29.4	31.0	25.4	24.7	28.9	28.0	24.1	23.4	72	72	77	78	69	62	69.5	64.5
26	48.0	48.0	46.1	47.5	40.4	34.6	48.4	49.8	29.5	31.0	25.4	24.7	29.0	28.1	24.1	23.5	71	71	77	77	75	65.5	75	68.5
27	48.1	48.1	46.2	47.6	40.5	34.6	50.9	52.3	29.5	30.8	25.5	24.8	29.0	28.2	24.1	23.8	72	72	78	78	79	68.5	79	71
28	48.2	48.2	46.3	47.7	40.6	34.7	53.5	54.7	29.6	31.2	25.5	24.7	29.1	28.2	24.2	23.6	72	73	77	77	52	52	48.5	50.5
29	48.3	48.3	46.4	47.8	40.7	34.7	48.9	44.0	29.7	31.5	25.6	24.8	29.1	28.3	24.2	23.7	44	50	47	51	52	50	52	51
30	44.1	42.9	42.1	43.1	41.2	34.8	44.7	41.8	29.7	31.6	25.7	24.9	29.2	28.3	24.2	23.6	39	40	42	46	48	49	46	48
31	42.2	40.9	40.4	41.2	41.3	34.1	44.0	42.5	29.8	31.4	25.8	24.9	29.3	28.5	24.2	23.6	38	42	41	45	49	49.5	45.5	48

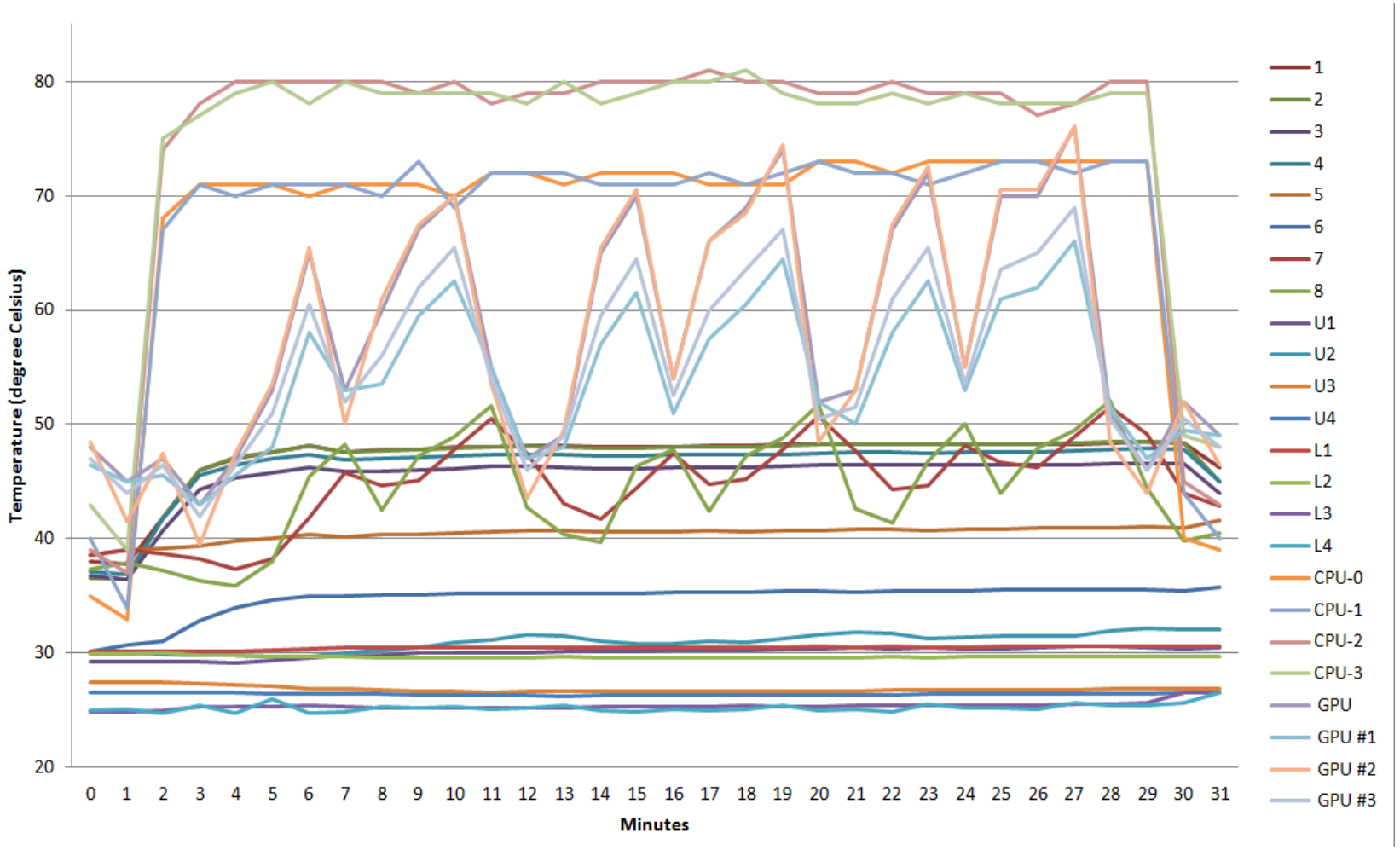

Figure C.2 Alienware temperature measurements with 100% workload (full data)

Table C.2 Thermal data collected with 100% workload

	DATA LOGGER																TAT TOOLS				GPU-Z			
Minute	1	2	3	4	5	6	7	8	U1	U2	U3	U4	L1	L2	L3	Amb	CPU-0	CPU-1	CPU-2	CPU-3	GPU	GPU #1	GPU #2	GPU #3
0	38.0	36.6	36.8	37.1	38.6	30.2	38.6	37.4	29.2	30.0	27.4	26.6	30.2	29.9	24.9	25.0	35	40	39	43	48	46.5	48.5	47
1	37.8	36.4	36.5	36.9	39.0	30.7	39.0	37.9	29.2	30.0	27.4	26.6	30.2	29.9	24.9	25.1	33	34	37	39	45	45	41.5	44
2	41.8	41.8	40.7	41.7	39.2	31.1	38.7	37.2	29.2	29.9	27.4	26.6	30.2	30.0	25.0	24.8	68	67	74	75	47	45.5	47.5	46.5
3	46.0	46.0	44.3	45.5	39.4	32.9	38.3	36.3	29.2	29.8	27.3	26.6	30.2	29.8	25.3	25.4	71	71	78	77	43	43	39.5	42
4	47.0	47.1	45.3	46.5	39.8	34.0	37.3	35.9	29.1	29.8	27.2	26.5	30.2	29.8	25.3	24.7	71	70	80	79	47	45.5	47.5	46.5
5	47.6	47.6	45.8	47.0	40.1	34.6	38.2	38.0	29.4	29.7	27.1	26.4	30.3	29.7	25.3	26.0	71	71	80	80	53	48	53.5	51
6	48.1	48.1	46.2	47.4	40.4	35.0	41.8	45.4	29.6	29.7	26.9	26.4	30.4	29.7	25.4	24.8	70	71	80	78	65	58	65.5	60.5
7	47.6	47.6	45.9	46.9	40.2	35.0	45.8	48.3	29.8	30.0	26.9	26.4	30.5	29.7	25.3	24.9	71	71	80	80	53	53	50	52
8	47.8	47.7	45.9	47.0	40.4	35.1	44.6	42.5	29.8	30.3	26.8	26.4	30.5	29.6	25.2	25.3	71	70	80	79	60	53.5	61	56
9	47.8	47.8	46.0	47.1	40.4	35.1	45.1	47.2	30.0	30.5	26.7	26.3	30.5	29.6	25.2	25.2	71	73	79	79	67	59.5	67.5	62
10	48.0	47.9	46.1	47.2	40.5	35.2	47.8	48.9	30.0	30.9	26.7	26.3	30.5	29.6	25.2	25.3	70	69	80	79	70	62.5	70	65.5
11	48.0	48.0	46.3	47.4	40.6	35.2	50.5	51.6	30.0	31.2	26.6	26.3	30.5	29.6	25.2	25.1	72	72	78	79	55	55	53.5	54
12	48.1	48.1	46.3	47.4	40.7	35.2	47.5	42.7	30.0	31.6	26.7	26.3	30.5	29.6	25.2	25.2	72	72	79	78	47	47	43.5	46
13	48.1	48.0	46.2	47.4	40.7	35.2	43.1	40.4	30.2	31.5	26.7	26.2	30.5	29.7	25.2	25.4	71	72	79	80	49	48	49.5	49
14	48.0	47.9	46.1	47.2	40.6	35.2	41.7	39.7	30.2	31.0	26.7	26.3	30.5	29.6	25.3	25.0	72	71	80	78	65	57	65.5	59.5
15	48.0	47.9	46.1	47.2	40.6	35.2	44.4	46.3	30.2	30.8	26.7	26.3	30.5	29.6	25.3	24.9	72	71	80	79	70	61.5	70.5	64.5
16	48.0	48.0	46.2	47.3	40.6	35.3	47.5	47.8	30.3	30.8	26.7	26.3	30.5	29.6	25.3	25.1	72	71	80	80	54	51	54	52.5
17	48.1	48.0	46.2	47.4	40.7	35.3	44.8	42.4	30.3	31.0	26.7	26.3	30.5	29.6	25.3	25.0	71	72	81	80	66	57.5	66	60
18	48.1	48.0	46.2	47.3	40.6	35.3	45.2	47.2	30.3	30.9	26.7	26.3	30.5	29.6	25.4	25.1	71	71	80	81	69	60.5	68.5	63.5
19	48.2	48.1	46.3	47.4	40.7	35.4	47.8	48.8	30.4	31.3	26.7	26.3	30.5	29.6	25.3	25.4	71	72	80	79	74	64.5	74.5	67
20	48.2	48.3	46.4	47.5	40.7	35.4	50.7	51.7	30.4	31.6	26.7	26.3	30.6	29.6	25.3	25.0	73	73	79	78	52	52	48.5	50.5
21	48.3	48.3	46.4	47.6	40.8	35.3	47.7	42.6	30.5	31.8	26.7	26.3	30.5	29.6	25.4	25.1	73	72	79	78	53	50	53	51.5
22	48.2	48.3	46.4	47.6	40.8	35.4	44.3	41.4	30.4	31.7	26.8	26.3	30.6	29.7	25.4	24.9	72	72	80	79	67	58	67.5	61
23	48.2	48.2	46.4	47.5	40.7	35.4	44.7	46.8	30.5	31.3	26.8	26.4	30.5	29.6	25.4	25.5	73	71	79	78	72	62.5	72.5	65.5
24	48.2	48.3	46.4	47.6	40.8	35.4	48.1	50.1	30.4	31.4	26.8	26.4	30.5	29.7	25.4	25.2	73	72	79	79	55	53	55	53.5
25	48.3	48.3	46.4	47.6	40.8	35.5	46.7	44.0	30.4	31.5	26.8	26.4	30.6	29.7	25.4	25.2	73	73	79	78	70	61	70.5	63.5
26	48.2	48.3	46.4	47.6	40.9	35.5	46.2	47.9	30.5	31.5	26.8	26.4	30.6	29.7	25.4	25.1	73	73	77	78	70	62	70.5	65
27	48.3	48.4	46.5	47.7	40.9	35.5	48.9	49.5	30.6	31.5	26.8	26.4	30.6	29.7	25.5	25.7	73	72	78	78	76	66	76	69
28	48.4	48.5	46.6	47.8	40.9	35.5	51.5	52.1	30.6	32.0	26.9	26.4	30.6	29.7	25.5	25.4	73	73	80	79	51	51.5	48.5	50.5
29	48.5	48.5	46.6	47.9	41.1	35.5	49.2	44.4	30.5	32.2	26.9	26.4	30.6	29.7	25.7	25.4	73	73	80	79	46	47	44	46
30	48.4	48.4	46.6	47.8	41.0	35.4	44.0	39.8	30.4	32.1	26.9	26.5	30.6	29.7	26.6	25.7	40	44	45	49	52	49.5	52	50.5
31	46.2	45.0	44.0	45.0	41.6	35.8	42.9	40.5	30.5	32.1	26.9	26.5	30.6	29.7	26.6	26.5	39	40	43	48	49	49	46.5	48

APPENDIX D

INTEGRATED TE MODULE MEASUREMENTS

All of the units are in ˚C for temperature data (represented in black) and in mV for electrical data (represented in red) for the tables presented in this section.

Table D.1 Data collected from scenario 1 (TAT set to 80%, without TE, without 3DMark)

Min	CPU-0	CPU-1	CPU-2	CPU-3	1	2	3	4	5	6	7	8	Amb
0	35	40	39	42	38,3	37,5	37,3	37,2	39,7	33,2	38,2	37,5	26,5
1	70	70	75	76	45,0	45,8	44,6	44,3	40,1	34,6	38,3	36,9	26,6
2	71	71	77	77	47,0	47,7	46,4	46,1	40,5	36,2	37,6	35,9	26,7
3	72	72	78	78	47,9	48,5	47,3	47,0	41,0	37,1	37,2	35,7	26,5
4	72	73	79	79	48,4	49,1	47,7	47,5	41,3	37,6	36,9	35,5	26,5
5	73	73	79	80	48,7	49,4	48,1	47,8	41,6	37,9	36,7	35,4	26,7
6	73	73	79	80	48,9	49,6	48,3	48,0	41,7	38,2	36,6	35,3	27,0
7	74	74	79	79	49,1	49,8	48,4	48,2	41,9	38,3	36,4	35,2	27,2
8	73	74	79	79	49,2	49,9	48,6	48,3	42,0	38,4	36,4	35,2	26,5
9	75	74	79	79	49,3	50,0	48,7	48,4	42,0	38,5	36,4	35,2	26,7
10	75	75	79	79	49,4	50,0	48,8	48,5	42,1	38,6	36,4	35,2	26,6
11	73	74	79	79	49,5	50,1	48,8	48,5	42,2	38,6	36,4	35,2	27,1
12	74	74	79	79	49,5	50,2	48,9	48,6	42,1	38,7	36,4	35,2	26,7
13	75	75	79	79	49,6	50,2	48,9	48,6	42,2	38,7	36,4	35,2	26,6
14	74	74	79	79	49,6	50,3	49,0	48,7	42,2	38,7	36,3	35,2	26,5
15	74	75	79	80	49,6	50,3	49,0	48,7	42,2	38,8	36,4	35,2	26,6
16	74	75	79	80	49,6	50,3	49,0	48,7	42,2	38,8	36,4	35,2	26,7
17	75	75	79	80	49,6	50,3	49,0	48,7	42,2	38,8	36,3	35,1	26,7
18	74	75	80	79	49,6	50,3	49,0	48,7	42,2	38,8	36,3	35,2	26,6
19	75	75	79	80	49,7	50,4	49,0	48,7	42,2	38,8	36,4	35,2	26,6
20	75	75	79	80	49,7	50,4	49,0	48,8	42,2	38,8	36,3	35,2	26,6
21	75	75	79	79	49,7	50,4	49,1	48,8	42,2	38,9	36,3	35,2	26,8
22	75	75	80	80	49,7	50,4	49,1	48,8	42,2	38,9	36,3	35,2	26,7
23	75	75	79	79	49,7	50,4	49,1	48,8	42,2	38,9	36,4	35,2	27,3
24	74	75	80	80	49,7	50,4	49,1	48,8	42,2	38,9	36,4	35,2	26,6
25	74	74	79	80	49,7	50,4	49,1	48,8	42,2	38,9	36,4	35,2	26,5
26	74	74	79	80	49,8	50,4	49,1	48,8	42,2	38,9	36,4	35,2	26,7
27	74	74	79	80	49,8	50,4	49,1	48,8	42,2	38,9	36,4	35,2	26,6
28	74	74	79	79	49,7	50,4	49,1	48,8	42,2	39,0	36,3	35,2	26,5

29	74	74	79	79	49,7	50,5	49,1	48,8	42,3	39,0	36,3	35,3	26,6
30	74	74	79	80	49,8	50,5	49,1	48,8	42,3	39,0	36,4	35,2	27,1
31	75	75	79	80	49,7	50,4	49,1	48,9	42,2	39,0	36,4	35,2	27,9
32	74	74	80	80	49,7	50,4	49,1	48,8	42,2	39,0	36,3	35,2	27,3
33	73	74	79	79	49,7	50,4	49,1	48,8	42,2	38,9	36,3	35,2	27,3
34	75	74	80	79	49,8	50,4	49,1	48,8	42,2	38,9	36,3	35,2	27,1
35	55	58	59	63	49,7	50,4	49,2	48,9	42,2	39,0	36,3	35,1	26,5
36	42	47	45	48	45,8	45,1	44,6	44,6	42,7	38,9	36,5	35,8	26,7
37	39	43	42	45	42,4	41,6	41,3	41,2	42,5	37,2	37,2	36,6	26,9
38	39	43	41	44	41,1	40,2	40,0	39,9	42,2	36,1	37,7	36,9	26,9
39	43	45	47	48	40,3	39,4	39,2	39,1	41,9	35,4	38,0	37,2	26,8
40	38	42	41	44	39,9	39,0	38,8	38,7	41,8	35,0	38,3	37,4	26,9

Table D.2 Data collected from scenario 2 (TAT set to 100%, without TE without 3DMark)

Min	CPU-0	CPU-1	CPU-2	CPU-3	1	2	3	4	5	6	7	8	Amb
0	32	36	36	39	34,7	33,9	33,6	33,4	35,6	30,4	34,6	34,1	26,3
1	68	67	75	74	41,5	42,2	41,1	40,9	36,5	31,8	34,9	34,0	26,5
2	70	69	77	76	44,2	44,8	43,6	43,2	37,2	33,7	34,9	33,7	26,2
3	71	71	78	77	45,2	45,8	44,6	44,2	37,9	34,8	34,7	33,6	26,2
4	71	71	79	78	46,0	46,6	45,3	45,0	38,5	35,4	34,7	33,6	26,7
5	72	72	79	78	46,6	47,1	45,9	45,6	39,1	35,9	34,8	33,7	26,3
6	72	72	79	79	47,0	47,6	46,3	46,0	39,4	36,3	34,8	33,8	26,2
7	72	72	81	79	47,3	47,9	46,6	46,4	39,7	36,6	34,9	33,9	26,6
8	73	73	81	80	47,6	48,2	46,9	46,6	40,0	36,8	35,0	34,0	26,5
9	74	73	81	80	47,9	48,4	47,2	46,9	40,2	37,0	35,1	34,1	26,4
10	73	73	80	79	48,0	48,6	47,4	47,0	40,4	37,2	35,2	34,2	26,6
11	74	73	80	80	48,2	48,7	47,5	47,2	40,5	37,4	35,3	34,2	26,4
12	73	73	80	79	47,7	48,3	47,1	46,5	40,3	37,1	35,3	34,0	26,6
13	72	73	79	79	47,4	47,9	46,7	46,3	40,2	36,9	35,0	34,0	26,5
14	73	72	79	78	47,3	47,9	46,7	46,2	40,1	36,8	35,0	33,9	26,5
15	73	71	79	78	47,3	47,8	46,7	46,2	40,1	36,8	35,0	33,9	26,7
16	73	72	79	78	47,2	47,9	46,7	46,2	40,1	36,8	35,0	33,9	26,5
17	72	72	79	79	47,3	47,9	46,7	46,2	40,1	36,8	35,0	33,9	26,4
18	72	71	79	78	47,3	47,9	46,7	46,3	40,1	36,9	35,0	33,9	26,8
19	72	73	79	79	47,4	47,9	46,7	46,3	40,2	36,8	35,0	33,9	26,8
20	72	72	79	78	47,3	47,9	46,7	46,2	40,2	36,9	35,0	33,9	26,7
21	72	72	79	78	47,3	48,0	46,8	46,3	40,2	36,9	35,0	34,0	26,4
22	72	72	79	78	47,4	48,0	46,8	46,3	40,2	37,0	35,0	34,0	26,4
23	72	72	80	79	47,4	48,0	46,8	46,3	40,2	36,9	35,1	34,0	26,8
24	72	72	80	79	47,5	48,0	46,9	46,4	40,3	36,9	35,1	34,0	26,3

25	73	72	79	79	47,5	48,1	46,9	46,4	40,3	37,0	35,3	34,4	26,4
26	73	72	79	78	47,5	48,1	46,9	46,4	40,3	37,0	35,5	34,5	26,6
27	72	72	80	79	47,6	48,2	47,0	46,5	40,3	37,0	35,6	34,6	26,4
28	72	73	80	79	47,6	48,2	47,0	46,5	40,4	37,1	35,7	34,7	26,3
29	72	72	80	79	47,7	48,2	47,0	46,6	40,4	37,1	35,8	34,7	26,4
30	73	73	80	79	47,6	48,2	47,1	46,6	40,4	37,1	35,8	34,9	26,5
31	73	73	80	79	47,7	48,3	47,1	46,6	40,4	37,2	35,9	34,8	26,4
32	72	72	80	79	47,7	48,3	47,1	46,6	40,5	37,1	35,9	34,9	26,3
33	74	73	80	79	47,7	48,3	47,1	46,7	40,5	37,2	35,9	34,9	26,7
34	73	73	80	80	47,8	48,3	47,2	46,7	40,5	37,2	35,9	34,8	26,4
35	41	46	45	50	47,8	48,3	47,2	46,6	40,5	37,2	35,9	34,9	26,5
36	38	41	42	46	42,6	41,7	41,4	41,3	41,2	36,8	36,2	35,6	26,7
37	37	40	40	44	40,4	39,4	39,3	39,2	41,1	35,5	36,8	36,2	26,4
38	37	39	43	45	39,5	38,6	38,5	38,4	41,0	34,7	37,3	36,6	26,4
39	38	40	41	45	39,1	38,1	38,0	37,9	40,8	34,3	37,6	36,7	26,5
40	34	39	39	43	38,8	37,8	37,7	37,6	40,7	33,9	37,8	36,9	26,5

Table D.3 Data collected from scenario 3 (TAT set to 80%, with TE without 3DMark)

Time	CPU 0-3				Voc	VL	TH	TC	ΔT	1	2	3	4	5	6	7	8	Amb
0	36	38	41	43	**11,53**	**4,00**	36,8	33,8	**3,0**	37,3	36,3	36,3	36,1	36,0	32,8	35,5	35,7	27,5
1	62	62	69	68	**24,68**	**9,69**	39,7	34,7	**5,0**	38,8	38,7	38,2	38,2	36,8	33,3	36,3	36,1	27,5
2	70	70	76	76	**34,97**	**11,65**	46,8	38,6	**8,2**	45,6	45,8	45,0	45,0	37,4	36,1	36,7	36,0	27,9
3	70	72	76	76	**36,39**	**11,97**	47,9	39,5	**8,4**	46,9	47,0	46,1	46,3	37,8	37,7	36,7	35,6	27,5
4	71	72	77	77	**37,21**	**11,97**	48,8	40,1	**8,7**	47,7	47,9	46,9	47,1	38,3	38,6	36,6	35,6	27,9
5	71	73	78	78	**37,58**	**12,18**	49,3	40,5	**8,8**	48,3	48,4	47,5	47,7	38,8	39,3	36,7	35,6	27,5
6	72	74	78	79	**37,85**	**13,20**	49,7	40,9	**8,8**	48,7	48,8	47,8	48,1	39,1	39,6	36,8	35,7	27,5
7	73	74	78	78	**38,03**	**12,52**	50,0	41,2	**8,8**	49,0	49,1	48,1	48,5	39,3	39,9	36,8	35,8	27,5
8	73	74	79	78	**38,16**	**11,44**	50,2	41,3	**8,9**	49,2	49,3	48,3	48,7	39,5	40,2	36,9	35,9	28,0
9	73	74	78	78	**38,17**	**11,64**	50,4	41,5	**8,9**	49,4	49,5	48,5	48,9	39,6	40,3	37,0	35,9	27,5
10	73	75	78	78	**38,20**	**12,34**	50,5	41,7	**8,8**	49,6	49,6	48,6	49,0	39,8	40,4	37,0	36,0	27,6
11	73	74	79	79	**38,24**	**12,26**	50,6	41,8	**8,8**	49,7	49,8	48,8	49,1	39,9	40,6	37,0	36,0	27,6
12	73	75	78	79	**38,27**	**11,46**	50,8	41,8	**9,0**	49,8	49,9	48,9	49,3	40,0	40,7	37,1	36,1	27,7
13	73	74	80	80	**38,31**	**11,68**	50,8	41,9	**8,9**	49,9	50,0	48,9	49,4	40,1	40,7	37,1	36,1	28,0
14	74	75	79	80	**38,38**	**12,07**	50,9	42,0	**8,9**	49,9	50,0	49,0	49,4	40,1	40,8	37,2	36,1	27,9
15	74	75	79	79	**38,40**	**11,90**	51,0	42,4	**8,6**	50,0	50,1	49,1	49,5	40,1	40,8	37,2	36,2	27,9
16	74	73	80	79	**38,44**	**11,80**	51,1	42,1	**9,0**	50,1	50,2	49,2	49,5	40,2	40,9	37,3	36,3	27,8
17	74	74	79	79	**38,49**	**12,39**	51,0	42,2	**8,8**	50,1	50,2	49,2	49,6	40,2	40,9	37,3	36,2	27,9
18	74	76	79	79	**38,48**	**12,40**	51,1	42,2	**8,9**	50,2	50,2	49,3	49,7	40,3	41,0	37,3	36,2	27,9

19	73	74	80	79	**38,45**	**12,40**	51,2	42,3	**8,9**	50,2	50,3	49,3	49,7	40,3	41,0	37,3	36,3	27,7
20	74	75	79	79	**38,49**	**11,69**	51,2	42,3	**8,9**	50,2	50,3	49,3	49,7	40,3	41,0	37,3	36,3	27,7
21	74	75	80	79	**38,49**	**11,56**	51,3	42,3	**9,0**	50,2	50,4	49,3	49,8	40,3	41,1	37,3	36,3	27,7
22	74	75	79	79	**38,52**	**11,80**	51,3	42,3	**9,0**	50,3	50,4	49,3	49,8	40,4	41,1	37,4	36,3	27,7
23	74	75	79	79	**38,53**	**11,60**	51,3	42,3	**9,0**	50,3	50,4	49,4	49,8	40,4	41,1	37,4	36,3	27,8
24	74	74	80	80	**38,53**	**11,57**	51,3	42,4	**8,9**	50,3	50,4	49,4	49,8	40,4	41,1	37,4	36,3	27,9
25	74	75	78	79	**38,56**	**12,11**	51,3	42,4	**8,9**	50,3	50,4	49,4	49,8	40,4	41,2	37,4	36,3	28,0
26	74	74	79	80	**38,55**	**11,77**	51,4	42,4	**9,0**	50,4	50,5	49,4	49,9	40,4	41,2	37,4	36,4	27,8
27	73	74	79	79	**38,59**	**11,44**	51,4	42,4	**9,0**	50,4	50,5	49,5	49,9	40,5	41,2	37,4	36,3	27,7
28	72	73	79	79	**37,20**	**10,90**	51,0	42,3	**8,7**	50,2	50,3	49,1	49,6	40,2	41,1	37,4	36,3	27,7
29	72	73	78	78	**36,09**	**10,92**	50,1	41,7	**8,4**	49,3	49,4	48,3	48,8	39,9	40,6	37,2	36,0	28,3
30	72	72	78	78	**35,88**	**11,38**	49,9	41,5	**8,4**	49,0	49,2	48,0	48,5	39,6	40,4	37,0	35,9	28,0
31	72	72	77	78	**35,57**	**11,13**	49,7	41,4	**8,3**	48,9	49,0	47,9	48,4	39,5	40,2	37,0	35,8	28,0
32	71	73	78	78	**35,85**	**11,59**	49,6	41,3	**8,3**	48,8	48,9	47,8	48,3	39,4	40,1	36,8	35,7	27,8
33	71	73	78	78	**35,81**	**10,70**	49,5	41,2	**8,3**	48,7	48,8	47,7	48,2	39,4	40,0	36,8	35,7	28,2
34	71	72	79	78	**35,82**	**11,06**	49,5	41,1	**8,4**	48,7	48,7	47,7	48,1	39,3	40,0	36,7	35,7	28,2
35	44	48	49	53	**35,81**	**10,80**	49,4	41,1	**8,3**	48,6	48,6	47,6	48,1	39,3	39,9	36,8	35,6	28,1
36	39	42	44	48	**19,35**	**5,50**	44,2	39,3	**4,9**	44,7	43,6	43,4	43,6	40,2	39,5	36,9	36,4	27,7
37	39	42	42	46	**14,05**	**4,55**	41,5	37,9	**3,6**	42,1	41,0	40,9	41,1	40,4	37,9	37,7	37,3	27,6
38	37	40	41	44	**12,24**	**4,50**	40,4	37,4	**3,0**	41,1	39,9	39,9	40,0	40,3	36,9	38,3	37,7	27,6
39	38	41	42	45	**11,35**	**3,48**	39,9	37,0	**2,9**	40,5	39,4	39,4	39,5	40,2	36,3	38,7	38,1	27,7
40	37	40	42	45	**10,93**	**3,33**	39,5	36,8	**2,7**	40,2	39,2	39,1	39,2	40,2	35,9	39,1	38,3	27,6

Table D.4 Data collected from scenario 4 (TAT set to 100%, with TE without 3DMark)

Time	CPU 0-3				Voc	VL	TH	TC	ΔT	1	2	3	4	5	6	7	8	Amb
0	34	40	37	42	**11,40**	**3,43**	35,9	33,1	**2,8**	36,5	35,5	35,5	35,2	35,7	32,0	35,0	35,2	27,0
1	68	68	76	75	**31,93**	**10,50**	44,9	37,6	**7,3**	43,8	43,9	43,4	43,3	38,2	34,6	38,0	37,1	27,1
2	72	71	78	77	**35,78**	**11,12**	47,6	39,2	**8,4**	46,6	46,6	45,9	45,9	38,3	36,9	37,9	36,6	27,1
3	73	72	80	79	**37,27**	**11,68**	48,6	39,9	**8,7**	47,7	47,7	46,9	47,0	38,7	38,1	37,6	36,4	27,2
4	73	73	80	79	**36,03**	**11,17**	48,4	40,0	**8,4**	47,7	47,6	46,7	46,9	38,7	38,7	37,5	36,1	27,4
5	74	73	80	78	**35,93**	**10,70**	48,4	40,0	**8,4**	47,6	47,6	46,7	46,9	38,6	38,7	37,2	36,0	27,2
6	72	73	80	79	**36,00**	**10,71**	48,5	40,1	**8,4**	47,7	47,7	46,7	47,0	38,7	38,8	37,1	35,9	27,0
7	72	72	80	79	**36,04**	**9,94**	48,6	40,1	**8,5**	47,8	47,8	46,8	47,1	38,7	38,9	37,0	35,8	27,2
8	72	72	80	79	**35,94**	**10,16**	48,7	40,3	**8,4**	47,8	47,8	46,9	47,2	38,8	39,0	36,9	35,9	27,2
9	72	73	79	79	**36,09**	**10,39**	48,7	40,3	**8,4**	47,9	47,9	47,0	47,3	38,7	39,0	36,9	35,8	27,2
10	73	73	80	80	**36,14**	**10,43**	48,8	40,3	**8,5**	48,0	48,0	47,0	47,4	38,8	39,1	36,9	35,8	27,3
11	73	73	80	80	**36,16**	**10,07**	48,8	40,3	**8,5**	48,0	48,0	47,1	47,4	38,8	39,2	36,9	35,9	27,5
12	73	73	79	79	**36,01**	**10,15**	48,9	40,5	**8,4**	48,0	48,1	47,1	47,4	38,8	39,2	36,9	35,8	27,4
13	73	72	80	79	**36,20**	**10,75**	49,0	40,5	**8,5**	48,1	48,1	47,1	47,5	38,9	39,3	36,9	35,8	27,3
14	72	72	80	79	**36,18**	**10,45**	48,9	40,5	**8,4**	48,1	48,1	47,2	47,5	38,9	39,3	36,9	35,9	27,5

15	72	72	80	79	**36,19**	**10,33**	49,0	40,6	**8,4**	48,2	48,2	47,2	47,6	38,8	39,3	36,9	35,9	27,2
16	74	73	80	79	**36,07**	**10,29**	49,0	40,6	**8,4**	48,2	48,2	47,2	47,6	38,9	39,3	36,9	35,9	27,2
17	72	72	80	80	**36,20**	**10,53**	49,0	40,6	**8,4**	48,2	48,2	47,3	47,7	38,9	39,3	36,9	35,8	27,8
18	72	73	80	79	**36,23**	**11,04**	49,0	40,6	**8,4**	48,3	48,3	47,3	47,6	39,0	39,4	36,9	35,9	27,4
19	73	73	79	79	**36,21**	**10,79**	49,1	40,6	**8,5**	48,3	48,3	47,3	47,7	38,9	39,4	36,9	35,9	27,3
20	73	72	80	79	**36,13**	**10,69**	49,1	41,0	**8,1**	48,3	48,3	47,3	47,7	38,9	39,4	36,9	35,9	27,3
21	73	73	80	79	**36,21**	**10,75**	49,1	40,7	**8,4**	48,3	48,3	47,3	47,7	39,0	39,4	36,9	35,9	27,2
22	73	73	80	79	**36,24**	**10,74**	49,1	40,7	**8,4**	48,3	48,4	47,4	47,7	38,9	39,4	37,0	35,9	27,6
23	74	73	80	80	**36,24**	**10,85**	49,1	40,7	**8,4**	48,3	48,3	47,4	47,8	39,0	39,5	37,0	35,9	27,6
24	73	72	80	79	**36,23**	**10,85**	49,1	41,1	**8,0**	48,4	48,3	47,3	47,7	38,9	39,5	36,9	35,9	27,3
25	72	72	81	80	**36,28**	**10,81**	49,1	40,7	**8,4**	48,3	48,4	47,4	47,8	38,9	39,5	37,0	36,0	27,2
26	72	73	81	80	**36,29**	**10,87**	49,1	40,8	**8,3**	48,4	48,4	47,4	47,8	39,0	39,5	37,0	36,0	27,9
27	73	72	80	79	**36,29**	**10,89**	49,2	41,1	**8,1**	48,3	48,4	47,4	47,8	38,9	39,5	37,0	36,0	27,2
28	73	73	80	79	**36,30**	**11,19**	49,2	40,8	**8,4**	48,4	48,4	47,4	47,8	38,9	39,5	37,0	35,9	27,4
29	72	72	80	80	**36,32**	**11,48**	49,2	40,8	**8,4**	48,4	48,4	47,4	47,8	39,0	39,5	37,0	36,0	27,4
30	73	74	80	79	**36,33**	**11,54**	49,2	41,2	**8,0**	48,4	48,4	47,4	47,8	39,0	39,5	37,0	36,0	27,9
31	73	73	80	79	**36,34**	**11,52**	49,2	41,2	**8,0**	48,4	48,5	47,5	47,9	39,0	39,6	37,0	36,0	27,3
32	72	73	80	79	**36,36**	**11,75**	49,2	40,8	**8,4**	48,5	48,5	47,5	47,9	39,0	39,6	37,1	36,0	27,5
33	72	73	81	80	**36,29**	**10,87**	49,1	40,8	**8,3**	48,4	48,4	47,4	47,8	39,0	39,5	37,0	36,0	27,9
34	73	74	80	79	**36,33**	**11,54**	49,2	41,2	**8,0**	48,4	48,4	47,4	47,8	39,0	39,5	37,0	36,0	27,9
35	72	73	80	79	**36,36**	**11,75**	49,2	40,8	**8,4**	48,5	48,5	47,5	47,9	39,0	39,6	37,1	36,0	27,5
36	41	46	45	48	**20,61**	**6,58**	44,6	39,2	**5,4**	45,1	44,0	43,8	44,0	39,9	39,4	37,1	36,3	27,2
37	39	43	42	45	**14,25**	**4,75**	41,2	37,6	**3,6**	41,9	40,7	40,6	40,8	40,1	37,7	37,7	37,2	27,4
38	38	41	41	45	**12,03**	**3,98**	40,0	37,0	**3,0**	40,6	39,6	39,5	39,7	40,0	36,5	38,2	37,5	27,2
39	33	39	39	42	**9,62**	**3,12**	36,7	34,3	**2,4**	37,4	36,3	36,3	36,2	38,3	33,2	37,7	37,0	27,1
40	33	39	38	40	**9,49**	**2,93**	36,3	34,0	**2,3**	37,0	35,9	36,0	35,9	37,7	33,1	37,5	36,7	27,1

Table D.5 Data collected from scenario 5 (TAT set to 80%, with TE and 3DMark)

Time	**CPU 0-3**				**Voc**	**VL**	**TH**	**TC**	**ΔT**	**1**	**2**	**3**	**4**	**5**	**6**	**7**	**8**	**Amb**
0	34	39	39	43	**12,71**	**4,60**	37,3	34,6	**2,7**	37,9	36,9	36,8	36,7	37,4	33,9	37,3	37,1	27,7
1	62	64	69	70	**32,57**	**11,36**	45,2	37,9	**7,3**	43,9	44,1	43,5	43,5	37,8	35,3	37,9	37,2	27,9
2	69	71	75	76	**35,81**	**11,75**	47,9	39,6	**8,3**	46,8	47,0	46,1	46,2	38,2	37,5	37,9	36,7	28,0
3	71	71	77	77	**36,58**	**11,44**	49,0	40,4	**8,6**	47,9	48,1	47,1	47,4	38,6	38,8	37,7	36,6	27,9
4	71	72	79	78	**37,90**	**11,43**	49,7	40,9	**8,8**	48,6	48,8	47,7	48,1	39,0	39,4	37,7	36,5	28,1
5	73	74	79	79	**38,37**	**11,71**	50,2	41,2	**9,0**	49,1	49,2	48,2	48,6	39,4	39,9	37,5	36,6	28,0
6	72	72	79	80	**38,53**	**11,53**	50,5	41,5	**9,0**	49,4	49,6	48,5	48,9	39,6	40,3	37,6	36,7	27,8
7	72	72	79	78	**36,37**	**10,44**	49,7	41,2	**8,5**	48,8	48,9	47,7	48,2	39,3	40,1	37,8	36,7	27,8
8	72	72	78	78	**36,22**	**10,57**	49,6	41,2	**8,4**	48,6	48,8	47,7	48,2	39,4	40,0	38,7	38,7	27,9
9	72	72	78	79	**36,41**	**10,78**	49,7	41,2	**8,5**	48,7	48,8	47,7	48,2	39,5	40,1	40,1	39,9	28,7
10	71	71	78	78	**36,47**	**10,81**	49,7	41,3	**8,4**	48,8	48,9	47,8	48,3	39,5	40,0	39,8	38,4	27,9

11	72	73	78	79	**36,56**	**10,97**	49,8	41,3	**8,5**	48,9	49,0	47,9	48,4	39,5	40,1	39,9	39,6	28,1
12	73	73	78	78	**36,68**	**10,83**	49,9	41,4	**8,5**	49,0	49,0	48,0	48,5	39,6	40,2	40,8	40,1	27,8
13	72	72	79	79	**36,82**	**11,12**	50,0	41,5	**8,5**	49,1	49,2	48,1	48,6	39,7	40,2	41,8	41,0	28,2
14	73	74	78	78	**36,91**	**10,98**	50,1	41,5	**8,6**	49,1	49,2	48,1	48,7	39,7	40,2	41,0	38,8	28,0
15	72	73	79	79	**36,69**	**12,04**	50,1	41,6	**8,5**	49,1	49,2	48,1	48,7	39,7	40,2	39,8	38,1	28,5
16	73	74	78	78	**36,78**	**11,11**	50,0	41,6	**8,4**	49,1	49,2	48,2	48,7	39,7	40,3	39,7	39,2	28,0
17	73	73	79	78	**36,82**	**11,85**	50,1	41,6	**8,5**	49,2	49,3	48,2	48,7	39,7	40,3	40,9	40,4	28,5
18	72	73	79	78	**36,74**	**12,71**	50,2	41,6	**8,6**	49,2	49,3	48,2	48,7	39,8	40,4	40,7	39,1	28,3
19	73	73	79	79	**36,79**	**12,27**	50,1	41,6	**8,5**	49,2	49,3	48,2	48,8	39,8	40,4	40,1	39,2	27,9
20	72	73	78	78	**36,84**	**11,64**	50,2	41,6	**8,6**	49,3	49,3	48,2	48,8	39,8	40,4	41,0	40,2	28,0
21	71	74	79	78	**36,95**	**10,76**	50,3	41,7	**8,6**	49,3	49,4	48,3	48,9	39,8	40,4	41,9	41,0	28,1
22	73	73	79	79	**36,98**	**11,54**	50,3	41,7	**8,6**	49,3	49,5	48,3	49,0	39,9	40,4	41,7	39,5	28,1
23	72	73	78	79	**36,84**	**10,88**	50,3	41,8	**8,5**	49,3	49,5	48,4	48,9	39,8	40,4	40,1	38,2	28,1
24	72	72	78	77	**36,77**	**10,53**	50,2	41,7	**8,5**	49,4	49,4	48,3	48,8	39,8	40,4	39,4	38,0	28,1
25	73	74	79	79	**36,74**	**10,59**	50,2	41,8	**8,4**	49,3	49,4	48,3	48,8	39,7	40,5	40,2	39,9	28,0
26	74	74	78	79	**36,89**	**10,40**	50,3	41,8	**8,5**	49,4	49,4	48,4	48,9	39,9	40,5	41,3	40,7	28,1
27	72	73	78	78	**36,81**	**10,32**	50,3	41,8	**8,5**	49,4	49,5	48,3	48,9	39,8	40,5	40,5	39,0	28,0
28	73	75	79	79	**36,87**	**10,45**	50,3	41,8	**8,5**	49,4	49,5	48,3	49,0	39,9	40,5	40,7	40,1	28,2
29	73	74	79	79	**36,98**	**12,88**	50,4	41,8	**8,6**	49,4	49,5	48,4	49,0	39,9	40,5	41,5	40,7	28,1
30	73	75	79	80	**37,10**	**10,65**	50,4	41,8	**8,6**	49,4	49,6	48,5	49,1	39,9	40,5	42,3	41,5	28,3
31	74	74	79	79	**37,10**	**13,69**	50,5	41,8	**8,7**	49,5	49,6	48,5	49,1	40,0	40,6	41,3	39,1	28,5
32	74	74	79	79	**37,00**	**10,60**	50,4	41,8	**8,6**	49,4	49,6	48,5	49,1	39,9	40,5	39,8	37,9	28,1
33	73	73	79	80	**36,85**	**11,40**	50,4	41,8	**8,6**	49,4	49,5	48,4	49,0	39,9	40,5	39,0	37,4	28,0
34	72	73	79	79	**36,68**	**10,33**	50,3	41,8	**8,5**	49,4	49,5	48,4	48,9	39,8	40,5	38,5	37,0	28,1
35	72	73	79	79	**36,57**	**10,30**	50,2	41,8	**8,4**	49,3	49,4	48,3	48,8	39,8	40,4	38,1	36,7	28,1
36	41	45	48	50	**20,77**	**6,60**	45,4	40,1	**5,3**	45,8	44,8	44,5	44,8	40,7	40,2	38,0	37,3	28,1
37	39	42	44	44	**15,08**	**4,61**	42,4	38,6	**3,8**	42,9	41,9	41,7	42,0	41,0	38,6	38,7	38,2	28,1
38	37	40	42	46	**12,95**	**3,66**	41,3	38,0	**3,3**	41,8	40,8	40,7	40,9	40,9	37,5	39,3	38,6	28,0
39	37	40	42	46	**11,78**	**3,56**	40,6	37,7	**2,9**	41,2	40,2	40,1	40,3	40,9	37,0	39,7	38,9	28,1
40	37	40	42	46	**11,24**	**3,40**	40,3	37,5	**2,8**	40,9	39,8	39,8	39,9	40,8	36,5	39,9	39,2	28,1

Table D.6 Data collected from scenario 6 (TAT set to 100%, with TE and 3DMark)

Time	**CPU 0-3**				**Voc**	**VL**	**TH**	**TC**	**ΔT**	**1**	**2**	**3**	**4**	**5**	**6**	**7**	**8**	**Amb**
0	37	42	42	45	**11,40**	**3,85**	37,8	35,1	**2,7**	38,5	37,5	37,4	37,3	38,0	34,2	38,0	37,5	27,7
1	63	64	74	73	**33,68**	**10,93**	45,9	38,4	**7,5**	44,7	44,9	44,2	44,3	38,2	35,7	38,3	37,4	27,6
2	71	70	78	78	**36,60**	**11,36**	48,4	39,9	**8,5**	47,2	47,4	46,5	46,7	38,5	37,8	38,1	36,8	27,6
3	73	73	80	79	**37,89**	**11,75**	49,5	40,7	**8,8**	48,4	48,5	47,5	47,8	39,0	39,0	37,8	36,6	28,3
4	74	73	80	79	**36,68**	**11,41**	49,2	40,7	**8,5**	48,3	48,4	47,3	47,7	38,9	39,5	37,6	36,3	27,8
5	72	72	80	79	**36,73**	**11,42**	49,4	40,8	**8,6**	48,4	48,5	47,4	47,8	39,1	39,6	37,4	36,3	27,7
6	73	72	80	80	**36,85**	**12,02**	49,6	41,0	**8,6**	48,6	48,7	47,6	48,0	39,2	39,7	37,3	36,1	28,1

7	72	71	81	81	**36,99**	**11,78**	49,7	41,1	**8,6**	48,8	48,8	47,8	48,2	39,3	39,8	37,4	36,5	27,8
8	73	73	80	79	**37,13**	**12,77**	49,8	41,2	**8,6**	48,9	49,0	47,9	48,3	39,4	40,0	38,2	38,2	27,7
9	73	73	80	79	**37,33**	**11,82**	50,0	41,3	**8,7**	49,0	49,1	48,0	48,5	39,5	40,2	39,7	39,4	27,8
10	72	71	81	81	**37,47**	**11,93**	50,1	41,4	**8,7**	49,1	49,2	48,2	48,6	39,6	40,2	39,5	37,9	28,4
11	72	71	81	81	**37,67**	**12,03**	50,2	41,5	**8,7**	49,3	49,3	48,3	48,7	39,6	40,3	39,0	37,9	27,9
12	74	73	80	80	**37,69**	**12,29**	50,3	41,5	**8,8**	49,3	49,4	48,3	48,9	39,7	40,4	40,0	39,4	27,7
13	74	73	80	80	**37,73**	**12,42**	50,4	41,7	**8,7**	49,4	49,5	48,4	48,9	39,8	40,4	41,2	40,4	27,9
14	74	73	79	80	**37,85**	**12,11**	50,4	41,7	**8,7**	49,5	49,5	48,4	49,0	39,7	40,4	41,3	39,4	28,2
15	73	74	80	80	**37,91**	**12,12**	50,5	41,7	**8,8**	49,5	49,6	48,5	49,1	39,8	40,5	39,9	38,2	28,0
16	74	74	80	79	**37,95**	**11,72**	50,5	41,7	**8,8**	49,6	49,7	48,6	49,1	39,8	40,5	39,2	37,7	28,2
17	74	74	81	80	**37,93**	**11,85**	50,5	41,7	**8,8**	49,6	49,7	48,6	49,1	39,9	40,5	40,1	39,7	28,2
18	74	74	81	80	**37,88**	**12,18**	50,6	41,8	**8,8**	49,6	49,7	48,6	49,1	39,8	40,6	40,9	39,6	27,8
19	74	73	78	79	**38,06**	**12,41**	50,6	41,8	**8,8**	49,7	49,7	48,7	49,2	39,9	40,6	39,9	38,4	27,9
20	74	74	81	80	**37,94**	**13,53**	50,6	41,8	**8,8**	49,7	49,8	48,7	49,2	39,9	40,6	40,2	39,7	27,9
21	74	74	81	80	**37,93**	**13,98**	50,6	41,9	**8,7**	49,7	49,7	48,7	49,2	39,9	40,6	41,0	40,2	27,8
22	75	74	81	81	**38,00**	**12,53**	50,6	41,9	**8,7**	49,7	49,8	48,7	49,2	39,9	40,6	41,8	41,0	27,9
23	75	74	81	81	**37,96**	**11,26**	50,7	41,9	**8,8**	49,7	49,8	48,8	49,3	40,0	40,6	40,7	38,6	27,9
24	75	75	80	80	**37,99**	**12,17**	50,7	41,9	**8,8**	49,7	49,8	48,7	49,3	39,9	40,6	39,6	37,8	27,8
25	74	74	81	81	**37,93**	**11,97**	50,7	41,9	**8,8**	49,7	49,8	48,7	49,3	39,9	40,6	39,4	39,0	27,8
26	74	74	81	80	**37,94**	**11,50**	50,7	41,9	**8,8**	49,7	49,8	48,7	49,3	39,9	40,7	40,7	40,1	28,3
27	75	74	80	80	**37,97**	**12,36**	50,7	41,9	**8,8**	49,7	49,9	48,8	49,3	39,9	40,7	40,5	38,6	28,0
28	75	75	82	80	**38,03**	**12,10**	50,7	42,0	**8,7**	49,8	49,9	48,8	49,4	39,9	40,7	39,6	38,3	27,8
29	74	75	81	79	**38,01**	**12,39**	50,7	41,9	**8,8**	49,8	49,9	48,8	49,3	39,9	40,7	40,5	39,8	27,8
30	74	75	80	80	**38,02**	**12,68**	50,7	42,0	**8,7**	49,8	49,9	48,7	49,3	39,9	40,7	41,5	40,6	28,3
31	74	74	80	80	**38,03**	**13,71**	50,8	42,0	**8,8**	49,8	49,9	48,8	49,4	40,0	40,7	41,8	39,9	28,0
32	75	74	81	81	**38,01**	**12,50**	50,8	42,0	**8,8**	49,8	49,9	48,8	49,4	40,0	40,7	40,2	38,1	27,8
33	75	75	81	80	**37,87**	**12,22**	50,7	42,0	**8,7**	49,8	49,8	48,8	49,3	39,9	40,7	39,0	37,2	27,9
34	74	74	80	80	**37,68**	**12,22**	50,6	41,9	**8,7**	49,7	49,8	48,7	49,3	39,9	40,7	38,3	36,8	28,0
35	74	74	81	80	**37,57**	**12,20**	50,6	41,9	**8,7**	49,7	49,7	48,7	49,2	39,8	40,6	37,9	36,5	27,9
36	44	48	52	53	**23,83**	**12,07**	46,9	40,8	**6,1**	47,2	46,3	45,9	46,2	40,6	40,6	37,7	36,6	27,8
37	39	42	43	47	**16,05**	**4,83**	42,8	38,8	**4,0**	43,4	42,3	42,2	42,4	41,3	38,9	38,3	37,7	27,8
38	39	42	42	46	**13,30**	**3,78**	41,3	38,0	**3,3**	41,9	40,8	40,7	40,9	41,0	37,6	38,8	38,2	27,7
39	37	41	42	45	**11,92**	**3,81**	40,6	37,6	**3,0**	41,2	40,1	40,0	40,2	40,8	36,9	39,2	38,5	27,7
40	37	40	44	46	**11,41**	**3,79**	40,2	37,3	**2,9**	40,8	39,7	39,7	39,8	40,7	36,5	39,5	38,8	28,0

APPENDIX E

ANSYS ICEPAK SIMULATION RESULTS

For the meshing process **hexa unstructured mesh** has been selected among three standard meshing options. The iteration number was set to 50 for the solver and the ambient temperature was adjusted to be 30˚C. For the size of the meshes a relative ratio of 1/40 of the maximum lengths has been taken for all dimensions

Table E.1 Overview of the Full Simulation without TE

Overview of solution Full-Simulation00_30amb, Wed Jul 25 00:17:34 Turkey Daylight Time 2012

Mass flow rates:

Object	Specified	Calculated
opening.1	0.0 kg/s	0.005818 kg/s
cabinet_default_side_maxz	n/a	-0.009537 kg/s
grille_gfx	n/a	0.01425 kg/s
grille_gfx.1	n/a	-1.482e-005 kg/s
grille_gfx.1.1	n/a	-0.0002486 kg/s
grille_gfx.2	n/a	-0.002017 kg/s
grille.1	n/a	0.01873 kg/s
blower_gfx	n/a	0.001833 kg/s
blower.1	n/a	0.001833 kg/s

Volume flow rates:

Object	Specified	Calculated
opening.1	n/a	0.005009 m3/s
cabinet_default_side_maxz	n/a	-0.008211 m3/s
grille_gfx	n/a	0.01227 m3/s
grille_gfx.1	n/a	-1.276e-005 m3/s
grille_gfx.1.1	n/a	-0.0002141 m3/s
grille_gfx.2	n/a	-0.001737 m3/s
grille.1	n/a	0.01613 m3/s
blower_gfx	n/a	0.001578 m3/s
blower.1	n/a	0.001578 m3/s

Fan operating points:

blower_gfx volume flow = 1.578e-003 m3/s, pressure rise = 35.550406724662 N/m2

Heat flows for objects with power specified:

Object	Specified	Calculated
HEX	1 W	0.9805 W
blower_gfx hub	1 W	-288.7 W
blower.1 hub	1 W	-72.8 W
GFX_Source	50.0	50 W
CPU_Source	35.0	35 W

Heat flows for openings, walls, grilles, and fans:

opening.1	0 W

cabinet_default_side_maxz -110.1 W

grille_gfx 71.34 W

grille_gfx.1 -2.473 W

grille_gfx.1.1 -1.498 W

grille_gfx.2 -13.1 W

grille.1 92.77 W

blower_gfx -96.23 W

blower.1 -24.27 W

Maximum temperatures:

GFX_Source 77.15 C

CPU_Source 78.42 C

HEX 43.66 C

RAM 30.87 C

WLAN 32.56 C

WPAN 30.94 C

battery 31.08 C

block.5 30.91 C

block.6 30.91 C

dvd_rom 30.83 C

harddisk 31 C

GFX_Block_2 56.65 C

GFX_heat_plate 59.73 C

block.g1 57.32 C

block.g2 57.25 C

block.g3 56.53 C

block.g4	56.52 C
BGA.1	52.58 C
Die_gfx	77.11 C
Socket and Pins_gfx	54.16 C
CPU_Block	51.62 C
CPU_Block.1	46.47 C
block.1	46.55 C
block.2	46.82 C
block.3	45.96 C
block.4	45.95 C
BGA	47.72 C
Die	78.42 C
Socket and Pins	49.45 C
pcb.4	31.85 C
pcb_inout	32.55 C
pcb_gfx	56.62 C
pcb.1	50.52 C
pcb.2	47.44 C
pcb.3	31.34 C

Table E.2 Detailed report of the Full Simulation without TE

Problem definition

Time variation: steady

Variables solved: temperature, flow

Radiation: YES

Flow regime: turbulent

Overview of solution Full-Simulation00_30amb, Wed Jul 25 03:07:16 Turkey Daylight Time 2012

Mass flow rates:

Object Specified Calculated

opening.1 0.0 kg/s 0.005818 kg/s

cabinet_default_side_maxz n/a -0.009537 kg/s

grille_gfx n/a 0.01425 kg/s

grille_gfx.1 n/a -1.482e-005 kg/s

grille_gfx.1.1 n/a -0.0002486 kg/s

grille_gfx.2 n/a -0.002017 kg/s

grille.1 n/a 0.01873 kg/s

blower_gfx n/a 0.001833 kg/s

blower.1 n/a 0.001833 kg/s

Volume flow rates:

Object Specified Calculated

opening.1 n/a 0.005009 m3/s

cabinet_default_side_maxz n/a -0.008211 m3/s

grille_gfx n/a 0.01227 m3/s

grille_gfx.1 n/a -1.276e-005 m3/s

grille_gfx.1.1 n/a -0.0002141 m3/s

grille_gfx.2 n/a -0.001737 m3/s

grille.1 n/a 0.01613 m3/s

blower_gfx n/a 0.001578 m3/s

blower.1 n/a 0.001578 m3/s

Fan operating points:

blower_gfx volume flow = 1.578e-003 m3/s, pressure rise = 35.550406724662 N/m2

Heat flows for objects with power specified:

Object Specified Calculated

HEX 1 W 0.9805 W

blower_gfx hub 1 W -288.7 W

blower.1 hub 1 W -72.8 W

GFX_Source 50.0 50 W

CPU_Source 35.0 35 W

Heat flows for openings, walls, grilles, and fans:

opening.1 0 W

cabinet_default_side_maxz -110.1 W

grille_gfx 71.34 W
grille_gfx.1 -2.473 W
grille_gfx.1.1 -1.498 W
grille_gfx.2 -13.1 W
grille.1 92.77 W
blower_gfx -96.23 W
blower.1 -24.27 W

Maximum temperatures:
GFX_Source 77.15 C
CPU_Source 78.42 C
HEX 43.66 C
RAM 30.87 C
WLAN 32.56 C
WPAN 30.94 C
battery 31.08 C
block.5 30.91 C
block.6 30.91 C
dvd_rom 30.83 C
harddisk 31 C
GFX_Block_2 56.65 C
GFX_heat_plate 59.73 C
block.g1 57.32 C
block.g2 57.25 C
block.g3 56.53 C
block.g4 56.52 C
BGA.1 52.58 C
Die_gfx 77.11 C
Socket and Pins_gfx 54.16 C
CPU_Block 51.62 C
CPU_Block.1 46.47 C
block.1 46.55 C
block.2 46.82 C
block.3 45.96 C
block.4 45.95 C
BGA 47.72 C
Die 78.42 C
Socket and Pins 49.45 C
pcb.4 31.85 C
pcb_inout 32.55 C
pcb_gfx 56.62 C
pcb.1 50.52 C
pcb.2 47.44 C
pcb.3 31.34 C

Overall totals:
power = -275.5 W

mass flow through boundaries = 0.02483 kg/s

volume flow through boundaries = 0.02138 m3/s

Heat sources

Block "BGA":	power = 0.0 W
	dims = 36 x 0.66 x 35.0 mm
Block "BGA.1":	power = 0.0 W
	dims = 40 x 0.66 x 40.0 mm
Block "CPU_Block":	power = 0.0 W
	dims = 50 x 3 x 40.0 mm
Block "CPU_Block.1":	power = 0.0 W
	dims = 40 x 3 x 25.0 mm
Block "Die":	power = 0.0 W
	dims = -13.6 x 0.79 x 10.371 mm
Block "Die_gfx":	power = 0.0 W
	dims = 13.6 x 0.79 x 10.371 mm
Block "GFX_Block_2":	power = 0.0 W
	dims = -50 x 6.2 x 16.0 mm
Block "GFX_heat_plate":	power = 0.0 W
	dims = 47.5 x 2.3 x 40.0 mm
Block "HEX":	power = 1.0 W
	dims = 30 x 2 x 30.0 mm
Block "RAM":	power = 0.0 W
	dims = 70 x -6.6 x 55.0 mm
Block "Socket and Pins":	power = 0.0 W
	dims = -36 x 1.47 x -35.0 mm
Block "Socket and Pins_gfx":	power = 0.0 W
	dims = 40 x 1.47 x 40.0 mm
Block "WLAN":	power = 0.0 W
	dims = 30 x 4 x 30.0 mm
Block "WPAN":	power = 0.0 W
	dims = 30 x 2 x 18.0 mm
Block "battery":	power = 0.0 W
	dims = -172 x 18 x 77.0 mm
Block "block.1":	power = 0.0 W
	dims = 9 x 5 x 125.0 mm
Block "block.2":	power = 0.0 W
	dims = 9 x 5 x 114.0 mm
Block "block.3":	power = 0.0 W
	dims = 92 x 5 x 9.0 mm
Block "block.4":	power = 0.0 W
	dims = 103 x 5 x 9.0 mm
Block "block.5":	power = 0.0 W
	dims = 62 x 4 x 55.0 mm
Block "block.6":	power = 0.0 W

	dims = 40 x 4 x 30.0 mm
Block "block.g1":	power = 0.0 W
	dims = 9 x 5 x 102.0 mm
Block "block.g2":	power = 0.0 W
	dims = 9 x 5 x 90.0 mm
Block "block.g3":	power = 0.0 W
	dims = 74 x 5 x 9.0 mm
Block "block.g4":	power = 0.0 W
	dims = 85 x 5 x 9.0 mm
Block "dvd_rom":	power = 0.0 W
	dims = 130 x 13 x 126.0 mm
Block "harddisk":	power = 0.0 W
	dims = -100 x 10 x 72.0 mm
Blower "blower.1":	power = 1.0 W
	dims = 0.07 x 0.0108 x 0.07 m
Blower "blower_gfx":	power = 1.0 W
	dims = 0.07 x 0.0108 x 0.07 m
Plate "CPU_TIM":	power = 0.0 W
	dims = 10.4 x -13.6 mm
Plate "GFX_TIM":	power = 0.0 W
	dims = 40 x 40 mm
Plate "Substrate":	power = 0.0 W
	dims = -35 x 36 mm
Plate "Substrate_gfx":	power = 0.0 W
	dims = 40 x 40 mm
Plate "plate.1":	power = 0.0 W
	dims = 10.4 x -13.6 mm
Plate "underfill":	power = 0.0 W
	dims = 10.4 x 13.6 mm
Source "CPU_Source":	power = 0.0 W
	dims = 8 x -11.6 mm
Source "GFX_Source":	power = 0.0 W
	dims = 8 x 11.6 mm

Fans

No fans are present

Vents

Ventres "cabinet_default_side_maxz":	loss coeff = 0.0 m/s
	dims = 0.405 x 0.033 m
Ventres "grille.1":	loss coeff = 0.0 m/s
	dims = 80 x -190 mm
Ventres "grille_gfx":	loss coeff = 0.0 m/s
	dims = 80 x 60 mm
Ventres "grille_gfx.1":	loss coeff = 0.0 m/s

	dims = 0.015 x 0.08 m
Ventres "grille_gfx.1.1":	loss coeff = 0.0 m/s
	dims = 0.015 x 0.08 m
Ventres "grille_gfx.2":	loss coeff = 0.0 m/s
	dims = 80 x -60 mm

Table E.3 Overview of the Full Simulation with TE integrated

Overview of solution Full-Simulation_with_ferro, Wed Jul 25 20:26:49 Turkey Daylight Time 2012

Mass flow rates:

Object	Specified	Calculated
opening.1	0.0 kg/s	0.009443 kg/s
cabinet_default_side_maxz	n/a	-0.0113 kg/s
grille_gfx	n/a	0.01386 kg/s
grille_gfx.1	n/a	-0.0001098 kg/s
grille_gfx.1.1	n/a	-0.0002958 kg/s
grille_gfx.2	n/a	-0.002421 kg/s
grille.1	n/a	0.01857 kg/s
blower_gfx	n/a	0.001833 kg/s
blower.1	n/a	0.001692 kg/s

Volume flow rates:

Object	Specified	Calculated
opening.1	n/a	0.008131 m3/s
cabinet_default_side_maxz	n/a	-0.009726 m3/s
grille_gfx	n/a	0.01194 m3/s
grille_gfx.1	n/a	-9.452e-005 m3/s
grille_gfx.1.1	n/a	-0.0002547 m3/s
grille_gfx.2	n/a	-0.002085 m3/s
grille.1	n/a	0.01599 m3/s

blower_gfx	n/a	0.001578 m3/s
blower.1	n/a	0.001457 m3/s

Fan operating points:

blower_gfx volume flow = 1.578e-003 m3/s, pressure rise = 35.550406724662 N/m2

Heat flows for objects with power specified:

Object	Specified	Calculated
HEX	1 W	0.9816 W
blower_gfx hub	1 W	-275.9 W
blower.1 hub	1 W	-25.65 W
GFX_Source	35.0	35 W
CPU_Source	35.0	35 W

Heat flows for openings, walls, grilles, and fans:

opening.1	0 W
cabinet_default_side_maxz	-109.5 W
grille_gfx	69.33 W
grille_gfx.1	-2.266 W
grille_gfx.1.1	-1.747 W
grille_gfx.2	-15.61 W
grille.1	91.63 W
blower_gfx	-91.96 W
blower.1	-8.551 W

Maximum temperatures:

GFX_Source	62.41 C
CPU_Source	75.91 C
HEX	42.66 C
RAM	30.63 C
WLAN	32.46 C
WPAN	30.97 C
battery	30.86 C
block.5	30.79 C
block.6	30.81 C
dvd_rom	30.88 C
harddisk	30.99 C
GFX_Block_2	48.06 C
GFX_heat_plate	50.21 C
block.g1	48.53 C
block.g2	48.48 C
block.g3	47.97 C
block.g4	47.97 C
BGA.1	45.42 C
Die_gfx	62.38 C
Socket and Pins_gfx	46.5 C
BiTe.1	44.5 C
TE bottom.1	44.5 C
TE top.1	33.75 C
CPU_Block	49.38 C
CPU_Block.1	44.35 C

block.1	44.44 C
block.2	44.69 C
block.3	43.85 C
block.4	43.84 C
BGA	46.19 C
Die	75.91 C
Socket and Pins	47.76 C
pcb.4	31.06 C
pcb_inout	32.64 C
pcb_gfx	48.04 C
pcb.1	46.1 C
pcb.2	45.94 C
pcb.3	31.04 C

Table E.4 Detailed report of the Full Simulation with TE integrated

Problem definition

Time variation: steady
Variables solved: temperature, flow
Radiation: YES
Flow regime: turbulent

Overview of solution Full-Simulation_with_ferro, Wed Jul 25 20:26:49 Turkey Daylight Time 2012

Mass flow rates:

Object Specified Calculated

opening.1 0.0 kg/s 0.009443 kg/s

cabinet_default_side_maxz n/a -0.0113 kg/s

grille_gfx n/a 0.01386 kg/s

grille_gfx.1 n/a -0.0001098 kg/s

grille_gfx.1.1 n/a -0.0002958 kg/s

grille_gfx.2 n/a -0.002421 kg/s

grille.1 n/a 0.01857 kg/s

blower_gfx n/a 0.001833 kg/s

blower.1 n/a 0.001692 kg/s

Volume flow rates:

Object Specified Calculated

opening.1 n/a 0.008131 m3/s

cabinet_default_side_maxz n/a -0.009726 m3/s

grille_gfx n/a 0.01194 m3/s

grille_gfx.1 n/a -9.452e-005 m3/s

grille_gfx.1.1 n/a -0.0002547 m3/s

grille_gfx.2 n/a -0.002085 m3/s

grille.1 n/a 0.01599 m3/s

blower_gfx n/a 0.001578 m3/s

blower.1 n/a 0.001457 m3/s

Fan operating points:

blower_gfx volume flow = 1.578e-003 m3/s, pressure rise = 35.550406724662 N/m2

Heat flows for objects with power specified:

Object Specified Calculated

HEX 1 W 0.9816 W

blower_gfx hub 1 W -275.9 W

blower.1 hub 1 W -25.65 W

GFX_Source 35.0 35 W

CPU_Source 35.0 35 W

Heat flows for openings, walls, grilles, and fans:

opening.1 0 W

cabinet_default_side_maxz -109.5 W
grille_gfx 69.33 W
grille_gfx.1 -2.266 W
grille_gfx.1.1 -1.747 W
grille_gfx.2 -15.61 W
grille.1 91.63 W
blower_gfx -91.96 W
blower.1 -8.551 W

Maximum temperatures:
GFX_Source 62.41 C
CPU_Source 75.91 C
HEX 42.66 C
RAM 30.63 C
WLAN 32.46 C
WPAN 30.97 C
battery 30.86 C
block.5 30.79 C
block.6 30.81 C
dvd_rom 30.88 C
harddisk 30.99 C
GFX_Block_2 48.06 C
GFX_heat_plate 50.21 C
block.g1 48.53 C
block.g2 48.48 C
block.g3 47.97 C
block.g4 47.97 C
BGA.1 45.42 C
Die_gfx 62.38 C
Socket and Pins_gfx 46.5 C
BiTe.1 44.5 C
TE bottom.1 44.5 C
TE top.1 33.75 C
CPU_Block 49.38 C
CPU_Block.1 44.35 C
block.1 44.44 C
block.2 44.69 C
block.3 43.85 C
block.4 43.84 C
BGA 46.19 C
Die 75.91 C
Socket and Pins 47.76 C
pcb.4 31.06 C
pcb_inout 32.64 C
pcb_gfx 48.04 C
pcb.1 46.1 C

pcb.2 45.94 C

pcb.3 31.04 C

Overall totals:

power = -230.6 W

mass flow through boundaries = 0.02184 kg/s

volume flow through boundaries = 0.0188 m3/s

Heat sources

Block "BGA":	power = 0.0 W
	dims = 36 x 0.66 x 35.0 mm
Block "BGA.1":	power = 0.0 W
	dims = 40 x 0.66 x 40.0 mm
Block "BiTe.1":	power = 0.0 W
	dims = 6.05 x 2 x 6.05 mm
Block "CPU_Block":	power = 0.0 W
	dims = 50 x 3 x 40.0 mm
Block "CPU_Block.1":	power = 0.0 W
	dims = 40 x 3 x 25.0 mm
Block "Die":	power = 0.0 W
	dims = -13.6 x 0.79 x 10.371 mm
Block "Die_gfx":	power = 0.0 W
	dims = 13.6 x 0.79 x 10.371 mm
Block "GFX_Block_2":	power = 0.0 W
	dims = -50 x 6.2 x 16.0 mm
Block "GFX_heat_plate":	power = 0.0 W
	dims = 47.5 x 2.3 x 40.0 mm
Block "HEX":	power = 1.0 W
	dims = 30 x 2 x 30.0 mm
Block "RAM":	power = 0.0 W
	dims = 70 x -6.6 x 55.0 mm
Block "Socket and Pins":	power = 0.0 W
	dims = -36 x 1.47 x -35.0 mm
Block "Socket and Pins_gfx":	power = 0.0 W
	dims = 40 x 1.47 x 40.0 mm
Block "TE bottom.1":	power = 0.0 W
	dims = 6.05 x 0.3 x 7.62 mm
Block "TE top.1":	power = 0.0 W
	dims = 6.05 x 0.3 x 6.05 mm
Block "WLAN":	power = 0.0 W
	dims = 30 x 4 x 30.0 mm
Block "WPAN":	power = 0.0 W
	dims = 30 x 2 x 18.0 mm
Block "battery":	power = 0.0 W
	dims = -172 x 18 x 77.0 mm
Block "block.1":	power = 0.0 W

	dims = 9 x 5 x 125.0 mm
Block "block.2":	power = 0.0 W
	dims = 9 x 5 x 114.0 mm
Block "block.3":	power = 0.0 W
	dims = 92 x 5 x 9.0 mm
Block "block.4":	power = 0.0 W
	dims = 103 x 5 x 9.0 mm
Block "block.5":	power = 0.0 W
	dims = 62 x 4 x 55.0 mm
Block "block.6":	power = 0.0 W
	dims = 40 x 4 x 30.0 mm
Block "block.g1":	power = 0.0 W
	dims = 9 x 5 x 102.0 mm
Block "block.g2":	power = 0.0 W
	dims = 9 x 5 x 90.0 mm
Block "block.g3":	power = 0.0 W
	dims = 74 x 5 x 9.0 mm
Block "block.g4":	power = 0.0 W
	dims = 85 x 5 x 9.0 mm
Block "dvd_rom":	power = 0.0 W
	dims = 130 x 13 x 126.0 mm
Block "harddisk":	power = 0.0 W
	dims = -100 x 10 x 72.0 mm
Blower "blower.1":	power = 1.0 W
	dims = 0.07 x 0.0108 x 0.07 m
Blower "blower_gfx":	power = 1.0 W
	dims = 0.07 x 0.0108 x 0.07 m
Plate "CPU_TIM":	power = 0.0 W
	dims = 10.4 x -13.6 mm
Plate "GFX_TIM":	power = 0.0 W
	dims = 40 x 40 mm
Plate "Substrate":	power = 0.0 W
	dims = -35 x 36 mm
Plate "Substrate_gfx":	power = 0.0 W
	dims = 40 x 40 mm
Plate "plate.1":	power = 0.0 W
	dims = 10.4 x -13.6 mm
Plate "underfill":	power = 0.0 W
	dims = 10.4 x 13.6 mm
Source "CPU_Source":	power = 0.0 W
	dims = 8 x -11.6 mm
Source "GFX_Source":	power = 0.0 W
	dims = 8 x 11.6 mm

Fans

No fans are present

Vents

Ventres "cabinet_default_side_maxz":	loss coeff = 0.0 m/s
	dims = 0.405 x 0.033 m
Ventres "grille.1":	loss coeff = 0.0 m/s
	dims = 80 x -190 mm
Ventres "grille_gfx":	loss coeff = 0.0 m/s
	dims = 80 x 60 mm
Ventres "grille_gfx.1":	loss coeff = 0.0 m/s
	dims = 0.015 x 0.08 m
Ventres "grille_gfx.1.1":	loss coeff = 0.0 m/s
	dims = 0.015 x 0.08 m
Ventres "grille_gfx.2":	loss coeff = 0.0 m/s
	dims = 80 x -60 mm